

Studies of the Lifetime and Degradation of Li-Ion Cells

by

John Christopher Burns

Submitted in partial fulfillment of the requirements  
for the degree of Doctor of Philosophy

at

Dalhousie University  
Halifax, Nova Scotia  
June 2015

© Copyright by John Christopher Burns, 2015

*To my wife*

# Table of Contents

<b>List of Tables</b> .....	<b>v</b>
<b>List of Figures</b> .....	<b>vi</b>
<b>Abstract</b> .....	<b>xii</b>
<b>List of Abbreviations and Symbols Used</b> .....	<b>xiii</b>
<b>Acknowledgements</b> .....	<b>xv</b>
<b>Chapter 1 Introduction</b> .....	<b>1</b>
<b>Chapter 2 Lithium-ion Batteries</b> .....	<b>5</b>
2.1 Fundamental Principles .....	5
2.2 “Next Generation” Electrode Materials.....	8
2.3 Electrolytes .....	9
2.4 Electrochemical Behavior.....	13
<b>Chapter 3 Background on Experimental Techniques</b> .....	<b>23</b>
3.1 High Precision Coulometry .....	23
3.1a Symmetric Cells.....	26
3.1b Differential Voltage Analysis .....	30
3.2 Cell Storage .....	32
3.3 Electrochemical Impedance Spectroscopy .....	33
<b>Chapter 4 Electrolyte Additive Testing in Cells with Gradual Capacity Loss....</b>	<b>36</b>
4.1 Experimental Details .....	36
4.2 Results and Analysis.....	38
4.3 Summary.....	46
4.4 How Coulombic Efficiency Evolves with Cell Lifetime.....	50
<b>Chapter 5 Impedance Reducing Additives</b> .....	<b>58</b>
5.1 Impact of HQ-115 on Cell Performance.....	58
5.2 Impact of Trimethoxyboroxine on Cell Performance.....	64

<b>Chapter 6</b>	<b>Impact of Electrolyte Containing Intentionally Added Water .....</b>	<b>74</b>
6.1	Background.....	74
6.2	Cells with Graphite Negative Electrodes.....	75
6.3	Cells with Lithium Titanate Negative Electrodes.....	84
<b>Chapter 7</b>	<b>Electrolyte Additive Testing in “Zero-Fade” Cells.....</b>	<b>98</b>
7.1	Experimental Details .....	99
7.2	Results.....	100
<b>Chapter 8</b>	<b>Application-Based Performance Testing .....</b>	<b>113</b>
8.1	Uses of High Precision Coulometry for Battery Management.....	113
8.2	Impact of Charge Rate on Performance.....	114
<b>Chapter 9</b>	<b>Conclusions and Future Work.....</b>	<b>123</b>
9.1	Conclusions.....	123
9.2	Future Work.....	126
<b>Bibliography</b>	<b>.....</b>	<b>132</b>
<b>Appendix A: Request for Permission to Reproduce or Re-Publish ECS Material</b>	<b>.....</b>	<b>141</b>

## List of Tables

Table 4.1	A list of the different additives tested in the 120 mAh prismatic cells including molecular formula and abbreviated name.....	37
-----------	---	----

## List of Figures

Figure 2.1	The structures of $\text{LiCoO}_2$ and $\text{CoO}_2$ that exist through lithiation and delithiation process. ....	7
Figure 2.2	The structures of $\text{LiC}_6$ and $\text{C}_6$ (graphite) that exist through the lithiation and delithiation process. ....	7
Figure 2.3	The structure of commonly used carbonates as solvents for electrolyte in Li-ion cells. ....	10
Figure 2.4	Schematic of a cylindrically wound cell. ....	14
Figure 2.5	Schematic of coin cell parts and coin cell assembly. ....	14
Figure 2.6	The potential versus specific capacity for four common positive and negative electrode materials. ....	16
Figure 2.7	Panel a) shows the potential versus specific capacity for an LCO electrode half cell. Panel b) shows the potential versus specific capacity for a graphite electrode. ....	17
Figure 2.8	Panel a) shows the discharge capacity (left) and coulombic efficiency (right) versus cycle number. Panel b) shows the voltage versus capacity for 24 cycles of a $\text{LiCoO}_2$ /graphite cell. ....	18
Figure 2.9	Schematic showing the potential versus capacity curves for a positive and negative electrode along with the voltage versus capacity for the full cell. ....	21
Figure 3.1	Photograph of the 60-channel HPC system at Dalhousie University. ....	24
Figure 3.2	A comparison of the precision (or noise) (panel a) and accuracy (panel b) of coulombic efficiency measurements made with a Maccor 4000 series charger, the HPC and the UHPC measured in parts per million. ...	25
Figure 3.3	Photo of the 100-channel UHPC system at Dalhousie University. ....	26
Figure 3.4	Panel a) shows the voltage versus relative capacity (0 - 1) of a graphite half cell along with the charge and discharge endpoint capacities versus cycle number (insert). Panel b) shows a schematic of how slippage of electrodes should occur in a symmetric cell leading to capacity loss. ....	27
Figure 3.5	Panel a) shows the discharge (left) and charge (right) endpoint capacities versus cycle number for a graphite symmetric cell. Panel b) shows the voltage versus specific capacity for the same graphite symmetric cell. ....	28
Figure 3.6	Panel a) shows the specific capacity versus cycle number for a graphite symmetric cell with a linear fit to calculate fade rate. Panel b)	

	shows the measured coulombic efficiency of the graphite symmetric cell along with the calculated coulombic efficiency. ....	29
Figure 3.7	Cell voltage (black, left) and differential voltage (red, right) versus capacity for a $\text{LiCoO}_2/\text{graphite}$ cell. ....	31
Figure 3.8	A schematic circuit (left) showing the simplest representation of a Li-ion cell. The resulting Nyquist plot for the left circuit is shown on the right. ....	34
Figure 4.1	A photograph of the prismatically wound cells used for electrolyte additives testing. ....	36
Figure 4.2	Voltage versus capacity (%) curves for High Voltage LCO (a, d, g), Low Voltage LCO (b, e, h) and NMC (c, f, i) cells containing control electrolyte with 2% VC (a, b, c), 1% VC (d, e, f) or no VC (g, h, i) cycling at $C/20$ at $40^\circ\text{C}$ . ....	39
Figure 4.3	Charge endpoint capacity (a, b, c), discharge capacity (d, e, f) and coulombic efficiency (g, h, i) versus cycle number for High Voltage LCO (a, d, g), Low Voltage LCO (b, e, h) and NMC (c, f, i) cells cycling at $C/20$ at $40^\circ\text{C}$ . ....	41
Figure 4.4	Cell voltage versus time during open circuit storage for High Voltage LCO (a), Low Voltage LCO (b) and NMC (c) cells at $40^\circ\text{C}$ . ....	42
Figure 4.5	Impedance spectra in the form of Nyquist plots for High Voltage LCO (a, d, g), Low Voltage LCO (b, e, h) and NMC (c, f, i) cells containing control electrolyte with 2% VC (a, b, c), 1% VC (d, e, f) or no VC (g, h, i) after cycling on the HPC at $C/20$ at $40^\circ\text{C}$ . ....	43
Figure 4.6	Normalized discharge capacity versus cycle number for High Voltage LCO (a), Low Voltage LCO (b) and NMC (c) cells cycling at $C/10$ at $55^\circ\text{C}$ after cycling on the HPC. ....	45
Figure 4.7	A summary of electrolytes tested in Low Voltage LCO cells showing the fade rate, charge slippage, CIE/h and discharge slippage measured on the HPC. ....	47
Figure 4.8	A summary of electrolytes tested in High Voltage LCO cells showing the fade rate, charge slippage, CIE/h and discharge slippage measured on the HPC. ....	48
Figure 4.9	A summary of electrolytes tested in NMC cells showing the fade rate, charge slippage, CIE/h and discharge slippage measured on the HPC. ....	49
Figure 4.10	Long term cycling showing fractional capacity versus time for LCO/graphite cells cycling at $37^\circ\text{C}$ . ....	52
Figure 4.11	Charge endpoint capacity, discharge capacity and coulombic efficiency versus time collected on the UHPC system for cells after different amounts of cycling time. ....	54

Figure 4.12	Summary of UHPC data showing the charge slippage rate and coulombic efficiency as a function of cell age in years. ....	55
Figure 4.13	Impedance spectra presented in the form of a Nyquist plot of pair cells from each group collected at 3.9 V and 10°C after UHPC cycling tests. ...	56
Figure 5.1	Charge endpoint capacity (a, b, c), discharge capacity (d, e, f) and coulombic efficiency (g, h, i) versus cycle number for High Voltage LCO (a, d, g), Low Voltage LCO (b, e, h) and NMC (c, f, i) cells cycling at C/20 at 40°C. ....	59
Figure 5.2	Cell voltage versus time during open circuit storage for High Voltage LCO (a, b), Low Voltage LCO (c, d) and NMC (e, f) cells at 40°C during a first (a, c, e) and second (b, d, f) storage period. ....	61
Figure 5.3	Impedance spectra in the form of Nyquist plots for High Voltage LCO (a, d, g, j), Low Voltage LCO (b, e, h, k) and NMC (c, f, i, l) cells containing control electrolyte with 2% VC + 2% HQ-115 (a, b, c), 2% HQ-115 (d, e, f), 2% VC (g, h, i) or no additives (j, k, l) after cycling on the HPC at C/20 at 40°C. ....	62
Figure 5.4	Normalized discharge capacity versus cycle number for High Voltage LCO (a), Low Voltage LCO (b) and NMC (c) cells cycling at C/10 at 55°C after cycling on the HPC. ....	63
Figure 5.5	Charge Endpoint Capacity (a, b, c), discharge capacity (d, e, f) and coulombic efficiency (g, h, i) versus cycle number for High Voltage LCO (a, d, g), Low Voltage LCO (b, e, h) and NMC (c, f, i) cells cycling at C/20 at 40°C. ....	65
Figure 5.6	Cell voltage versus time during open circuit storage for High Voltage LCO (a, b), Low Voltage LCO (c, d) and NMC (e, f) cells at 40°C during a first (a, c, e) and second (b, d, f) storage period. ....	67
Figure 5.7	Impedance spectra in the form of Nyquist plots for High Voltage LCO (a, d, g, j), Low Voltage LCO (b, e, h, k) and NMC (c, f, i, l) cells containing control electrolyte with 2% VC + 0.3% TMOBX (a, b, c), 0.3% TMOBX (d, e, f), 2% VC (g, h, i) or no additives (j, k, l) after cycling on the HPC at C/20 at 40°C. ....	68
Figure 5.8	Normalized discharge capacity versus cycle number for High Voltage LCO (a), Low Voltage LCO (b) and NMC (c) cells cycling at C/10 at 55°C after cycling on the HPC. ....	70
Figure 6.1	The first cycle irreversible capacity loss (a, c) and swelling (%) during first cycle (b, d) for NMC/graphite (a, b) and LiCoO <sub>2</sub> /graphite (c, d) cells as a function of water content in either control (black), VC-containing (blue) or VC + HQ-115-containing (red) electrolyte. ....	76
Figure 6.2	Cycling data collected from the HPC for LiCoO <sub>2</sub> /graphite cells with constant current charge and discharge (~C/20) at 40°C. Shown are the charge end point capacity (a, b), discharge capacity (c, d) and coulombic efficiency (e, f) as a function of cycle number. ....	77



Figure 6.3	Cycling data collected from the HPC for NMC/graphite cells with constant current charge and discharge ( $\sim C/20$ ) at 40°C. Shown are the charge end point capacity (a, b), discharge capacity (c, d) and coulombic efficiency (e, f) as a function of cycle number. ....	78
Figure 6.4	A summary of data collected for LiCoO <sub>2</sub> /graphite cells showing the coulombic inefficiency (1 – CE), charge slippage rate, voltage drop during storage (V drop), and charge transfer resistance (R <sub>CT</sub> ) for each electrolyte formulation.....	80
Figure 6.5	A summary of data collected for NMC/graphite cells showing the coulombic inefficiency (1 – CE), charge slippage rate, voltage drop during storage (V drop), and charge transfer resistance (R <sub>CT</sub> ) for each electrolyte formulation.....	81
Figure 6.6	Long term cycling of the LiCoO <sub>2</sub> /graphite (a, b) and NMC/graphite (c, d) cells at $\sim C/10$ that were initially cycled on the HPC as well as cells containing 1000 ppm water in control electrolyte that were not cycled on the HPC.....	83
Figure 6.7	The swelling of the prismatic cell case during the formation cycle as a function of the amount of intentionally added water to the electrolyte. ....	85
Figure 6.8	Panel a) shows a schematic of the potential-capacity curves for the electrodes of a LTO-limited LCO/LTO cell. ....	86
Figure 6.9	Cycling data collected using the HPC for LCO/LTO cells with constant current charge and discharge ( $\sim C/20$ ) at 30 (a, c) and 60°C (b, d). ....	88
Figure 6.10	Cycling data collected from the HPC for LCO/LTO cells with constant current charge and discharge ( $\sim C/20$ ) at 30 (a, c, e) and 60°C (b, d, f). ....	89
Figure 6.11	Long term (4 years) cycling data from the manufacturer showing the normalized (%) (based on first cycle capacity) discharge capacity (with error bars based on the standard deviation of six cells) (a) and discharge voltage at 10% depth of discharge (b). ....	90
Figure 6.12	Open circuit voltage versus time during storage at 30 (a), 40 (b), 50 (c), and 60°C (d) for cells with different amounts of water added to the electrolyte.....	91
Figure 6.13	Area specific impedance spectra presented as Nyquist plot for data collected at 10°C for cells with different amounts of water added to the electrolyte before storage experiments. ....	92
Figure 6.14	Area specific impedance spectra presented as Nyquist plots for data collected at 10°C after cells were cycled on the HPC at 30 (a), 40 (b), 50 (c), and 60°C (d). ....	93
Figure 6.15	A summary of all measured parameters in HPC cycling, storage and impedance measurements as a function of the amount of water added to the electrolyte for each temperature.....	94

Figure 6.16	Normalized capacity (%) versus cycle number for three cells with control electrolyte and electrolyte containing 200, 1000 and 2000 ppm water (a) and the average for those cells with standard deviation error bars (b). Also shown in the normalized capacity versus cycle number for pairs of control cells and cells containing 1000 ppm water that were formed one week after being filled with electrolyte (c) and the averages for the two cells (d).....	96
Figure 7.1	Normalized discharge capacity (%) versus cycle number showing examples of gradual capacity loss (cells 1 and 2 in panel a)) and rapid “roll-over” capacity loss (cells 3 and 4 in panel b)).....	99
Figure 7.2	a) Capacity versus cycle number for the first 50 1C cycles, after low rate HPC cycling, of the NMC/graphite 18650 cells with the additives listed in the legend; b) coulombic efficiency for the same cells as a) measured during the first 16 C/20 cycles after formation using the high precision charger and c) capacity versus cycle number for the same cells as a) showing all 1C long term cycling data until failure at 1.6 Ah.....	101
Figure 7.3	Schematic model of a process that could cause “roll-over” failure in Li-ion cells with highly compressed negative electrodes after a sufficient number of charge-discharge cycles.....	102
Figure 7.4	Capacity versus cycle number for NMC/graphite cells cycling to different upper cut-off limits to illustrate the impact of high voltage on “roll-over” failure.....	103
Figure 7.5	SEM micrographs of uncycled electrodes and cycle electrodes from cells with VC + VEC + FEC electrolyte additives. ....	104
Figure 7.6	a) 1/(Charge slippage) [cycle/mAh] versus 1/(1 – CE) [no units] showing that oxidation reactions at the positive electrode account for almost exclusively for the departure of coulombic efficiency from the ideal value of 1.0000 and b) number of cycles to failure at 1.6 Ah (cycling at 1C) versus 1/(1 – CE). ....	106
Figure 7.7	The number of cycle until failure (capacity reaching 1.6 Ah) versus 1/(1 – CE) for the cells with known electrolyte compositions.....	107
Figure 7.8	Impedance spectra presented in Nyquist plots collected on cells after cycling on the HPC. The cells shown are (a) 1.5 wt.% VC, (b) FEC, (c) VC + FEC, (d) VC + VEC + FEC + PS, (e) 2UB, (f) 3UE, (g) 4UA and (h) 5UA. ....	108
Figure 7.9	Number of cycles to failure at 1.6 Ah (cycling at 1C) plotted as a function of both 1/(1 – CE) and charge transfer resistance ( $R_{CT}$ ) [ $\Omega$ ]. ....	109
Figure 7.10	Number of cycles to failure at 1.6 Ah (cycling at 1C) plotted as a function of both 1/(1 – CE) and 1500 x charge transfer resistance ( $1500 \cdot R_{CT}$ ) as a contour plot. ....	111

Figure 7.11	Capacity versus cycle number for NMC/graphite 18650 cells with a proprietary set of electrolyte additives cycled at 2A currents at 23°C and at 60°C.....	112
Figure 8.1	Schematic of coulombic efficiency versus charge rate with both the time dependent and charge rate dependent resolved curves (bottom) and the resulting CE versus rate curve (top) at different temperature. ....	115
Figure 8.2	Voltage versus capacity curves for pouch cells under test at 30°C during cycling with a two-step charge process from C/50 to 5C charge rates (a-h). ....	117
Figure 8.3	Capacity (a), coulombic efficiency (b) and coulombic inefficiency per hour (CIE/h) (c) versus time for pouch cells cycling at 30°C during cycling with a two-step charge process from C/50 to 5C charge rates. ....	118
Figure 8.4	A summary of fade (a), coulombic efficiency (b) and coulombic inefficiency per hour (CIE/h) (c) versus charge rate for all pouch cells at different temperatures and rates using both the single and two-stage charge process. ....	120
Figure 8.5	Photograph of the negative electrode after cycling for cells cycled at different rates and 12°C (a) and 50°C (b) to examine for confirmation of the occurrence of lithium plating. ....	122

## Abstract

Long lifetime Li-ion batteries (10 – 20+ years) are a key component in enabling applications such as electrified vehicles and grid storage for renewable power generation. However, undesirable parasitic reactions occur within Li-ion cells that can eventually limit their cycle life. These parasitic reactions can take many forms and manifest in different types of cell failure. In order to improve Li-ion cell lifetime, researchers and cell manufacturers must be able to understand the impact of small changes to the chemistry or manufacturing on cell lifetime without having to cycle cells until failure as it is too time consuming.

High precision coulometry has been suggested as a technique to detect small differences in the coulombic efficiency (ratio of charge delivered to charge stored during a cycle) of cells in the early cycles that should correlate to cell lifetime. This thesis examines cells with different failure modes and shows how high precision coulometry can be used, in conjunction with other techniques, to reliably determine the relative performance of cells in experiments that last only a few weeks. It was shown that coulombic efficiency could be used to predict the long term performance of cells that show either gradual fade or very little fade until “roll-over” failure with different electrolyte additives. The effect of age on coulombic efficiency was also studied showing the increase in coulombic efficiency with time but the presence of charge slippage even later in a cells life that can eventually lead to cell failure.

In addition to selecting cell chemistries that enable long lifetime, cycling conditions for different applications can also impact cell lifetime. In order to study some of these application demands, the impact of high rate charging has been studied using high precision coulometry to detect the onset of metallic lithium deposition which can limit lifetime. For the cells tested it was found lithium plating began at rates as low as  $C/2$  at  $12^{\circ}\text{C}$  but did not begin until  $2C$  when cycling at  $50^{\circ}\text{C}$ .

## List of Abbreviations and Symbols Used

ARC	Accelerating rate calorimetry
ATFEC	Allyl tris(2,2,2trifluoroethyl) carbonate
CE	Coulombic efficiency
CIE/h	Coulombic inefficiency per hour
CMC	Carboxymethyl cellulose
CPE	Constant phase element
$\Delta$	Endpoint slippages (specified by subscript)
DEC	Diethyl carbonate
DMC	Dimethyl carbonate
DOD	Depth of discharge
DSC	Differential scanning calorimetry
e	Electron charge, $1.602 \times 10^{-19}$ C
EC	Ethylene carbonate
EIS	Electrochemical impedance spectroscopy
EM-1	Tris (trimethylsilyl) phosphate
EMC	Ethyl methyl carbonate
FEC	Fluoroethylene carbonate
FTIR	Fourier transform infrared spectroscopy
HFiP	Tris(hexafluoro-iso-propyl)phosphate
HPC	High Precision Charger
HQ-115	lithium (bis) trifluoromethanesulfonimide
HVC	High voltage LiCoO <sub>2</sub> cells
I	Current (further described by subscript)
IRC	First cycle irreversible capacity loss
LiBOB	Lithium bis(oxalato)borate
LiDFOB	Lithium difluoro(oxalate)borate
LTO	Lithium titanate, Li <sub>4/3</sub> Ti <sub>5/3</sub> O <sub>2</sub>
LVC	Low voltage LiCoO <sub>2</sub> cells

m	Active electrode mass
NCA	$\text{Li}_x(\text{Ni}_{0.80}\text{Co}_{0.15}\text{Al}_{0.05})\text{O}_2$
NMC	$\text{Li}_x(\text{Ni}_{1/3}\text{Mn}_{1/3}\text{Co}_{1/3})\text{O}_2$
PC	Propylene carbonate
PS	1, 3-Propane sultone
PVDF	Polyvinylidene fluoride
q	Specific capacity (further described by subscript)
Q	Cell capacity (further described by subscript)
$R_{\text{CT}}$	Charge transfer resistance
SBR	Styrene-butadiene rubber
SEI	Solid Electrolyte Interphase
SEM	Scanning electron microscopy
t	Measured time for half cycle
TCEP	Tri( $\beta$ -chloromethyl) phosphate
TDFB	tris(pentafluorophenyl) borane
TEM	Tunneling electron microscopy
TMOBX	Trimethoxyboroxine
TPP	Triphenylphosphate
$\mu$	Chemical potential in joules per atom
UHPC	Ultra High Precision Charger
V	Cell voltage
VC	Vinylene carbonate
VEC	Vinyl ethylene carbonate
XPS	X-ray photoelectron spectroscopy

## **Acknowledgements**

Firstly I would like to thank Jeff Dahn for to opportunity to work in his lab for a number of years and for the flexibility he has given me. I could not have asked for more out of a supervisor than he has given me. The work, understanding and developments on the High Precision Charger would not have been possible without important contributions from Aaron Smith, Toby Bond and David Stevens. Much of the electrolyte work was done with Nupur Sinha and his contributions helped develop the understandings presented in this work. Many of the experiments conducted were part of industrially supported projects and I would like to thank my collaborators at 3M, Medtronic and E-One Moli Energy for their contributions. I have enjoyed my time in the lab and thank all of the group members that I have overlapped with for their help whenever it was needed and for making this lab an excellent place to work.

# Chapter 1 Introduction

Lithium-ion batteries are used in portable energy storage applications such as laptops, cell phone and portable power tools due to their high specific energy density relative to other rechargeable battery technologies such as nickel metal hydride (NiMH) [1]. Due to the large deployment of Li-ion batteries in portable applications, the use of the technology has expanded into packs for electric vehicle (and other modes of electric transportation such as scooters and bikes) and is a candidate for the choice of technology for grid energy scale storage. As the supply of energy shifts towards more renewable sources which are best used in conjunction with energy storage due to variations in power requirements on the grid scale and energy production rates from renewable sources such as wind or solar.

The first Li-ion cell was commercialized by Sony in 1991 and had a  $\text{LiCoO}_2$  positive electrode and a carbon negative electrode. In 2014, most of the Li-ion cells (where a battery is comprised of multiple cells) produced in the world used the same positive electrode and a graphite negative electrodes instead of the original carbon negative electrode. However, new applications such as electric vehicle packs and grid energy storage have increased the demands on the technology in terms of battery lifetime (or cycle life), energy storage (in terms of volumetric and gravimetric energy density), and power density all while trying to decrease production cost. Therefore, there are many aspects of Li-ion cells as well as battery design and engineering being researched across to world in attempts to improve the current state of the technology and see increased deployment of Li-ion batteries in these new applications.

For the past two decades the lifetime requirements of Li-ion cells were only several years because they were used in portable electronics which were typically replaced after 2-5 years (i.e. laptops and cell phones) and therefore there was no need for the cell lifetime to exceed the device lifetime. However, electric vehicles require a battery lifetime of at least 8 years (many electric vehicle manufacturers warranty the battery for up to 8 years [2–5]) and grid energy storage likely requires a  $> 20$  year lifetime to be commercially viable based on the cost required for a large scale energy



storage installation [6–9]. This leads to the issue of how a company can guarantee their battery will last for 8 years if they have not tested the battery for 8 years. Many researchers cycle batteries at elevated temperature to shorten the lifetime during lab experiments or cycle at very high rates (1 cycle per hour) to show a greater number of cycles in a shorter amount of time. However, for an electric vehicle the actual use of the battery will likely be one cycle per day as the user will drive the car during the day and recharge it overnight. Therefore, does an experiment showing 500 cycles of data that was collected over a 1 month experiment actually give an indication of the performance of that battery after 500 cycles by the user under the real conditions that would take 16-18 months? Unfortunately cycling under realistic conditions in lab experiments for many companies is not an option because when their experiment ends after, for example, 8 years, their technology is 8 years old and may be behind the new industry standards and, therefore may be obsolete.

The aim of this thesis is to present a new way to reliably evaluate long term cell performance in short term experiments using a technique referred to as high precision coulometry (in conjunction with other complementary experimental techniques) [10–12]. The premise behind high precision coulometry is that small differences in the coulombic efficiency of Li-ion cells in the early cycles can be indicative of the long term performance of those batteries under those cycling conditions. This comes from the fact that Li-ion cells degrade due to internal side reactions that slowly convert active components of the cell to inactive components and eventually lead to cell failure and these side reactions decrease the coulombic efficiency. Using this technique allows different cell chemistries to be compared in short experiments (roughly 1 month) and the chemistry with the highest efficiency to be selected as that which will show the longest cycle life under those conditions.

Chapter 2 will discuss Li-ion batteries in terms of the fundamental principles of operation as well as materials used. Basic electrochemical measurements of cell performance will also be presented. The important metrics resulting from the electrochemical tests will be discussed to show their importance for the Li-ion applications.

Chapter 3 will describe experimental techniques used with a heavy focus on high precision coulometry. High precision coulometry will be discussed in terms of the importance of the technique and the instrumentation required for relevant measurements. In addition to high precision coulometry, supplementary techniques such as differential voltage analysis, cell storage and impedance spectroscopy will be discussed.

Chapter 4 will present studies using high precision coulometry and other techniques on cells that show gradual degradation over time. These cells were studied to compare the effect of electrolyte formulation on performance using the same base electrode materials. It will also discuss what happens to coulombic efficiency during extended cycling presenting studies on cells that had been continually cycled by the manufacturer for up to 12 years before studying. This work was done in collaboration with Reza Fathi.

Chapter 5 will discuss several electrolyte additives from Chapter 4 that were studied in more detail. These additives showed interesting results in their short term measurements by dramatically reducing the cell impedance. The long term cycling performance will also be presented to illustrate how the use of precision short term measurements can be used to anticipate cell failure.

Chapter 6 will show studies on the impact of the addition of water to the electrolyte to cell performance using the same style cells from Chapter 4 that gradually degrade over time. Li-ion cells are typically manufactured in dry rooms with very low dew points and using materials that have minimal trace water present as it is believed that the presence of water in such an electrochemical cell accelerates degradation. Therefore water was intentionally added to the electrolyte to study the impact on cell performance.

Chapter 7 will present how changes to the electrolyte formulation of cells affect performance in cells that show a different failure mechanism. Some Li-ion cells show almost no loss in their ability to store energy from cycle to cycle until at some point in their life they fail very quickly. These types of cells are very interesting because without advanced techniques such as high precision coulometry it is very difficult to differentiate cell performance without cycling the cells until they actually fail which can be too long an experiment to be realistic for research and development purposes.

Chapter 8 will show other ways that high precision coulometry can be used to improve battery performance from an application perspective with respect to maximum charge rate capability. Much of the thesis to this point will have discussed how high precision coulometry can be used to study the chemistry within a cell and how it affects the lifetime, however there is a large opportunity to maximize cycle life by managing battery packs properly. Using the high precision charger, the impact of high charge rates on cell degradation was studied at different temperatures. Understanding how cycling conditions used in different applications impact cell lifetime is also important for enabling long lifetime cells.

Chapter 9 will summarize the work done in this thesis and how it can continue to be applied to improve the state of Li-ion technology. It will also discuss future directions that could be studied to further the understanding of cell failure and lifetime based on the results of this work.

## Chapter 2      Lithium-ion Batteries

### 2.1 Fundamental Principles

Lithium-ion batteries are comprised of multiple Li-ion cells. Each Li-ion electrochemical cell converts the difference in the chemical potential of lithium in two host materials into electrical energy through oxidation or reduction processes of the host materials as lithium is transferred between the electrodes within the cell and electrons through an external circuit [1]. A Li-ion cell contains two electrodes (coated on the respective current collectors to connect electrode material to the external circuit), electrolyte and a separator to electrically isolate the two electrodes within the cell while allowing  $\text{Li}^+$  transport between the electrodes. The voltage of a Li-ion cell is based the chemical potential of lithium atoms in the two electrode materials. Equation 2.1 shows the relationship between the voltage of the battery ( $V$  in volts) and the chemical potential of the lithium within the host material ( $\mu$  in joules) where  $e$  is the charge on an electron in coulombs.

$$V_{cell} = \frac{\mu_{negative} - \mu_{positive}}{e} \quad 2.1$$

There are many materials that can act as a host to lithium and therefore are candidates to be used as electrode materials. In order to increase the energy stored within the cell the voltage can be increased by choosing a positive electrode in which the chemical potential of lithium is low and a negative electrode in which the chemical potential of lithium is high to give a large difference. However, the chemical potential of lithium within the material is not the only consideration for choosing appropriate electrode materials as specific capacity (amount of lithium stored per unit mass or volume), cycle life and cost all contribute to the choice of materials.

As mentioned in Chapter 1, the first Li-ion battery was commercialized in 1991 using Li-ion cells containing  $\text{LiCoO}_2$  positive electrodes and carbon negative electrodes.

These materials, and most common Li-ion electrode materials, are intercalation electrodes which allow for the insertion and extraction of lithium from the structure with minimal change. For example,  $\text{Li}_x\text{CoO}_2$  can be lithiated and delithiated highly reversibly over the range  $0.5 \leq x \leq 1$  and achieve 150 mAh/g of capacity delithiated to 4.2 V vs. Li/Li<sup>+</sup> (average of 3.9 V) [13]. Figure 2.1 shows the structures of  $\text{LiCoO}_2$  and  $\text{CoO}_2$  that occur during the full lithiation and delithiation process. Another material with the same layered metal oxide structure as  $\text{LiCoO}_2$  that is commonly used has a mixture of transition metals in place of cobalt:  $\text{Li}[\text{NiMnCo}]\text{O}_2$  (NMC). This material was reported by Ohzuku and Makimura [14] in the form of equal concentration of nickel, manganese and cobalt and by Lu *et al.* [15] as a solid solution series. The  $\text{Li}[\text{Ni}_{1/3}\text{Mn}_{1/3}\text{Co}_{1/3}]\text{O}_2$  material can achieve 163 mAh/g when delithiated to 4.3 V vs. Li/Li<sup>+</sup> (average of 3.8 V) [16]. Variants of the equal metal content NMC can also be made with unequal metal contents such as  $\text{Li}[\text{Ni}_{0.5}\text{Mn}_{0.3}\text{Co}_{0.2}]\text{O}_2$  and  $\text{Li}[\text{Ni}_{0.42}\text{Mn}_{0.42}\text{Co}_{0.16}]\text{O}_2$  [17,18]. Other positive electrodes found in commercial cells include  $\text{Li}[\text{Ni}_{0.80}\text{Co}_{0.15}\text{Al}_{0.05}]\text{O}_2$  (NCA) (190 mAh/g at an average of 3.8 V),  $\text{LiMn}_2\text{O}_4$  (148 mAh/g at an average of 4 V [19]) and  $\text{LiFePO}_4$  (170 mAh/g at 3.4 V [20]).

Correspondingly as a lithium host at the negative electrode, graphite can rearrange the stacking sequence from ABAB... in the unlithiated state to AA... in the lithiated state ( $\text{LiC}_6$ ) and accommodate 372 mAh/g of capacity at an average of 0.1 V vs. Li/Li<sup>+</sup> [21]. The rearrangement of the graphite structure during lithiation results in a ~10% volume expansion [22]. Figure 2.2 shows the structure of graphite in the delithiated and lithiated ( $\text{LiC}_6$ ) states. Another common material used as a negative electrode is lithium titanate ( $\text{Li}_4\text{Ti}_5\text{O}_{12}$  called LTO) [23,24] which has a cubic spinel structure with a three dimensional array of tunnels that allow lithium transport into and out of the material. Due to the tunnel network that accommodates lithium ions, there is almost no expansion of the material during the lithiation and delithiation process. LTO is not as commonly used in commercial cells due to its lower specific capacity (175 mAh/g) and higher average potential (1.5 V vs. Li/Li<sup>+</sup>) relative to graphite, which leads to a lower capacity and energy cell. However, due to the lack of expansion during lithiation as well as operating at a less reductive potential, the cycle life of a Li-ion cell using LTO is better than those using a graphite electrode.

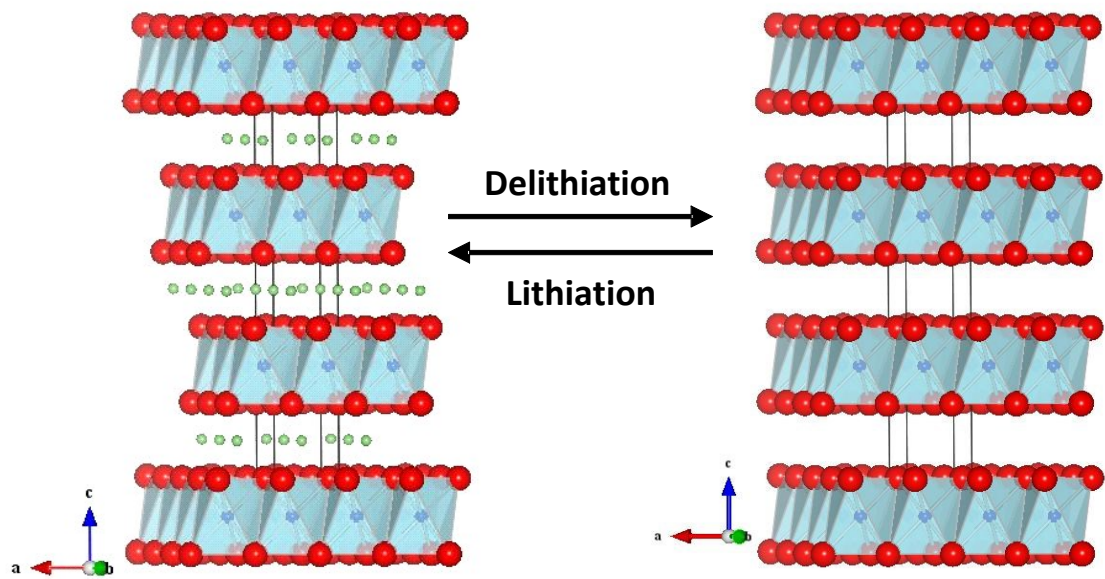


Figure 2.1 The structures of  $\text{LiCoO}_2$  and  $\text{CoO}_2$  that exist through lithiation and delithiation process. Lithium atoms are shown in green, oxygen in red and cobalt in blue.

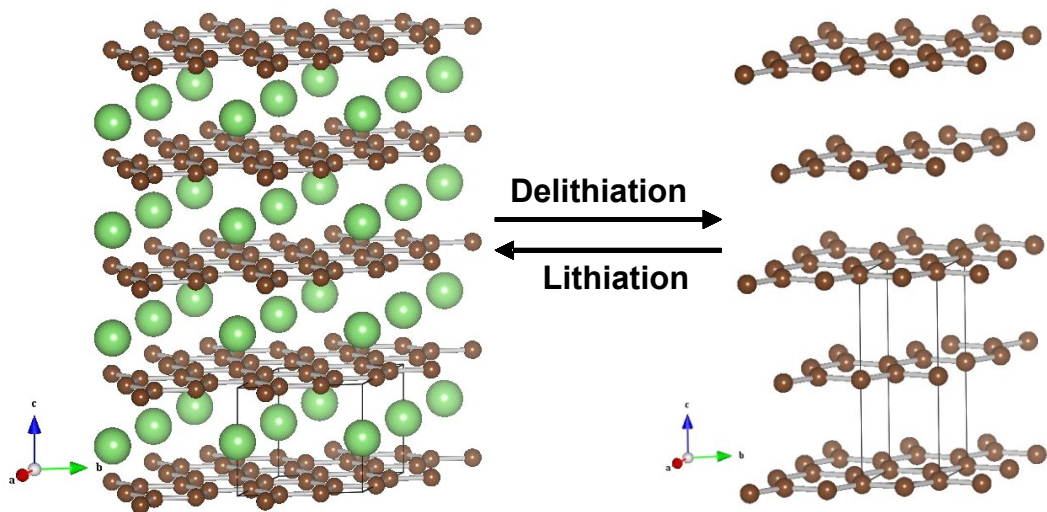


Figure 2.2 The structures of  $\text{LiC}_6$  and  $\text{C}_6$  (graphite) that exist through the lithiation and delithiation process. The lithium atoms are shown in green, carbon atoms are shown in brown.

The materials discussed above serve the role of the active electrode materials which host lithium as it is shuttled between the negative or positive electrode during charge and discharge, respectively. However, in order to make usable electrodes for Li-ion cells, the active material is mixed with a conductive additive to allow for better electron transport within the material as well as a binder to adhere the blend of materials together and to the current collector. Each electrode is cast onto a metallic foil to allow electrons to flow between the external circuit and the material during the oxidation/reduction processes. Positive electrode materials are typically cast on aluminum foil (due to the low cost, low weight and high electronic conductivity) while negative electrodes are typically cast on copper foil as aluminum alloys with lithium at  $\sim 0.26$  V [25] which is above the potentials reached by most negative electrodes. However, because the potential of LTO is  $\sim 1.5$  V vs. Li/Li<sup>+</sup> it can be cast on aluminum foil and is typically done so to reduce cost and weight.

## 2.2 “Next Generation” Electrode Materials

In order to reach higher energy densities, research is being conducted to find positive electrode materials that have higher specific capacity or can be charged to higher voltage to increase the cell voltage. Increasing the positive electrode potential can result in poor cycle life due to operating beyond the oxidative stability of the electrolyte which will be discussed in the next section. Correspondingly, research is done to find negative electrode materials that operate at a low potential such as graphite but have a higher specific capacity. These negative electrode materials are typically materials that alloy with lithium as they have a high theoretical capacity. Most of these materials are silicon, tin or aluminum-based and include Li<sub>15</sub>Si<sub>4</sub> (3579 mAh/g) [26], Li<sub>22</sub>Sn<sub>5</sub> (994 mAh/g) [27,28], LiAl (993 mAh/g) and Li<sub>9</sub>Al<sub>4</sub> (2234 mAh/g) [25]. Despite having high specific capacity and relatively low operating potentials, these materials have very poor cycle life due to the large structural changes associated with the alloying process. These structural changes can cause as much as 280% volume expansion (in the case of silicon) [29] which results in poor reversibility during cycling. The Sony Nexelion cell used a Sn-Co-C alloy

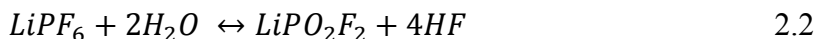
negative electrode [30] and other companies are starting to include small percentages of silicon in the graphite-based negative electrode in order to increase the negative electrode capacity.

A new class of positive electrode materials referred to as “5 V Positive Electrodes” [31] have recently emerged and gained research interest. Some of the more frequently studied materials include  $\text{LiNi}_{0.5}\text{Mn}_{1.5}\text{O}_4$  (147 mAh/g at 4.7 V),  $\text{LiCoPO}_4$  (167 mAh/g at 4.8 V) and  $\text{LiNiPO}_4$  (167 mAh/g at 5.1 V). Other materials are being investigated that may be charged to higher voltage to achieve greater specific capacity but do not operate continually at 5 V. Many of these are based on the NMC style material that contain excess lithium that is present in the transition metal layer to allow for higher specific capacity [32,33].

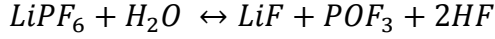
While these materials may be used in future Li-ion cell production (some are beginning to be used in specialized commercial cells now), many are still in the research stage and were not studied in this work. Recall that the goal of this thesis is to study cells for long life applications.

## 2.3 Electrolytes

In addition to the two electrodes, the third essential component of a Li-ion cell is the electrolyte. The electrolyte is comprised of a lithium salt dissolved in some mixture of solvents. The most common lithium salt used is lithium hexafluorophosphate ( $\text{LiPF}_6$ ). A 1 molar concentration of salt is typically present in the electrolyte. Lithium hexafluorophosphate is the most common salt due to its high conductivity ( $10^{-2}$  S/cm), lithium ion transference number ( $\sim 0.35$ ) [1] and low corrosion of the aluminum current collector at high potentials relative to other salts [34]. One concern about the use of  $\text{LiPF}_6$  is the reactivity with any trace water in the electrolyte to form hydrofluoric acid [35] which will be discussed further in Chapter 6.







2.3

Various other lithium salts have been studied for use in Li-ion cells including lithium tetrafluoroborate ( $\text{LiBF}_4$ ), lithium perchlorate ( $\text{LiClO}_4$ ), lithium bis(oxalato)borate ( $\text{LiBOB}$ ) and lithium (bis) trifluoromethanesulfonimide ( $(\text{LiN}(\text{SO}_2\text{CF}_3)_2$  referred to as HQ-115) [34,36,37].

The solvent systems used in Li-ion cells are typically comprised of carbonates such as ethylene carbonate (EC), ethyl methyl carbonate (EMC), diethyl carbonate (DEC), propylene carbonate (PC) and dimethyl carbonate (DMC) [35,38]. Figure 2.3 shows the structure of some of these common carbonates. These carbonates allow for high concentrations ( $> 1$  molar) of lithium salts to be dissolved and serve as good electrolytes. Typically the electrolyte solvent is a mixture of these and/or other solvents; two common blends of solvents used are EC:EMC (3:7 wt.) and EC:DEC (1:2: wt.). Other non-carbonate solvents such esters [39] and methyl butyrate [40] have been studied for special purpose applications such as wide operation temperature window or high power cells.

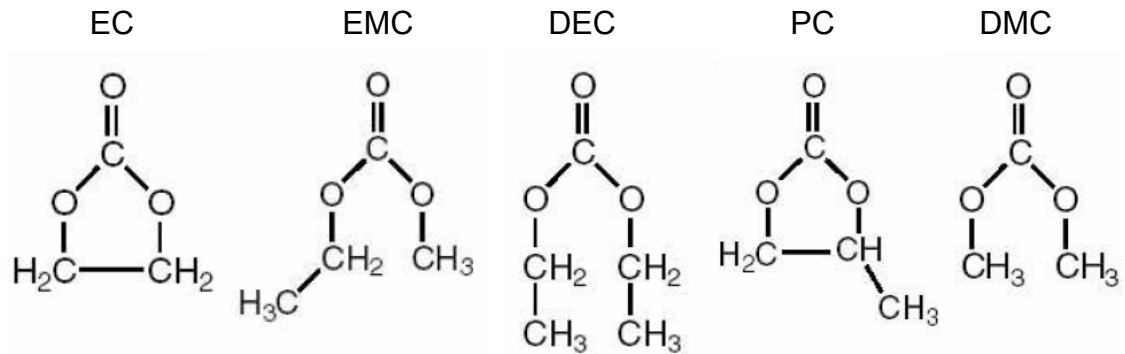


Figure 2.3 The structure of commonly used carbonates as solvents for electrolyte in Li-ion cells.

In addition to the salt and solvent used in electrolytes for Li-ion cells, different electrolyte additives are used to provide benefit for some performance metrics [35]. These additives are typically used in the 0.1 – 10 wt% range in the electrolyte. While many Li-ion cell manufacturers use the same electrode materials (i.e.  $\text{LiCoO}_2$  and graphite) the performance of their cells can vary greatly based on their choice of

electrolyte additives. Electrolyte additives can be used to extend lifetime [35,41–44], decrease cell impedance [45–50], limit gas generation during cycling [51–54] or to improve the safety of cells [55–61]. The impact of electrolyte additives can be quantified in many ways including electrochemically through cell cycling or electrochemical impedance spectroscopy (EIS). Other characterization of cell performance can be done by measuring gas generation through cell volume changes or by fundamental safety studies using accelerating rate calorimetry (ARC) or differential scanning calorimetry (DSC) [46,55,62–65]. The impact to the cell chemistry has been best studied through post mortem analysis of the surface films with techniques such as x-ray photoelectron spectroscopy (XPS) [66–70], scanning electron microscopy (SEM) [66,67,70,71], tunneling electron microscopy (TEM) [66,72–75], or fourier transform infrared spectroscopy (FTIR) [66,67,76–79].

One of the most commonly studied electrolyte additives is vinylene carbonate (VC) which is used to improve the lifetime of cells [80]. Its impact on the surface film between the graphite electrode and electrolyte known as the solid electrolyte interphase (SEI) (to be discussed in more detail in the next section) has been studied extensively [81–83] and benefits of the additive to the performance of the positive electrode have also been shown [82,84]. Other carbonates have also been studied as electrolyte additives such as vinyl ethylene carbonate (VEC) [77,85–88] and fluoroethylene carbonate (FEC) [89–93]. Many non-carbonate based electrolyte additives have also been studied and found to be beneficial for certain cell types. Additives such as tris(pentafluorophenyl) borane (TDFPB) [94], lithium difluoro(oxalate)borate (LiDFOB) [41], tris(hexafluoro-iso-propyl)phosphate (HFiP) [95] and many others have been shown to improve cycling performance in different types of cells.

Improvements to safety can be achieved by lowering the reactivity between the electrodes and electrolyte, by using additives that prevent overcharging of cells or through the use of flame retardant additives. Measurements on the reactivity of the electrode/electrolyte pairing are typically done using ARC or DSC with the positive electrode fully delithiated or the negative electrode fully lithiated to correspond to the charged state in a full cell [64]. Varying the choice of lithium salt (or using that lithium salt as an additive) can affect the safety characteristics just as the use of electrolyte

additives can. Jiang and Dahn [96] studied  $\text{LiPF}_6$  and  $\text{LiBOB}$ -based electrolytes with  $\text{LiCoO}_2$  and  $\text{Li}[\text{Ni}_{0.1}\text{Co}_{0.8}\text{Mn}_{0.1}]\text{O}_2$  and  $\text{LiFePO}_4$  positive electrodes. These studies showed that the thermal stability of the  $\text{LiPF}_6$ -containing electrolyte was better for the  $\text{LiCoO}_2$  and NMC positive electrodes but the  $\text{LiBOB}$  electrolyte was better for  $\text{LiFePO}_4$ . This also highlights that the choice of electrolytes for optimal safety (or performance) is highly dependent on the choice of electrodes. Examples of additives that have been claimed to improve safety include the use of 4-isopropyl phenyl diphenyl phosphate with  $\text{LiCoO}_2$  electrodes [97] and thiophene in  $\text{LiCoO}_2/\text{graphite}$  cells [46].

Additives can be used to prevent overcharging cells through shuttling charge within the cell or by polymerizing on the positive electrode surface to prevent further lithium deintercalation. Shuttle molecules such as 2,5-ditertbutyl-1,4-dimethoxybenzene [98] and dimethoxybenzene derivatives [99] have been reported to prevent further charging of cells by being reversibly oxidized and reduced once the positive electrode reaches the oxidation potential of the molecule. 2,4-ditertbutyl-1,4-dimethoxybenzene was shown to have very good performance in  $\text{LiFePO}_4/\text{LTO}$  cells and could prevent the cell from reaching both overcharged and overdischarged conditions. Additives that prevent overcharge through polymerization on the positive electrode include cyclohexyl benzene [58,100,101], tri( $\beta$ -chloromethyl) phosphate (TCEP) [58], biphenyl [60,61,101,102], diphenyl [103] and fluorobenzene [104]. Cyclohexyl benzene, for example, decomposes at 4.7 V vs.  $\text{Li}/\text{Li}^+$  and therefore can be used to prevent the positive electrode delithiating beyond that potential. TCEP oxidizes at a slightly higher potential, 4.75 V vs.  $\text{Li}/\text{Li}^+$ , but interestingly the oxidation potential of both additives decreases with increased cell temperature. Therefore these additives would provide greater overcharge protection at elevated temperature during which cell safety is a greater concern due to reactivity between the electrodes and electrolyte.

Other electrolyte additives can be used as flame retardants to prevent fire in such a failure of a cell. One example of such an additive is allyl tris(2,2,2-trifluoroethyl) carbonate (ATFEC) [56]. Large concentrations (up to 30 vol%) of ATFEC in 1 M  $\text{LiPF}_6$  in EC:DMC electrolyte showed increasing thermal stability. There was little to no adverse impact seen in the cycling performance of  $\text{LiCoO}_2/\text{graphite}$  cells when used up to 30 vol% but concentrations of 15 vol% were recommended as the electrolyte

conductivity begins decreasing at very high concentrations. Another flame retardant additive reported is triphenylphosphate (TPP) [57]. Adding 3% TPP to 1 M  $\text{LiPF}_6$  in EC:DEC electrolyte in NMC/graphite cells showed improved safety with minimal increase in cell impedance. Higher concentrations resulted in large impedance and therefore a decrease in achievable capacity at high rates. Many of the additives for safety compromise cycling or other performance metrics and therefore are used only at low levels to balance both the performance and safety of commercial cells.

## 2.4 Electrochemical Behavior

Li-ion cells can be made in numerous formats all using the same basic operation principles. One main distinction between cell formats is how the positive and negative electrodes are positioned relative to each other. Typically cells are made with layers of electrodes stacked on top of each other (with a layer of separator between each layer of electrodes) or with an electrode stack wound to fit in either a cylindrical or prismatic case. Another main distinction between cell formats is the enclosure containing the electrodes. Cell enclosures are typically either metal (giving a rigid cylindrical, coin-shaped or prismatic enclosure) or made of a soft pouch material. Figure 2.4 shows a schematic of a cylindrically wound cell. The most common size is referred to as an 18650 (18 mm diameter and 65 mm in length) where the layered electrode stack can be seen as it is wound around a central pin to hold the shape. The wound electrode stack is referred to as a “jelly roll”. As in a cylindrically wound cell, a prismatically wound cell has a similar electrode stack but is wound differently. This format allows for thinner format cells as are required in cell phones and tablets. The same prismatic jelly roll can be put in a pouch or hard-cased enclosure depending on the application.

Figure 2.5 shows a schematic coin cell assembly. A coin cell is a form of stacked electrode cell with only one layer of each electrode. A spring and spacer are included in the design of a coin cell to ensure that the two electrodes are in good contact with both the metal casings as electrical connections and the separator. Coin cells are the most common cell format for small-scale research as the winding process for electrodes

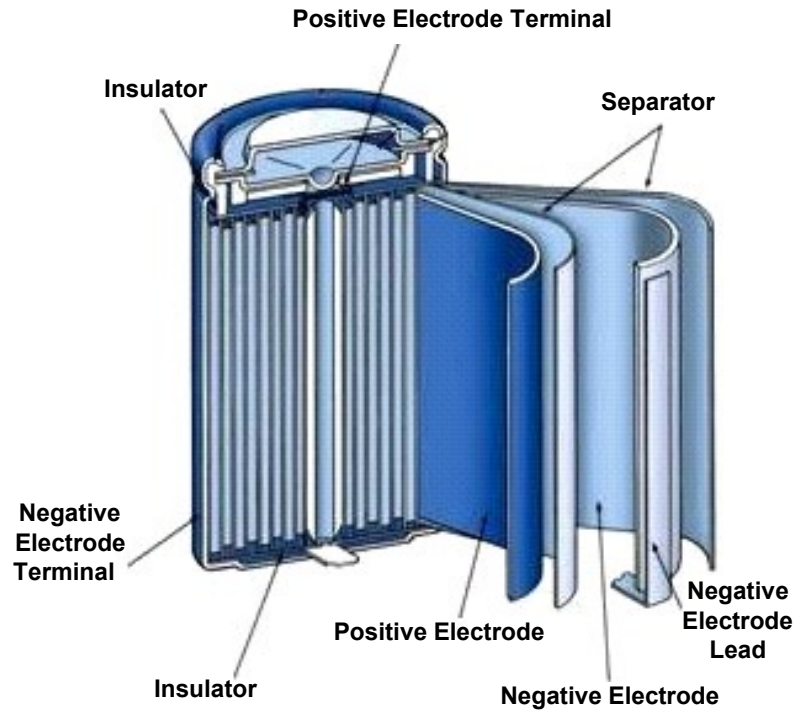


Figure 2.4 Schematic of a cylindrically wound cell.

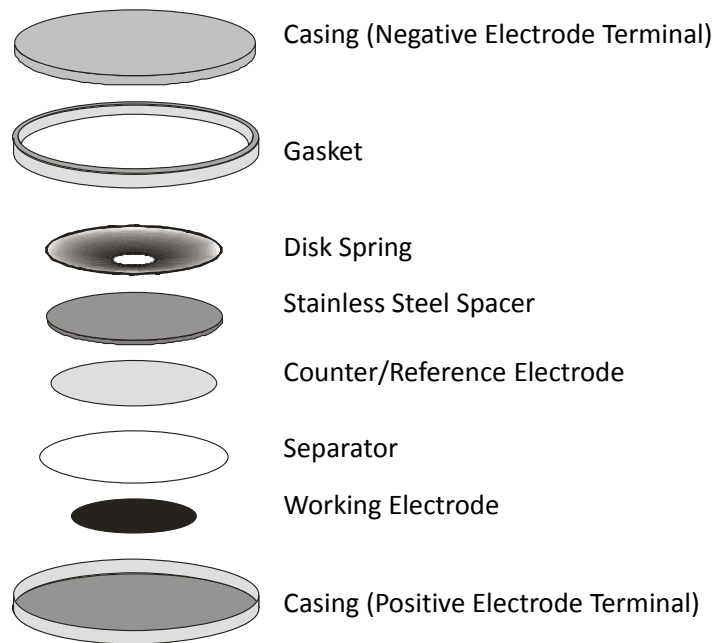


Figure 2.5 Schematic of coin cell parts and coin cell assembly.

requires additional equipment, as well as material, to make wound cells. Often coin cells are made with a lithium metal electrode which acts as both a reference and counter electrode in order to study the behavior of a single electrode material. This type of cell is referred to as a “half cell”. If a cell is made with two electrode materials that are not lithium metal it is referred to as a “full cell”. This thesis will present work from all of these style cells where the coin cells were made in-house but other cells were manufactured elsewhere.

Numerous electrode materials were mentioned in the previous section and different electrode potentials and specific capacities were given for each. The potential of an electrode material presented is an average potential during lithiation/delithiation process to a certain lithium content. The electrode potential typically varies with lithium content. Figure 2.6 shows the electrode potential versus specific capacity during a single delithiation/lithiation (charge/discharge) process of several of these common electrode materials (most of which were studied in this thesis). In order to achieve the highest energy density, a combination of both high capacity and high operating potential versus  $\text{Li}/\text{Li}^+$  (for positive electrodes, or low operating potential versus  $\text{Li}/\text{Li}^+$  for negative electrodes) is desirable. When measuring the capacity (Q) of a material it is typically made in a half cell configuration and a known current flow (I) is applied to the cell until the desired potential is reached. This allows the capacity (subscripted for charge or discharge) of the electrode to be measured and the specific capacity (q) of the material to be calculated using the active mass (m) (simplified if current is constant).

$$Q_{C/D} = \int I_{C/D}(t) * dt = I_{C/D} * t \quad 2.4$$

$$q_{C/D} = \frac{Q_{C/D}}{m_{active}} \quad 2.5$$

Figure 2.6 shows the potential versus capacity profiles for several common positive and negative electrode materials. Some materials do not show any potential change during part of charging process. This is due to the lithium intercalation process into the material which leads to the formation of a two phase material (one lithium rich and one lithium deficient) which stays at an equilibrium potential as one phase converts

to the other on during charge or discharge. This occurs in graphite through multiple phase transitions and in LTO through a single phase transition between the fully charged and discharged state. In a full cell, the cell voltage is derived from the difference between the positive and negative electrode potentials at the given state of charge. Therefore, for a negative electrode material, it is desirable to have a low potential vs.  $\text{Li}/\text{Li}^+$  and high specific capacity to achieve a high energy density full cell. For example, if a manufacturer chooses to make a cell with a  $\text{LiCoO}_2$  positive electrode and a graphite negative electrode, the average cell voltage will be  $\sim 3.8$  V. However, if the graphite negative electrode was replaced with an LTO electrode, the full cell voltage would drop to  $\sim 2.4$  V and the cell would store less energy for the same mass or volume of electrode materials (there would also be a loss in specific capacity due to the lower specific capacity of LTO compared to graphite).

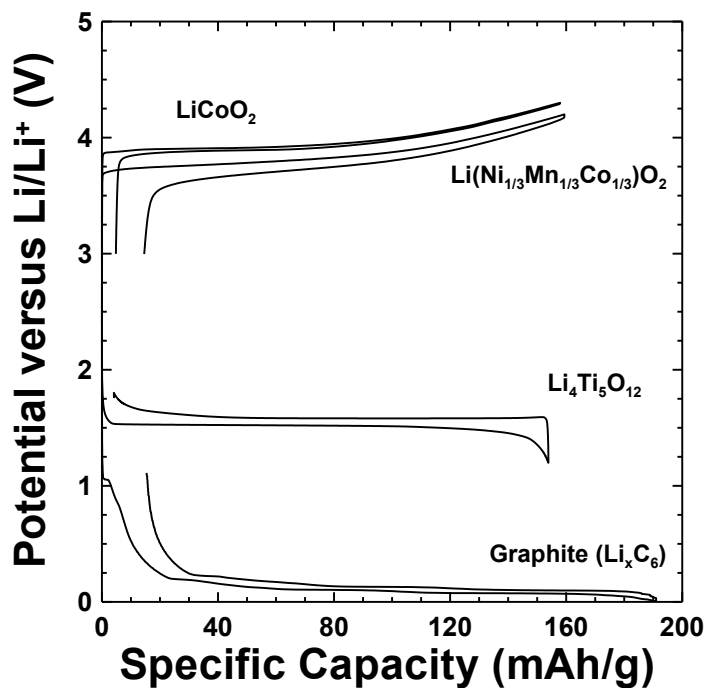


Figure 2.6 The potential versus specific capacity for four common positive and negative electrode materials. Note that the capacity axis for the graphite electrode has been divided by two for ease of viewing.

Figure 2.7 shows the potential versus specific capacity for a  $\text{LiCoO}_2$  electrode (panel a) and a graphite electrode (panel b) through the charging and discharging process.

As the electrodes are cycled through the first cycle, there is a large discrepancy between the capacity achieved during the first delithiation (discussion will be in terms of the positive electrode but is analogous for the negative electrode by exchanging delithiation for lithiation) and the capacity in the subsequent lithiation. This is due to reactions between the electrode material and the electrolyte and is referred to as (first cycle) irreversible capacity. The reaction between the electrode and electrolyte continues during subsequent cycles which causes each lithiation to be shorter than the previous delithiation.

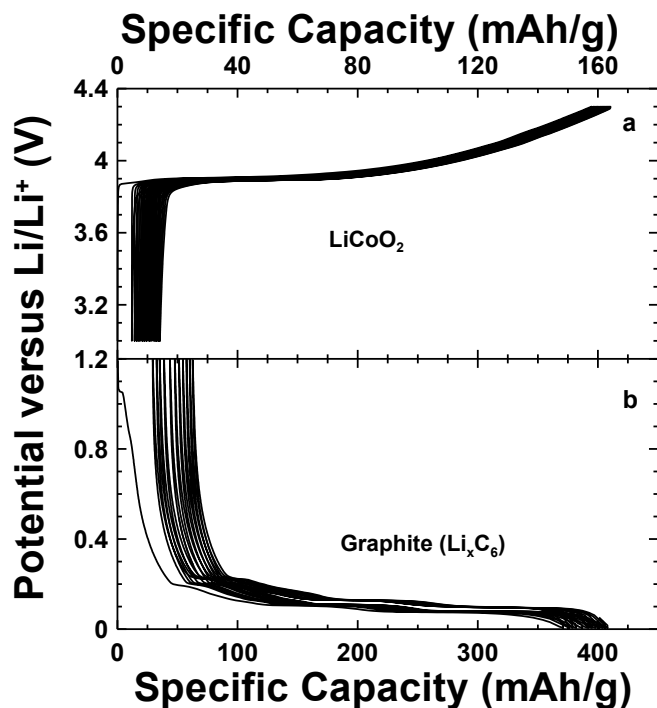


Figure 2.7 Panel a) shows the potential versus specific capacity for an LCO electrode half cell cycled between 3.0 and 4.3 V. Panel b) shows the potential versus specific capacity for a graphite electrode cycled between 0.005 and 1.2 V.

The reaction between the electrode and electrolyte results in the formation of a surface film on the electrode. This film has been extensively studied on the graphite electrode and is referred to as the solid electrolyte interphase (SEI) [105]. The reaction of lithiated graphite with the electrolyte causes the formation of this passivation film which reduces the rate of further electrolyte decomposition. The SEI on a graphite electrode contains organic and inorganic species such as Li<sub>2</sub>O, LiF, Li<sub>2</sub>CO<sub>3</sub>, polyolefins and semicarbontes [106]. The SEI is essential to the operation of Li-ion cells as it passivates against future reactions between the lithiated graphite and electrolyte. Without such a



film, the continual reaction would prevent the lithiation of graphite and a Li-ion cell could not operate. An analogous layer is formed on the positive electrode and referred to as the positive electrode SEI. The inefficiency due to the reaction between the electrode and electrolyte can be quantified by the coulombic efficiency (CE) of a positive electrode half cell which is the ratio of the discharge capacity ( $Q_D$ ) to the previous charge capacity ( $Q_C$ ), while for a negative electrode half cell the CE is the ratio of charge to discharge capacity, which is always less than 1.0000. Due to the coulombic efficiency being less than 1.0000, the electrodes appear to “slip” to high absolute capacities in the potential versus capacity plots. The rate of this slippage corresponds to the rate of the side reactions between the electrode and electrolyte that are not associated with lithium intercalation/deintercalation.

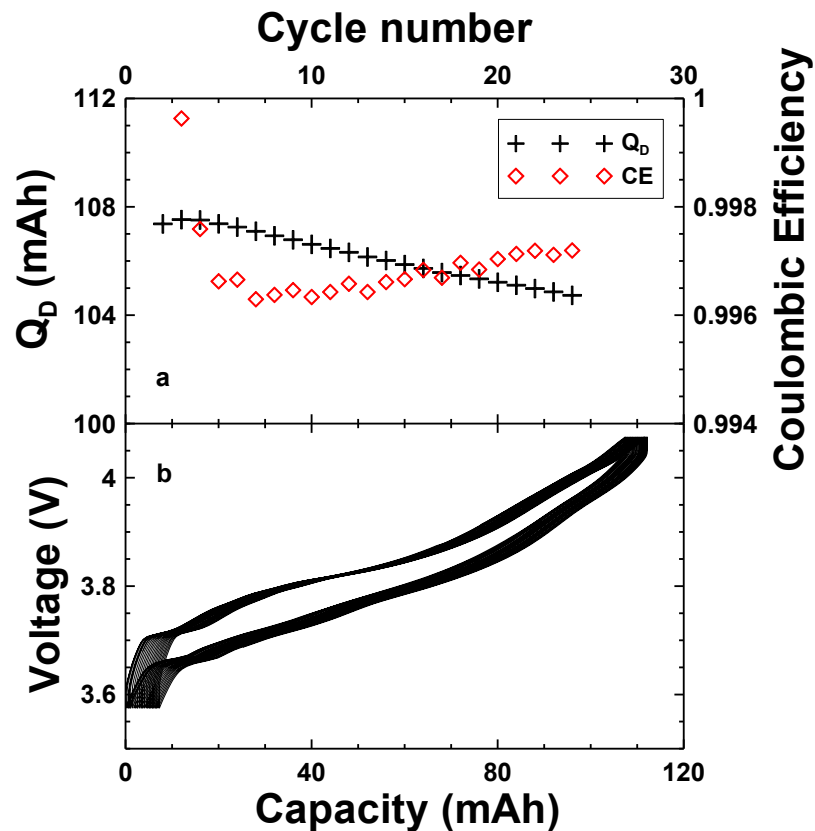


Figure 2.8 Panel a) shows the discharge capacity (left) and coulombic efficiency (right) versus cycle number. Panel b) shows the voltage versus capacity for 24 cycles of a LiCoO<sub>2</sub>/graphite cell cycled at C/10 rate at 40°C.

When constructing a full cell, these reactions between the electrode and electrolyte still occur and therefore there is still a first cycle irreversible capacity loss and continual slippage of the full cell voltage versus capacity curve to higher absolute capacities. Figure 2.8 shows the voltage curve of a  $\text{LiCoO}_2/\text{graphite}$  cell (panel b) along with the discharge capacity and coulombic efficiency (panel a) versus cycle number. Since the voltage of the full cell comes from the difference between the potentials of the positive and negative electrodes at the given state of charge, the features seen in both the positive and negative electrodes can be seen in the full cell. These features evolve over cycle number based on the different rates of slippage of the positive and negative electrodes due to the difference in reaction rates between the electrode and electrolyte at the positive and negative electrodes.

The slippage of the voltage versus capacity curve of a cell due to the reactions between the electrodes and electrolyte is very important to quantify to understand cell degradation. There are many types of these parasitic reactions that can occur at both electrodes but generally speaking they take three different forms [11]: 1) reduction reactions at the negative electrode, 2) oxidation reactions at the positive electrode and 3) “shuttle” type reactions in which an oxidation or reduction occurs and that oxidized or reduced species migrates to the other electrode and is subsequently reduced or oxidized. The bulk of these reactions involve reduction of the solvent molecules at the low potential of the graphite surface. Analogously, solvent molecules can be oxidized at the high potential of the positive electrode. This is one of the main issues surrounding the concept of the 5 V class of positive electrode materials, that the electrolyte is not stable to such a high potential is continually oxidized and degrades the cell.

The slippage occurs because of electron transfer at the electrode that is related to the side (or parasitic) reaction that is occurring and that is not associated with the lithium intercalation/deintercalation process occurring due to charging or discharge the cell. For example, if a solvent molecule is reduced at the negative electrode, an electron is transferred from the material therefore leaving a  $\text{Li}^+$  without an associated electron and an additional negative charge present in the electrolyte. Due to charge neutrality that must be maintained, the  $\text{Li}^+$  is therefore removed from the material and typically reacts to form a solid by-product on the surface of the electrode. This means that there is an

additional site for lithium intercalation after this process and thus the process has contributed to the delithiation of the negative electrode. If this reaction occurs during the lithiation of the graphite (charge of a full cell), then it will take more electron transfer through the external circuit (and associated  $\text{Li}^+$  transfer through the electrolyte) than should be required based on the specific capacity of the material because some of the charge is being “lost” to this side reaction. During the discharge of the full cell, electrolyte reduction contributes to the delithiation of the electrode and therefore the cell is discharged with less electron transfer through the external circuit than should be required. This process results in the slippage of the electrode to higher capacity and analogously occurs at the positive electrode with oxidation processes.

Quantifying the rate of slippage of the voltage curve therefore gives an indication of the rate at which these parasitic reactions occur within the cell. These parasitic reactions lead to cell degradation and eventual cell failure through numerous mechanisms including impedance rises on the electrodes due to the surface films, loss of electrolyte as the solvent is oxidized or reduced and “lithium inventory loss”. Lithium inventory loss [11] refers to the inability to access all of the lithium atoms within the cell due to the imbalance in parasitic reactions between the positive and negative electrodes. Figure 2.9 illustrates this loss of accessible capacity by showing a schematic of a positive and negative electrode potential curve along with a full cell voltage curve (calculated from the difference between the potentials of the positive and negative electrodes at a given state of charge) in an early cycle and later cycle. In the early cycles of a cell (shown in solid lines), the difference in capacity between when the negative electrode becomes fully delithiated (causing the cell voltage to drop rapidly and reach the discharge voltage limit) and when the positive electrode would be fully lithiated may be 10% due to the first cycle irreversible capacity loss. During subsequent cycles both the positive and negative electrodes slip to higher absolute capacity (or state of charge) but at different rates (later cycle shown in dashed lines). If the reactions at the negative electrode cause greater slippage than at the positive electrode the difference between the negative electrode delithiation and positive electrode lithiation will increase causing a decrease in capacity storage during each charge/discharge cycle.

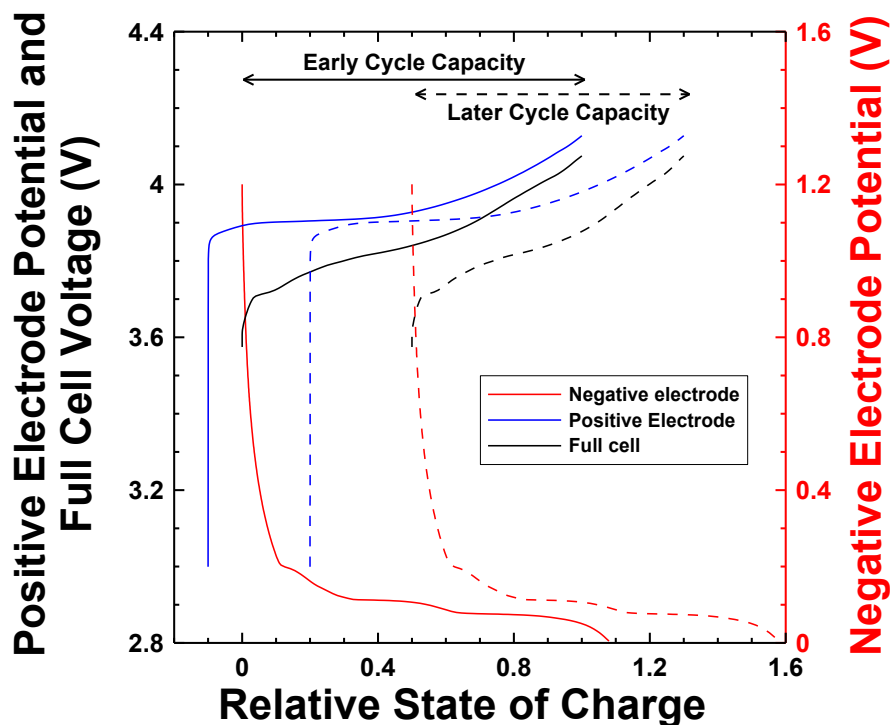


Figure 2.9 Schematic showing the potential versus capacity curves for a positive and negative electrode along with the voltage versus capacity for the full cell. The solid lines represent an early cycle illustration and the dashed lines represent a later cycle where electrode slippage has led to loss of lithium inventory.

Figure 2.9 shows how in a cell with a graphite negative electrode, the discharge capacity endpoint is controlled by the capacity at which the negative electrode becomes fully delithiated. The top of charge endpoint is determined from the positive electrode reaching a certain potential because the potential of the negative electrode is constant due to a two phase intercalation reaction of the graphite electrode at a high state of charge. Therefore, measuring the charge and discharge capacity endpoints can give insight into the reaction rates at the positive and negative electrodes. If differences can be detected in the slippage rates and coulombic efficiency of cells in the early cycles, it should give an indication in the stability of the chemistry within that cell and the rate of degradation. Cells with lower slippage rates and higher coulombic efficiencies should, therefore, have longer cycle lives and this should give a method of detecting cell performance in shorter experiments without having to cycle cells until failure. However, the performance of well-made Li-ion cells has reached a state where these inefficiencies are very small and

in order to measure them accurately, very accurate battery charging equipment must be used to ensure that measurements made are indicative of the cell performance and not influenced by errors and inaccuracies present in the testing equipment. This premise sparked the concept of high precision coulometry which is discussed in great detail in previous work [10,107] and will be reviewed in the next chapter.

## Chapter 3      Background on Experimental Techniques

### 3.1 High Precision Coulometry

As discussed in the previous chapter, cell failure due to parasitic reactions should be detectable in the early cycles with accurate measurements of the coulombic efficiency and capacity endpoint slippages. However, due to the very low reaction rates in well-made Li-ion cells, the ability to measure the slippage rates and coulombic efficiency are susceptible to inaccuracies introduced by the testing equipment. In 2010, Smith *et al.* [10] introduced a custom built battery testing system constructed of precision current sources and voltmeters made by Keithley Instruments that was able to measure the coulombic efficiency to an accuracy of 100 ppm. Figure 3.1 shows a photograph of the 60-channel, 100 mA maximum current, High Precision Charger (HPC) system constructed in Dr. Jeff Dahn's lab including the charging electronics and thermostats for cells. Maintaining constant cell temperature is important in minimizing measurement errors [10]. This system is comprised of Keithley 220, 224 and 6220 current sources along with Keithley 2000 6½ digital multimeters (used for voltage measurements).

In 2013, Bond *et al.* [108] showed how improvements could be made to the system design to further reduce noise and inaccuracy in measurements of the coulombic efficiency. Bond also characterized a commercially available battery testing system made by Maccor to show the inaccuracy and noise in the system to be significantly worse (over an order of magnitude in inaccuracy) and therefore could not be used to make precision measurements of the coulombic efficiency in attempts to compare cell lifetime in short term experiments. Figure 3.2 is taken from Bond's work and shows how the upgraded Ultra High Precision Charger (UHPC) outperforms the High Precision Charger. The difference between the systems is that the High Precision Charger relied on the accuracy of the Keithley current sources to be absolute and did not monitor the current flow and therefore simply calculated capacity using multiplication of current and time (see Equation 2.2). The UHPC included well characterized and thermally controlled precision resistors (0.01% tolerance, 0.2 ppm/°C) in series with the current output and

cell. The voltage drop across the resistor is then monitored with an additional voltmeter allowing for more accurate capacity calculations using an integral (see Equation 2.2). A different resistor is automatically switched in for every decade of current to improve measurement resolution of the voltmeter. Figure 3.3 shows the 100-channel, 3 A maximum current, UHPC system built in Dr. Dahn's lab. This system is comprised of Keithley 2602B current/voltage sources and Keithley 2002 8½ digit multimeters (used for voltage measurements at 7½ digits for better timing resolution).

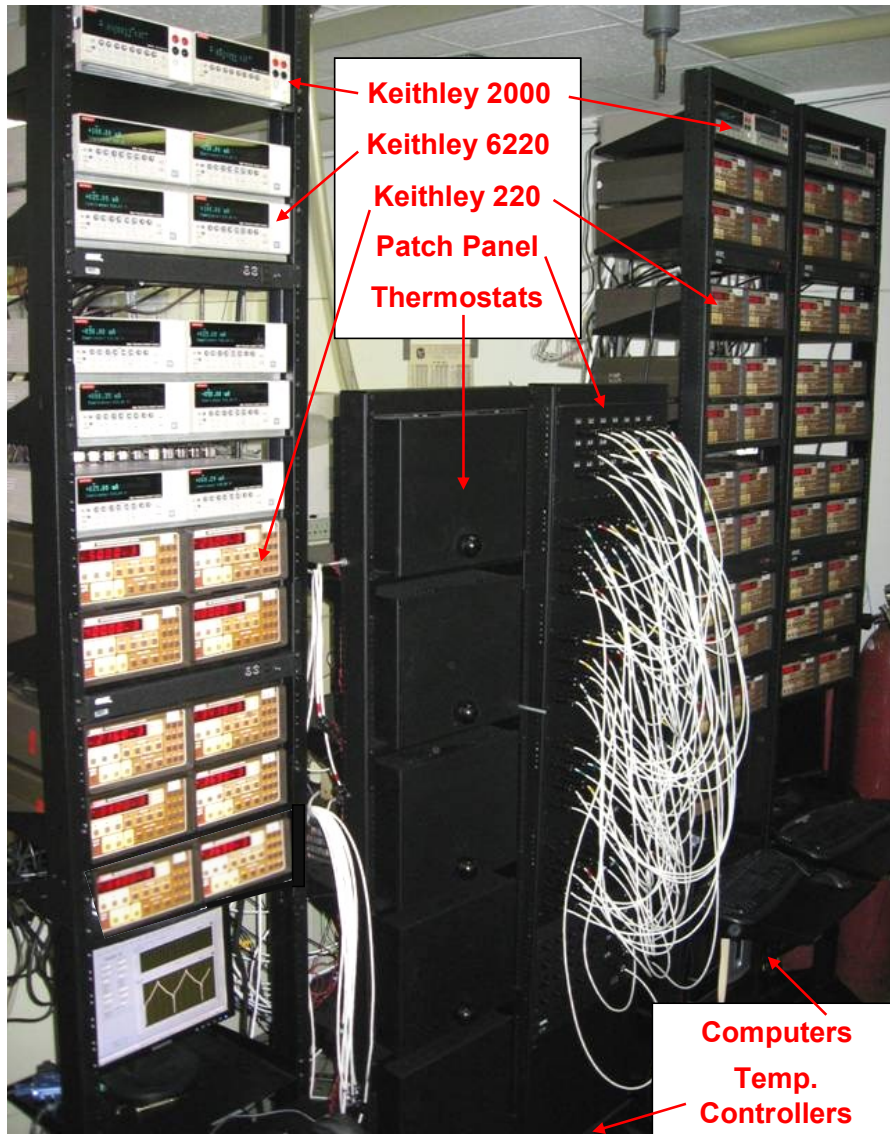


Figure 3.1 Photograph of the 60-channel HPC system at Dalhousie University.

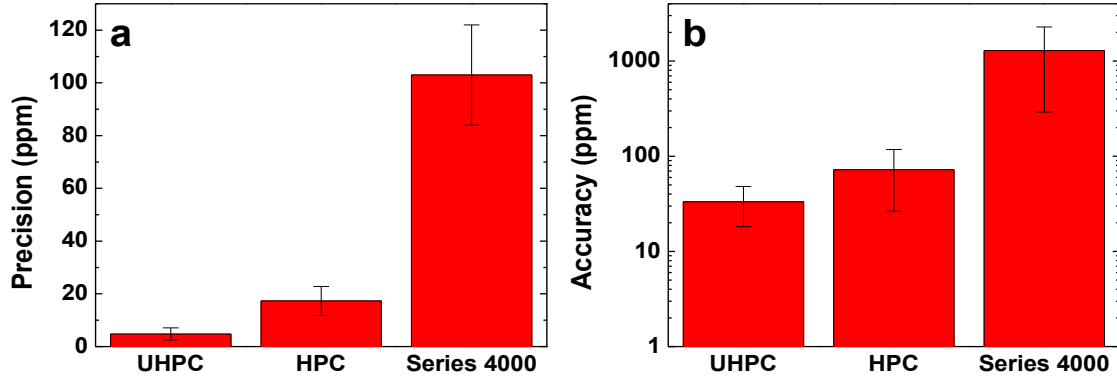


Figure 3.2 A comparison of the precision (or noise) (panel a) and accuracy (panel b) of coulombic efficiency measurements made with a Maccor 4000 series charger, the HPC and the UHPC measured in parts per million. Reproduced by permission of The Electrochemical Society [108].

In addition to the coulombic efficiency, both the charge and discharge endpoint capacities can be accurately monitored to compare the parasitic reaction rates between different cells. The charge endpoint capacity versus cycle number is plotted by taking the absolute capacity when the cell reaches the upper cutoff voltage each cycle and plotting that versus cycle number. As the voltage curve slips to higher capacity, so does the charge endpoint capacity. The rate of change of the charge endpoint capacity versus cycle number (which could also be plotted versus time) is referred to as charge endpoint slippage ( $\Delta_C$ ). Discharge endpoint capacity versus cycle number is found the same way by using the capacity at which the cell reaches the discharge voltage limit. However, the discharge endpoint slippage ( $\Delta_D$ ) is typically not discussed as it is mathematically related to the coulombic efficiency as seen below [11]

$$CE = \frac{Q_D}{Q_C} = \frac{Q_C - \Delta_D}{Q_C} = 1 - \frac{\Delta_D}{Q_C} \quad 3.1$$

The HPC and UHPC were used extensively in the work presented in this thesis in order to help compare the predicted cycle life of cells in short term experiments as well as understand how changes to the electrolyte or cell chemistry affect the short term parameters and anticipated lifetime.





Figure 3.3 Photo of the 100-channel UHPC system at Dalhousie University.

### *3.1a Symmetric Cells*

When examining a single electrode's performance in a half cell, the coulombic efficiency can be used as a metric for the stability of that system (electrode material and electrolyte) under the given conditions (voltage, temperature, cycling rate, etc.). However, due to high cost associated with building high precision charger systems relative to tradition charger systems there would ideally be a way to assess the performance using traditional charger systems. One way this can be done is through the use of symmetric cells [109]. Symmetric cells are assembled such that both the positive and negative electrodes are the same electrode material. One electrode must be lithiated

and the other delithiated in order to allow for lithium transfer. This leads to a cell with an average voltage of 0 V which therefore stores no energy but can be a useful tool for understanding electrode performance. While symmetric cells had not been used extensively in lithium-ion battery research [110], the technique has been used for studies of electrode impedance using impedance spectroscopy [47].

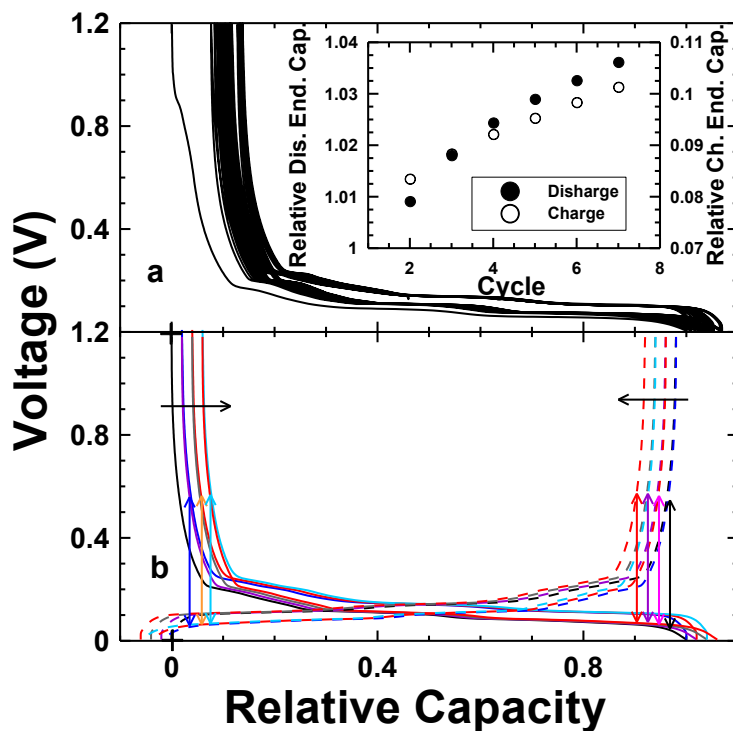


Figure 3.4 Panel a) shows the voltage versus relative capacity (0 - 1) of a graphite half cell along with the charge and discharge endpoint capacities versus cycle number (insert). Panel b) shows a schematic of how slippage of electrodes should occur in a symmetric cell leading to capacity loss. Different colors in panel b) indicate different subsequent half cycles. Reproduced by permission of The Electrochemical Society [109].

Since both electrodes of a symmetric cell are the same material, the rate of reactions between the electrode and electrolyte will be the same at either electrode, causing equal electrode slippage. Figure 3.4 shows a schematic of a graphite/graphite symmetric cell showing the two electrode potential curves and their direction of slippage as each electrode will slip in the direction of its lithiation. This leads to a cell that loses capacity at a rate based on the electrode slippage which is related to the coulombic efficiency of the electrode material. Therefore, unlike with a standard Li-ion cell design

with different positive and negative electrode materials, the coulombic efficiency can be calculated directly from the capacity loss rate (or fade with units of %/cycle).

$$CE = 1 - \frac{Fade}{2} \quad 3.2$$

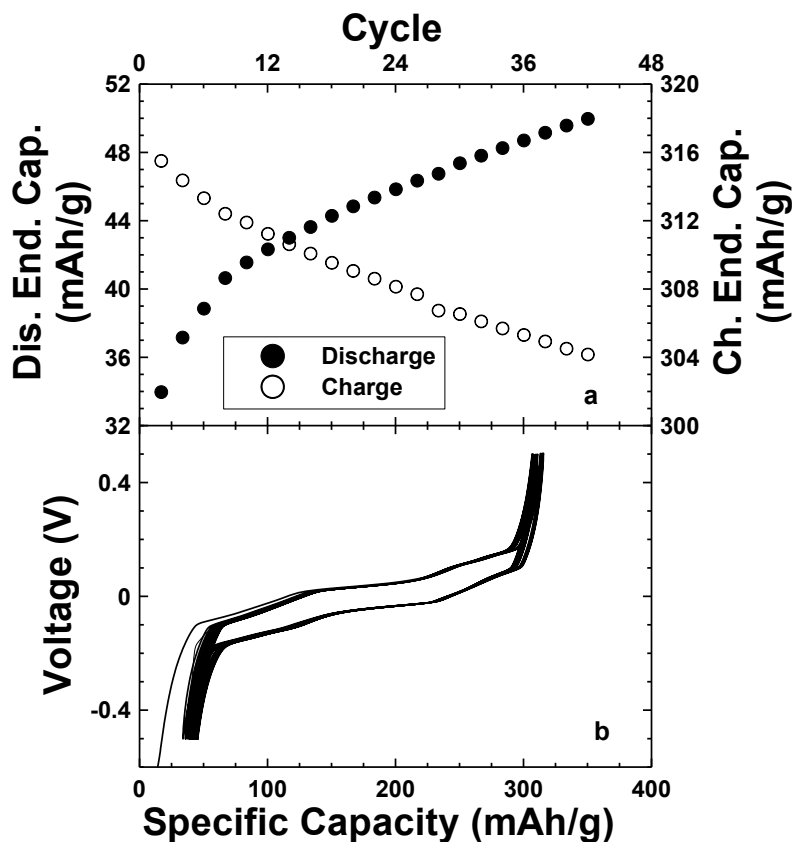


Figure 3.5 Panel a) shows the discharge (left) and charge (right) endpoint capacities versus cycle number for a graphite symmetric cell. Panel b) shows the voltage versus specific capacity for the same graphite symmetric cell. Reproduced by permission of The Electrochemical Society [109].

In order to confirm these predictions, graphite/graphite symmetric cells were assembled and run on the high precision charger system in order to measure the endpoint slippage rates and verify that they are equal and opposite and compare the actual measured coulombic efficiency to that calculated from the fade rate. Figure 3.5 shows the charge and discharge capacity endpoint capacities (panel a) versus cycle number and the voltage versus capacity curve (panel b) of a graphite/graphite symmetric cell. The slippage (slope of the capacity endpoint versus cycle curve) rates of the charge and

discharge endpoints are exactly equal and opposite which indicates that the reaction rates between the electrodes and electrolyte are equal as expected since they are the same material. Figure 3.6 shows a zoom in of the coulombic efficiency along with capacity over a given cycle range (cycles 30 - 44). The capacity loss versus cycle number curve can be fit very well with a linear fit which gives a fade rate that can be used in Equation 3.2 to calculate the coulombic efficiency. For this cycle range the coulombic efficiency is calculated to be  $0.99918 \pm 0.00050$  which agrees exactly with the measured values from the high precision charger (average over those cycles:  $0.99918 \pm 0.00020$ ). This shows that through the use of symmetric cells, traditional charger systems (which are adequate for measuring fade rates) can be used to assess the performance of electrode materials using the calculated coulombic efficiency without the use of a high precision charger system.

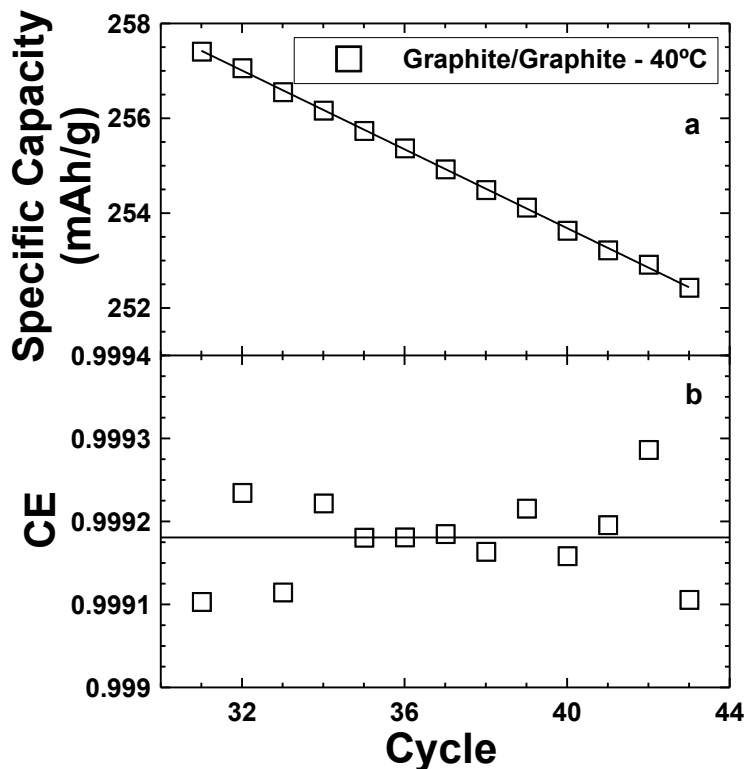


Figure 3.6 Panel a) shows the specific capacity versus cycle number for a graphite symmetric cell with a linear fit to calculate fade rate. Panel b) shows the measured coulombic efficiency of the graphite symmetric cell along with the calculated coulombic efficiency (line) using the fit from panel a) and Equation 3.2. Reproduced by permission of The Electrochemical Society [109].

Symmetric cells are very useful in understanding the interactions between a given electrode material and the electrolyte. However, in Li-ion cells there can be interactions between the positive and negative electrodes that can impact the cell performance [11]. These cannot happen in symmetric cells as there are not electrodes at both oxidation and reduction potentials. Since symmetric cells cannot capture this type of interaction, full cells must always be tested to validate the performance of an electrode for use in Li-ion cells.

All work showing the relationship between symmetric cell fade and coulombic efficiency was done by the author.

### ***3.1b Differential Voltage Analysis***

The parasitic reactions that occur at different rates on the positive and negative electrodes within a Li-ion cell cause unequal slippage of the two electrodes and therefore lead to a loss of lithium inventory as seen in Figure 2.9. However, there are also potential reasons for capacity loss that involve mechanical damage to the electrodes or impedance rises in the cell that can occur during long term cycling of cells. If a cell is cycled for its entire lifetime on a high precision charger system, the contributions to capacity loss from these three causes can be differentiated through the use of the charge and discharge endpoint data collected. Differential voltage analysis allows for cells that have been cycled (or aged) in any way to then be analyzed to determine how much of the capacity loss can be attributed to loss of lithium inventory compared to loss of active material (due to, for example, damage to the electrode material over time) [111,112]. There are only four parameters in differential voltage analysis [113]: positive electrode mass, positive electrode slippage (relative to zero being the full Li-ion cell in the discharged state), negative electrode active mass and negative electrode slippage. Therefore the active electrode masses can be compared between an early cycle and a later cycle to understand the extent of electrode damage.

Many Li-ion electrode materials show various features in the voltage versus capacity curves that come from the thermodynamics of lithium insertion into the electrode. The features from both the positive and negative electrode contribute to the

features seen in the full Li-ion cell and therefore these features can be used to assess the amount of active material in both electrodes along with the relative slippage of the positive and negative electrodes. Figure 3.7 shows the voltage and differential voltage ( $dV/dQ$ ) versus capacity curve of a full Li-ion cell (comprised of a  $\text{LiCoO}_2$  positive electrode and graphite negative electrode). Since the full cell  $dV/dQ$  comes from the  $dV/dQ$  of the individual electrodes, it can be fit if the  $dV/dQ$  versus capacity for each of the electrodes is known (which can easily be measured in a half cell). Software can be used to fit the full cell  $dV/dQ$  versus capacity and determine the contributions to capacity loss from parasitic reactions and mechanical failure of the electrodes. This is important to understand for long-life Li-ion cells if capacity loss comes from mechanical failure of the electrodes which is a cell engineering/design issue or all from reactions between the electrodes and electrolytes which may be mitigated with the use of different electrolyte formulations [88,114].

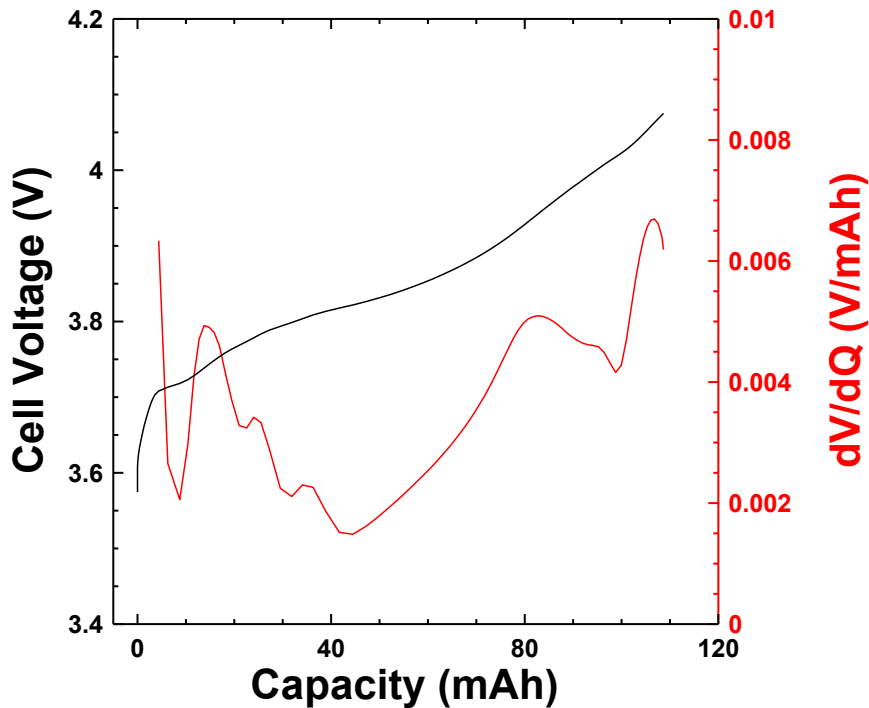


Figure 3.7 Cell voltage (black, left) and differential voltage (red, right) versus capacity for a  $\text{LiCoO}_2$ /graphite cell.

## 3.2 Cell Storage

Open circuit cell storage experiments are a simple way to compare the reaction rate of a given electrode/electrolyte combination. These experiments can occur in half cells to evaluate the performance of a single electrode or in a full cell configuration. In a full cell configuration (using a graphite negative electrode) open circuit storage measurements near the top of charge give an indication of the parasitic reaction rate at the positive electrode since at high states of charge the potential of the graphite electrode does not depend on the lithium content in the electrode because of the two-phase reaction occurring within the electrode upon insertion/removal of lithium. However, at these high states of charge the positive electrode potential does depend on the lithium content and therefore the only way the cell voltage can decrease during storage is for the lithium content of the positive electrode to change due to parasitic reactions causing a change in positive electrode potential and thus cell voltage. Figure 2.9 shows a schematic of  $\text{LiCoO}_2$  and graphite electrode potentials relative to the full cell voltage to clearly illustrate why changes in the cell voltage must come from changes to the lithium content in the positive electrode at high states of charge.

Open circuit storage measurements in a half cell are simpler since the potential of the lithium metal electrode is constant and therefore any changes in cell voltage come directly from the working electrode being studied in the cell. For electrode materials that have voltage versus capacity curves that vary with lithium content, the amount of charge transferred by parasitic reactions that have occurred can be estimated by comparing the change in cell voltage to the amount of capacity in that voltage region from the equilibrium voltage versus capacity curve. However, if the electrode material has plateaus in the voltage versus capacity curve (such as graphite), then this methodology does not work since there can be zero voltage change in the cell but a capacity change along one of the plateaus. The amount of capacity loss during storage periods however can be evaluated by cycling the cell before and after the storage periods and measuring the half cycle capacities. Sinha *et al.* [115] studied graphite electrodes through this type of storage process to evaluate the impact of different electrolyte additives on the parasitic reaction rates at the negative electrode.

This thesis will present work from simple open circuit storage experiments as well as automated cycling/storage experiments [116,117] to assess the performance of electrolyte additives in different cells using in-house built storage systems. The simple storage experiments were conducted on a system using of a Keithley 2700 scanning multimeter (to measure voltage) that is capable of measuring the voltage of 200 cells on test. The automated cycling/storage experiments were conducted using a system comprised of Keithley 220 current sources and Keithley 2000 digital multimeters (to measure voltage) [117]. The current sources are multiplexed such that the sources can be used to cycle cells while other cells are in a storage mode and only the open circuit voltage is being monitored.

### **3.3 Electrochemical Impedance Spectroscopy**

Parasitic reactions between the electrodes and electrolyte can result in a surface film forming (and evolving over time) on the electrode such as the SEI on graphite. These surface films can lead to impedance rises in the cell that decrease the ability for the cell to deliver high power and can eventually contribute to cell failure. Therefore understanding how different electrolyte formulations (or cycling conditions) affect the impedance in a cell is important for evaluating the overall performance, including lifetime, of the cells. Impedance measurements are made by sourcing a varying frequency AC voltage or current into the cell and measuring the corresponding current or voltage response. From this data the real and imaginary components of the impedance at each frequency can be calculated. In this thesis all impedance measurements were made using an AC voltage source (typically 10 mV) and measuring the current response.

The full cell impedance comes from the combinations of the positive and negative electrodes. Figure 3.8 shows a simple equivalent circuit that could represent the impedance of a lithium-ion cell. Each electrode/electrolyte interphase is modeled with a resistor in parallel with a capacitor to represent the resistance of transferring charge between the electrode and electrolyte and the capacitance due to charge build-up on the surface of the electrode and within the electrolyte forming a Helmholtz double layer. The



electrolyte can most simply be modeled with just a resistor to represent the resistance associated with moving charge through the electrolyte. These contributions are best analyzed in the form of a Bode plot where either the real or imaginary components of the impedance are plotted as a function of frequency. However, a more common way to view impedance data is in the form of a Nyquist plot where the negative imaginary component of the impedance is plotted versus the real component of the impedance. In a Nyquist plot, the sum of the resistive elements  $R_1$  and  $R_2$  in the cell can be taken as the difference between the high and low frequency intercepts with the real axis. Therefore, no extensive fitting of impedance spectra will be conducted in this work but instead just this sum of  $R_1$  and  $R_2$  will be given and referred to as the charge transfer resistance ( $R_{CT}$ ) of the full cell. Based on the values of the resistive and capacitive elements in the equivalent circuit, the semicircle could split into one semicircle for each RC element but the width of the total feature would still be the sum of  $R_1$  and  $R_2$ . Fitting of impedance spectra to quantitatively understand the contribution from each electrode is best done using symmetric cells [47]. Figure 3.9 shows the Nyquist plot for a  $\text{LiCoO}_2/\text{graphite}$  cell. As the measurement frequency varies from high to low, the data shifts towards higher real impedance values.

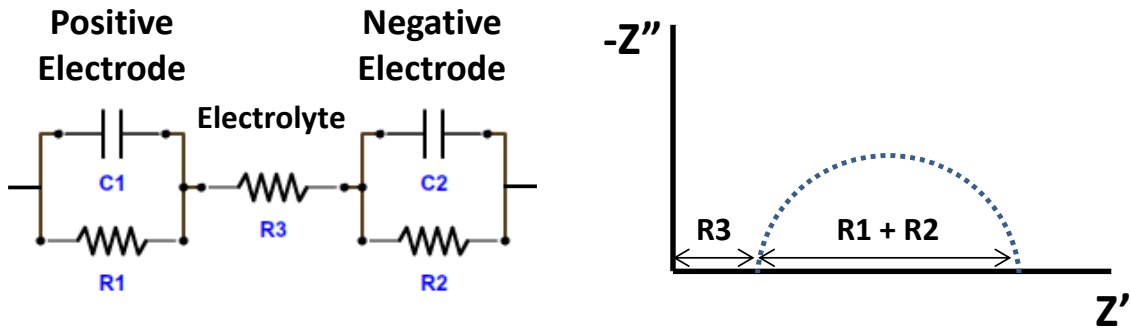


Figure 3.8 A schematic circuit (left) showing the simplest representation of a Li-ion cell with an electrode/electrolyte interphase at both electrodes represented by a parallel RC element and a purely resistive electrolyte. The resulting Nyquist plot for the left circuit is shown on the right if  $R_1 \cdot C_1 = R_2 \cdot C_2$ .

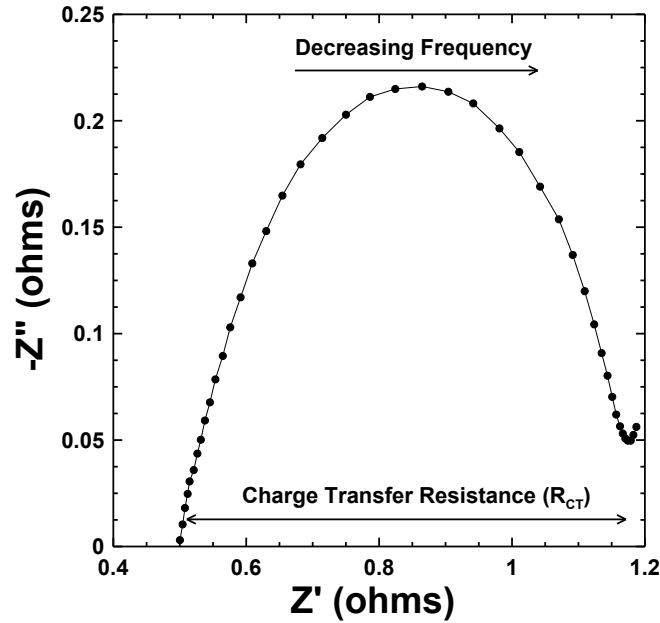


Figure 3.8 A Nyquist plot representation of the impedance spectra of a LiCoO<sub>2</sub>/graphite cell plotting the negative imaginary impedance ( $Z''$ ) versus real impedance ( $Z'$ ) measured at different frequencies.

There are different approaches to analyzing impedance spectra of Li-ion cells, many of which involve using equivalent circuits comprised of resistors and capacitors or constant phase elements (CPE) since the surface of an electrode is not modeled well by a simple capacitor [118,119]. The small low frequency “tail” seen in the Nyquist plot can be modeled with a Warburg element which comes from diffusion limitations at low frequency (close to DC). The simplest comparison between impedance spectra of different cells is using the full cell charge transfer resistance. This value is calculated as the difference in the impedance (real component) from the low frequency minimum to where the spectra crosses the real axis (or has a high frequency minimum) as illustrated in Figure 3.8. Note that while the term charge transfer resistance will be used here for simplicity, this value actually represents the sum of multiple contributions such as the particle/current collector interphase, ion transport through surface films and charge transfer resistance [118,119].

## Chapter 4      Electrolyte Additive Testing in Cells with Gradual Capacity Loss

### 4.1 Experimental Details

The electrolyte studies on cells that showed gradual capacity loss over time were done on commercially manufactured, prismatically wound, hard cased cells. The cells were hermetically sealed with the cell enclosure being attached to the negative electrode and a pin coming from the cell for connection to the positive electrode. Figure 4.1 shows a photo of one of these cells next to a quarter for size reference. The cells were made to be roughly 120 mAh capacity depending on the electrode materials and voltage limits used. Cells were made with one of two different positive electrode materials:  $\text{LiCoO}_2$  or  $\text{Li}[\text{Ni}_{0.42}\text{Mn}_{0.42}\text{Co}_{0.16}]\text{O}_2$ . All cells were made with a graphite [mesocarbon microbeads (MCMB)] negative electrode. Two types of  $\text{LiCoO}_2$ /graphite cells were studied with slightly different electrode masses such that one cell was used to charge to a lower upper cut-off voltage than the other while keeping the lithium content in the negative electrode at full state-of-charge the same. All cells were made with a base 1M  $\text{LiPF}_6$  in EC:EMC (3:7 wt.) electrolyte and then additives were included at their specified wt.%. Cells were made with very high reproducibility and variations in electrolyte and active positive or negative electrode masses were typically less than 2% [49,50,84].

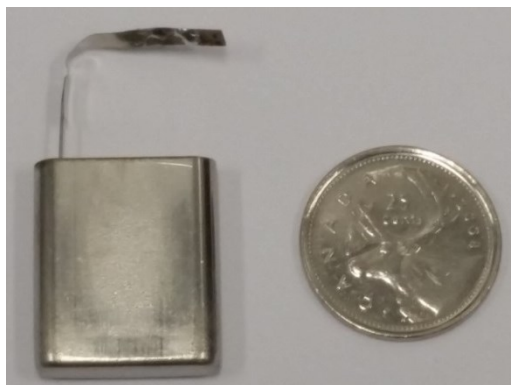


Figure 4.1      A photograph of the prismatically wound cells used for electrolyte additives testing (a Canadian quarter is shown for reference to cell size).

Several iterations of experiments were conducted on these types of cells with varying electrolytes. Table 4.1 shows a list of all the additives tested in full name, abbreviated name and chemical formula. Many of these additives were chosen as commonly used additives in these early studies to qualitatively validate the short term performance metrics through high precision coulometry with the studies conducted by numerous other research groups while others were novel additives being evaluated for the first time.

<b>Common Additive Name</b>	<b>Molecular Formula</b>	<b>Abbreviated Name</b>
Vinylene Carbonate	$C_3H_2O_3$	VC
Fluoroethylene Carbonate	$C_3H_3FO_3$	FEC
Lithium bis (trifluoromethanesulphonyl) imide	$Li N(CF_3SO_2)_2$	HQ or HQ-115
3M Proprietary	$Li_2(CF_3SO_2NSO_2(CF_2)_4SO_2NSO_2CF_3)_2$	DI
3M Proprietary	$LiOSO_2(CF_2)_3SO_2OLi$	DS
Trimethoxyboroxine	$C_3H_9B_3O_9$	TMOBX
3M Proprietary	$Li N(SO_2CF_2CF_2CF_2SO_2)$	CI
3M Proprietary	$FSO_2(CF_2)_3SO_2F$	DSF1
1, 3-Propanesultone	$(CH_2)_3SO_3$	PS
Tris (trimethylsilyl) phosphate	$PO(SiO(CH_3)_3)_3$	EM-1
3M Proprietary	$[C_3F_6 - C_2H_2F_2]_n$	LFC

Table 4.1 A list of the different additives tested in the 120 mAh prismatic cells including molecular formula and abbreviated name.

Cells were typically made in sets of four replicates such that two cells could undergo cycling experiments and two cells could undergo automated cycling/storage experiments independently and simultaneously. In order to compare the results of experiments that were conducted in several larger rounds, each round followed the same

protocol for testing. This ensured that all cells had impedance spectra measured at the same stage and the conditions of the experiments did not vary for different electrolytes. Upon arrival (after only a formation cycle conducted by the manufacturer) the cells were either put on the High Precision Charger for cycling or on the automated cycling/storage system for testing.

Cycling experiments were all conducted at 40°C at a charge/discharge rate of C/20 (6 mA). The cells referred to as “low voltage” LiCoO<sub>2</sub> (LVC) were cycled between 3.4 – 4.075 V and the cells referred to as “high voltage” LiCoO<sub>2</sub> (HVC) were cycled between 3.4 – 4.175 V. The NMC cells were cycled between 3.3 – 4.225 V. All cycling experiments lasted ~600 hours. Automated cycling/storage experiments [117] were conducted through the same voltage ranges and at the same cycling rate with storage times of ~560 hours measuring the open circuit voltage every 6 hours.

After cycling on the High Precision Charger, the cells were charged or discharged to 3.900 V after cycling and held at that voltage until the current reached ~100 μA in order to reach steady state. Impedance spectra were collected using a Maccor FRA 0356 at room temperature (21 ± 2°C). Impedance spectra were collected with ten points per decade over the range of 10 kHz – 1 mHz with a voltage drive amplitude of 2 mV. Ideally impedance spectra would have been collected up to 100 kHz but the equipment could not reach such high frequencies. After measuring impedance, the cells were moved to an older Maccor 2000 system and cycled over the appropriate voltage windows at 55°C and a 10 mA charge/discharge current. This was done to collect long term capacity fade data in order to verify the short term measurements of coulombic efficiency as valid metrics for predicting which cells would have better cycle lives.

## 4.2 Results and Analysis

Experimental design was determined by collaborators from Medtronic, 3M Company as well as the author and Dr. Jeff Dahn. All cell testing and analysis for the high precision coulometry and electrochemical impedance spectroscopy measurements were conducted by the author. Storage experiments were conducted by Dr. Nupur Sinha

in collaboration. All cells for electrolyte additive testing were manufactured at Medtronic. Some electrolyte additives were provided by 3M Company.

Many additives and additive combinations were studied using similar techniques in the same cell types. For clarity, the following will be a discussion in detail about the measurements and interpretation of data for a smaller set of data on cells containing different amounts of vinylene carbonate. A summary of performance metrics and a brief discussion of other interesting findings will be provided at the end of the section.

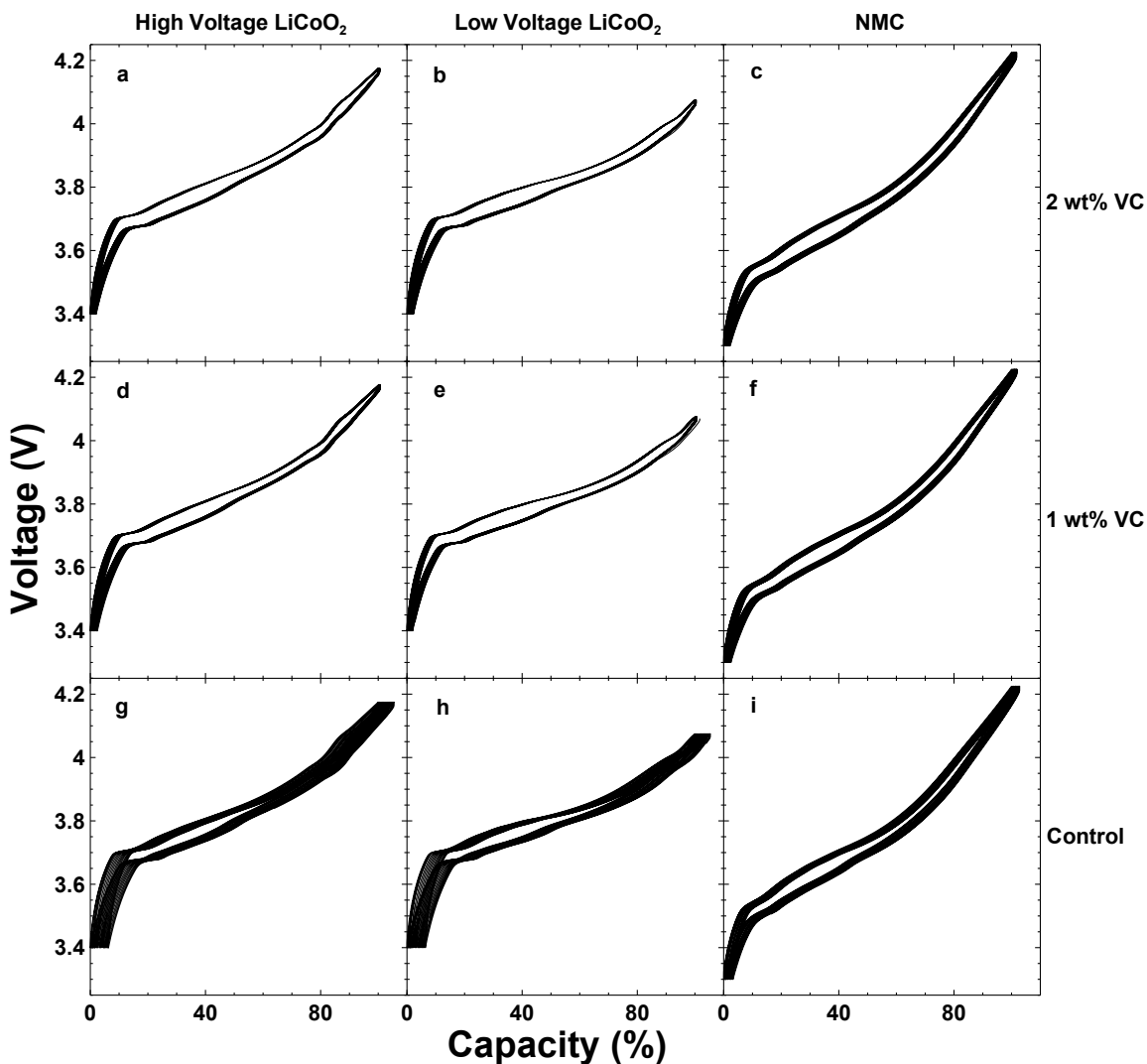


Figure 4.2 Voltage versus capacity (%) curves for High Voltage LCO (a, d, g), Low Voltage LCO (b, e, h) and NMC (c, f, i) cells containing control electrolyte with 2% VC (a, b, c), 1% VC (d, e, f) or no VC (g, h, i) cycling at C/20 at 40°C. Reproduced by permission of The Electrochemical Society [84].

The first data set always examined when evaluating cycling performance is the shape and changes in the voltage versus capacity curves. Figure 4.2 shows the voltage curves of the different cell types containing either the control electrolyte, control electrolyte with 1 wt.% VC or control electrolyte with 2 wt.% VC. These voltage curves slip to the right with continual cycling due to the inefficiencies within the cell caused by the parasitic reactions between the electrodes and electrolyte. It is clear from only the voltage curve that VC has a large impact on the cell performance (especially in the  $\text{LiCoO}_2$  cells) as the slippage rate of the curves is dramatically reduced when VC is added to the electrolyte. VC reduces both the capacity fade as well as almost completely eliminating the charge endpoint slippage in the  $\text{LiCoO}_2$  based cells. This implies that not only is VC beneficial at the negative electrode but also is impacting the reaction rate between the electrolyte and the positive electrode.

While the voltage curves give an initial indication of cell performance, examining the coulombic efficiency, capacity and charge endpoint versus cycle number give a detailed analysis of the voltage curves. Figure 4.3 shows this data for all the cells tested with pair cells shown in blue where available. By looking only at the discharge capacity (center row) it is very difficult to differentiate between cell performance over the first ~600 h of cycling that is occurring during these measurements. The cells with different electrolytes in a given cell type show very minimal difference in this capacity loss rate and therefore it is impossible to evaluate which of the cells would have the best cycle life (or long term performance). However, despite the minimal difference in capacity loss (fade) rates, there are clear differences in the coulombic efficiencies and charge endpoint slippage rates (slope of the charge endpoint capacity versus cycle number curve) between the different electrolytes within a given cell type.

The large benefit of using VC in terms of cycling performance in the early cycles is clear and this means that the parasitic reaction rates are lower and therefore the cell should have a longer cycle life. While there is a large improvement in performance with the addition of 1 wt.% VC to the electrolyte, the incremental improvement when comparing 2 wt.% VC to 1 wt.% VC is relatively small. Interestingly, the improvement in coulombic efficiency and charge endpoint slippage in the VC-containing cells is much smaller for the NMC cell chemistry compared to the  $\text{LiCoO}_2$  cells. Quantitatively using

the coulombic efficiency and endpoint slippage to predict cycle life depends on many factors (and will be discussed in the Chapter 7) and therefore comparing between the NMC and  $\text{LiCoO}_2$  cells is more complicated than simply comparing the efficiency and endpoint slippage between the cell chemistries. Regardless, this data qualitatively suggest that VC has an impact at both the positive and negative electrode in terms of lowering the rate of parasitic reactions which should manifest itself as a longer cycle life for those cells and the cells containing 2 wt.% should be slightly better than those containing only 1 wt.%.

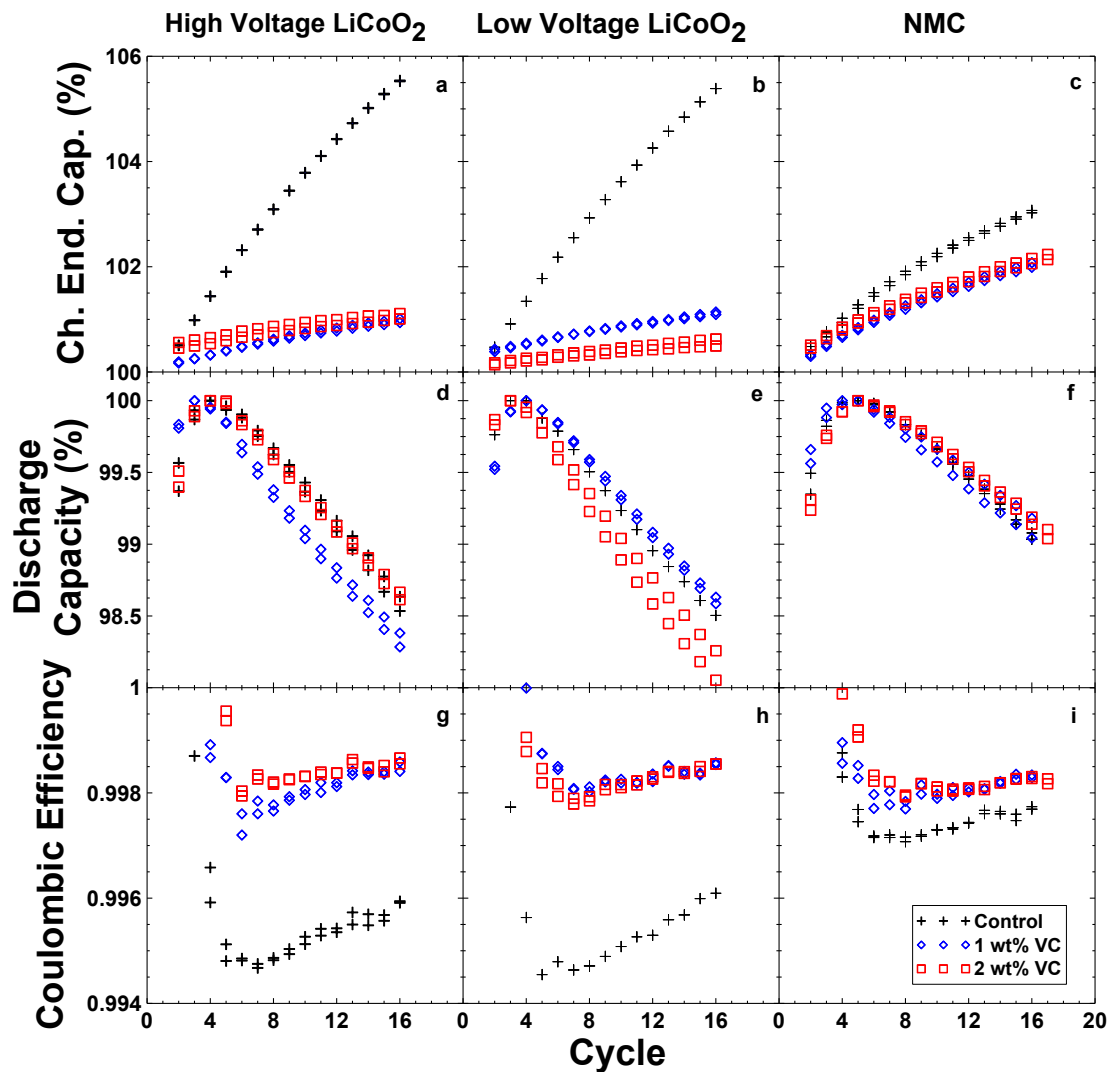


Figure 4.3 Charge endpoint capacity (a, b, c), discharge capacity (d, e, f) and coulombic efficiency (g, h, i) versus cycle number for High Voltage LCO (a, d, g), Low Voltage LCO (b, e, h) and NMC (c, f, i) cells cycling at C/20 at  $40^\circ\text{C}$ . Pair cells shown where available.



To complement the high precision cycling, automated cycling/storage experiments were conducted on cells of the same chemistry as well. Figure 4.4 shows the voltage versus storage time segments of the protocol. This allows a comparison of the self-discharge rate caused by parasitic reactions between the positive electrode and electrolyte. These results agree well with the cycling data for all three cell types in that there is a significant decrease in the voltage drop during storage when 1 wt.% VC is added and a slight decrease beyond that when 2 wt.% VC is present in the electrolyte. Once again this suggests that the cells with 2 wt.% VC should have the longest cycle life.

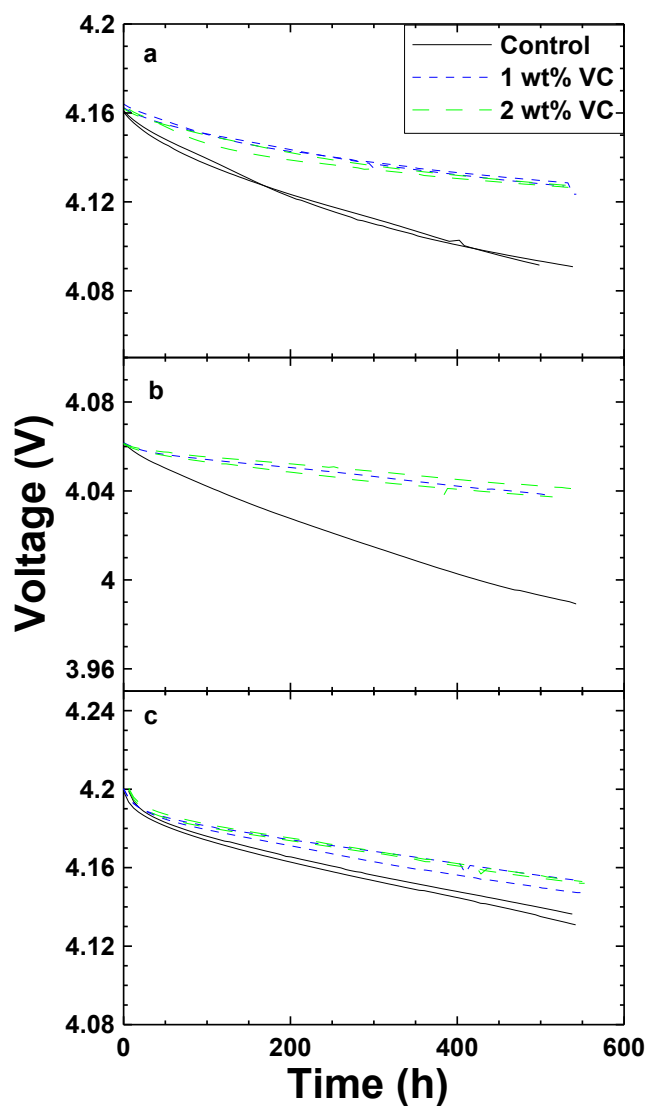


Figure 4.4 Cell voltage versus time during open circuit storage for High Voltage LCO (a), Low Voltage LCO (b) and NMC (c) cells at 40°C. Reproduced by permission of The Electrochemical Society [84].

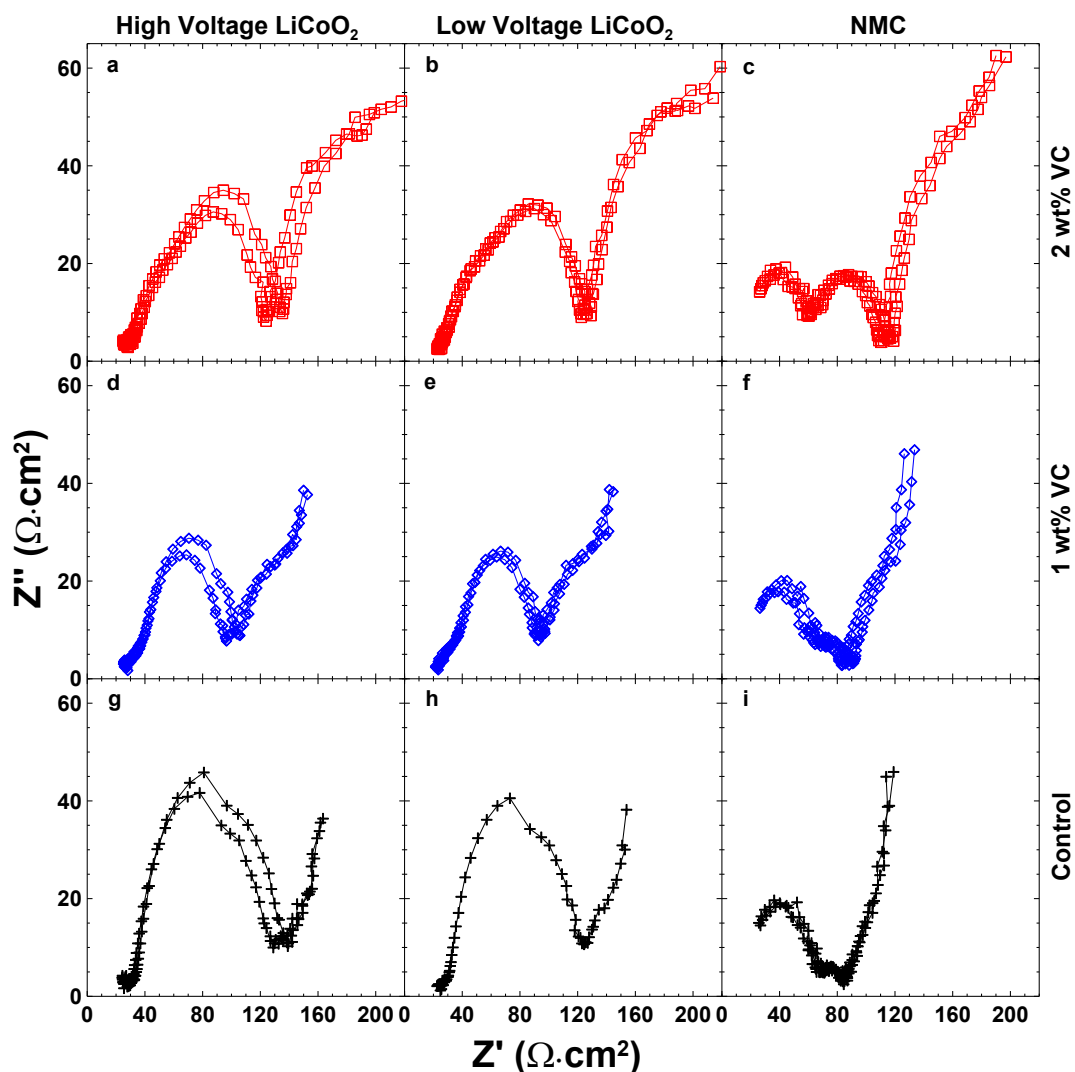


Figure 4.5 Impedance spectra in the form of Nyquist plots for High Voltage LCO (a, d, g), Low Voltage LCO (b, e, h) and NMC (c, f, i) cells containing control electrolyte with 2% VC (a, b, c), 1% VC (d, e, f) or no VC (g, h, i) after cycling on the HPC at C/20 at 40°C. Impedance spectra collected at room temperature and pair cells are shown where available.

Measurements of the coulombic efficiency, charge slippage and voltage drop during storage all give indications of the parasitic reaction rates which are important to minimize for long cycle life. However, another important metric is cell impedance as it can inhibit long cycle life and also decreases the ability of a cell to provide high power which is required for many applications of Li-ion cells. Many electrolyte additives that improve the coulombic efficiency and charge slippage do so by forming more passive surface films on the electrodes that therefore inhibit future electrolyte oxidation or

reduction further. However, these more passive films may be thicker and more resistive which would increase cell impedance and therefore measuring the impedance is important to quantify this.

Figure 4.5 shows the impedance spectra in the form of Nyquist plots for cells after cycling on the High Precision Charger. As discussed in the previous chapter the simplest analysis of such plots is to compare the width of the semicircular feature (or sum of two semicircular features as in the case of the NMC cells) as the full charge transfer resistance of the cell. From these impedance spectra it can be seen that for  $\text{LiCoO}_2$  cells, 1 wt.% VC added to the electrolyte actually decreases the total charge transfer resistance relative to control while the addition of 2 wt.% VC to the electrolyte increases the charge transfer resistance back to the same as the control electrolyte. In the NMC cells, the addition of 1 wt.% VC has minimal impact on the total charge transfer resistance while the addition of 2 wt.% VC does lead to an impedance increase. The features in the impedance spectra for the NMC cells come from the components at both the positive and negative electrode (at low and high frequency, respectively) [47,48]. Therefore, while the overall cell impedance can be examined, the impact of VC at both the positive and negative electrode can also be separated in these spectra. It appears that VC slightly lowers the impedance at the negative electrode (high frequency) and increases the impedance at the positive electrode (low frequency) likely due to a thicker and more stable SEI film formation on the graphite electrode.

After impedance spectra were collected, cells were put on an older charger system (Maccor 2000) and cycled at  $55^\circ\text{C}$  at a rate of C/10. This was done in order to validate all of the short term measurements made on the High Precision Charger that were used to predict which cells would have longer cycle lives. Figure 4.6 shows the normalized capacity versus cycle number collected during the longer term cycling. The temperature was elevated in order to increase the degradation rate as these cells were known to have very long lifetimes when cycled at only  $40^\circ\text{C}$  (to be discussed further in the Section 4.4). For all cells within a given cell type, the long term capacity retention agrees well with the short term metrics measured from the High Precision Charger in that 1 wt.% VC boasts a significant improvement in capacity retention compared to control with a marginal additional improvement seen when adding 2 wt.% VC to the electrolyte. Note that while

the coulombic efficiency for the NMC cells with control electrolyte was higher than that of the LiCoO<sub>2</sub> cells with control electrolyte the capacity retention is significantly worse. This reiterates that a comparison between different cell chemistries is not as simple as directly comparing the coulombic efficiency and charge slippage rates. However, since the temperature was changed between the short term high precision cycling and the long term cycling it is possible that there are degradation mechanisms that are much more heavily temperature dependent in the NMC cells compared to the LiCoO<sub>2</sub> cells such as manganese dissolution which can occur at high temperature. Therefore it is probable that if the high precision cycling was done at 55°C that the NMC control cells would have had much lower efficiency and worse charge slippage rates.

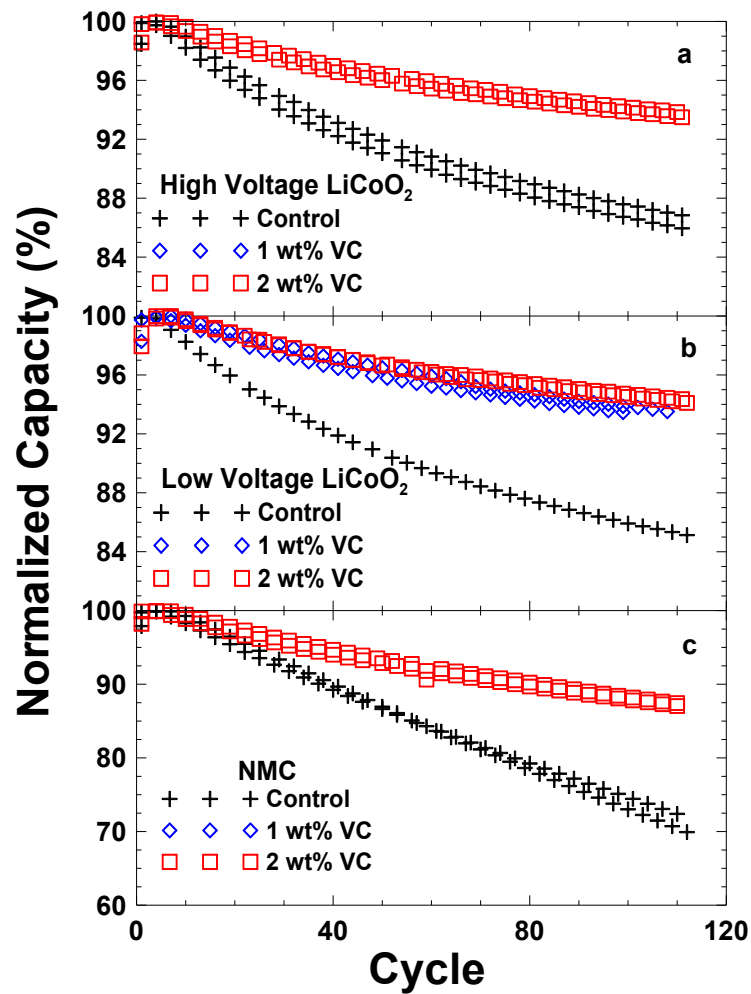


Figure 4.6 Normalized discharge capacity versus cycle number for High Voltage LCO (a), Low Voltage LCO (b) and NMC (c) cells cycling at C/10 at 55°C after cycling on the HPC (capacity renormalized at first cycle 55°C cycling).

### 4.3 Summary

Applying the same methodology as described in the previous section to many sets of cells with different electrolytes, comparative studies of the performance of numerous known and new electrolyte additives were performed. Figures 4.7 - 9 show summary bar charts of the high precision charger data collected on low voltage LiCoO<sub>2</sub>, high voltage LiCoO<sub>2</sub> and NMC cells, respectively. Shown is the coulombic inefficiency per hour ( $\text{CIE/h} = (1 - \text{CE})/(\text{hours per cycle})$ ), discharge slippage (%/cycle), charge slippage (%/cycle) and fade (%/cycle) to summarize the short term performance metrics. The additives are referred to in abbreviated form which can be referenced back to Table 4.1 for more detail. Those cells labeled with 100 or 1000 ppm refer to intentionally added water content which will be discussed further in Chapter 6. Each panel is ranked in ascending order except for fade which is ranked in the same order as CIE/h to show that short term capacity loss measurements do not always correlate with the coulombic efficiency. While it is true that many of the cells with lower CIE/h (or higher CE) show less fade during these short term experiments, there is no direct correlation between the two and it has been shown that CE is a better metric for predicting long term performance than the short term fade [44,84,120].

Most of the electrolyte additive combinations were studied under the same conditions in all three cell formats. One exception is the addition of added water to the electrolyte which was not studied in the high voltage LiCoO<sub>2</sub> cells. Based on the large number of cells made by a manufacturer for these studies they were spaced across multiple smaller builds of cells to study manageable subsets of cells at any given time. There is also data for control cells for the LiCoO<sub>2</sub> cells made over the course of many experimental runs that are labeled as “Control X” where the cells were made at different times to show consistency during the course of the experiments.

Almost all of these cells were put on for longer term cycle testing (as presented in the VC work in the previous section) and very good agreement was seen between the short term metrics and the long term performance. One electrolyte additive that showed unexpectedly good long term performance was trimethoxyboroxine (TMOBX) and it will be discussed in detail in the next Chapter. Therefore, based on the robust results found

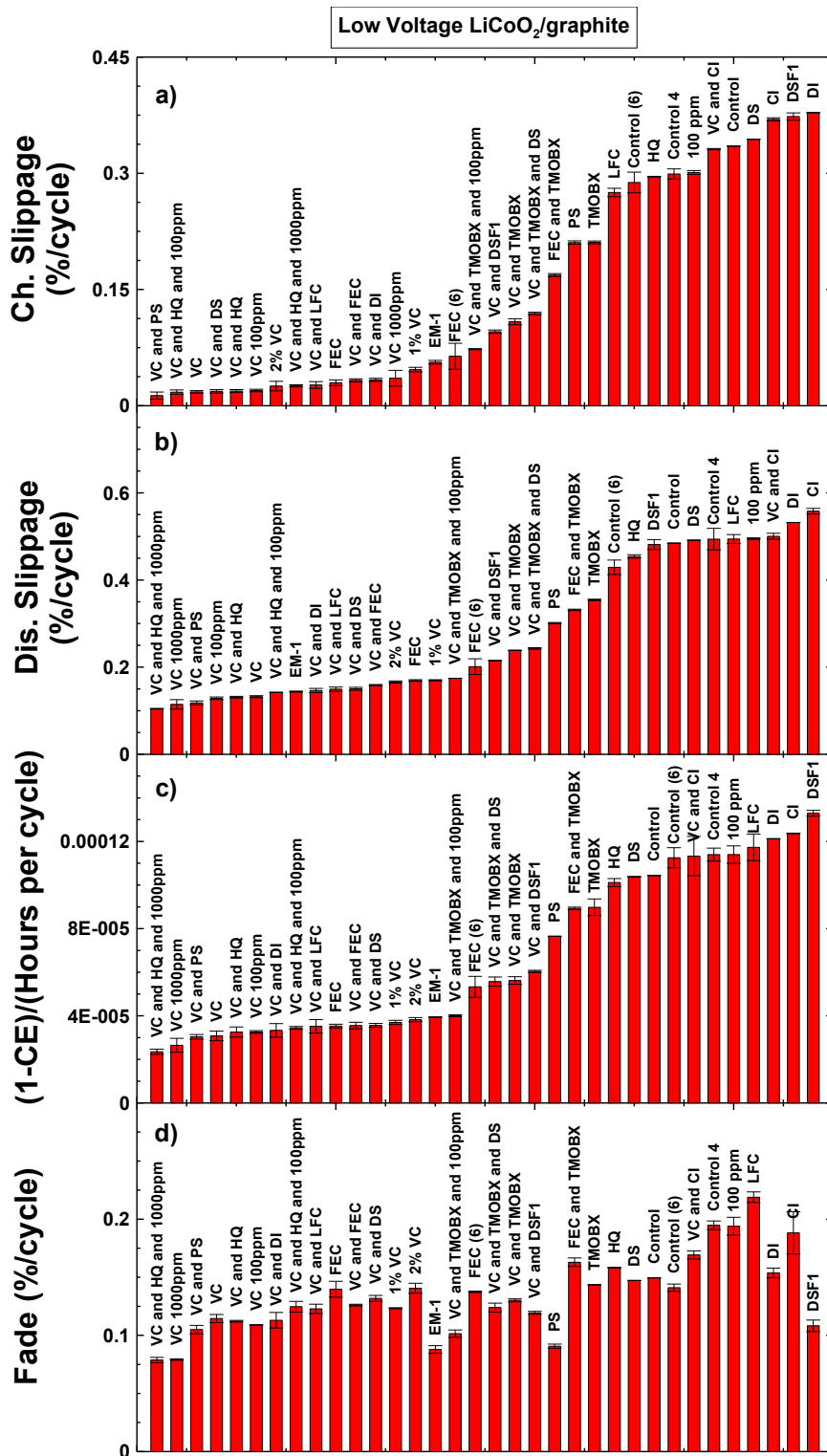


Figure 4.7 A summary of electrolytes tested in Low Voltage LCO cells showing the fade rate, charge slippage, CIE/h and discharge slippage measured on the HPC. Note that panel d) is in the same order as panel c) to show the lack of a direct correlation between fade and coulombic efficiency. Error bars represent the spread in pair cells.

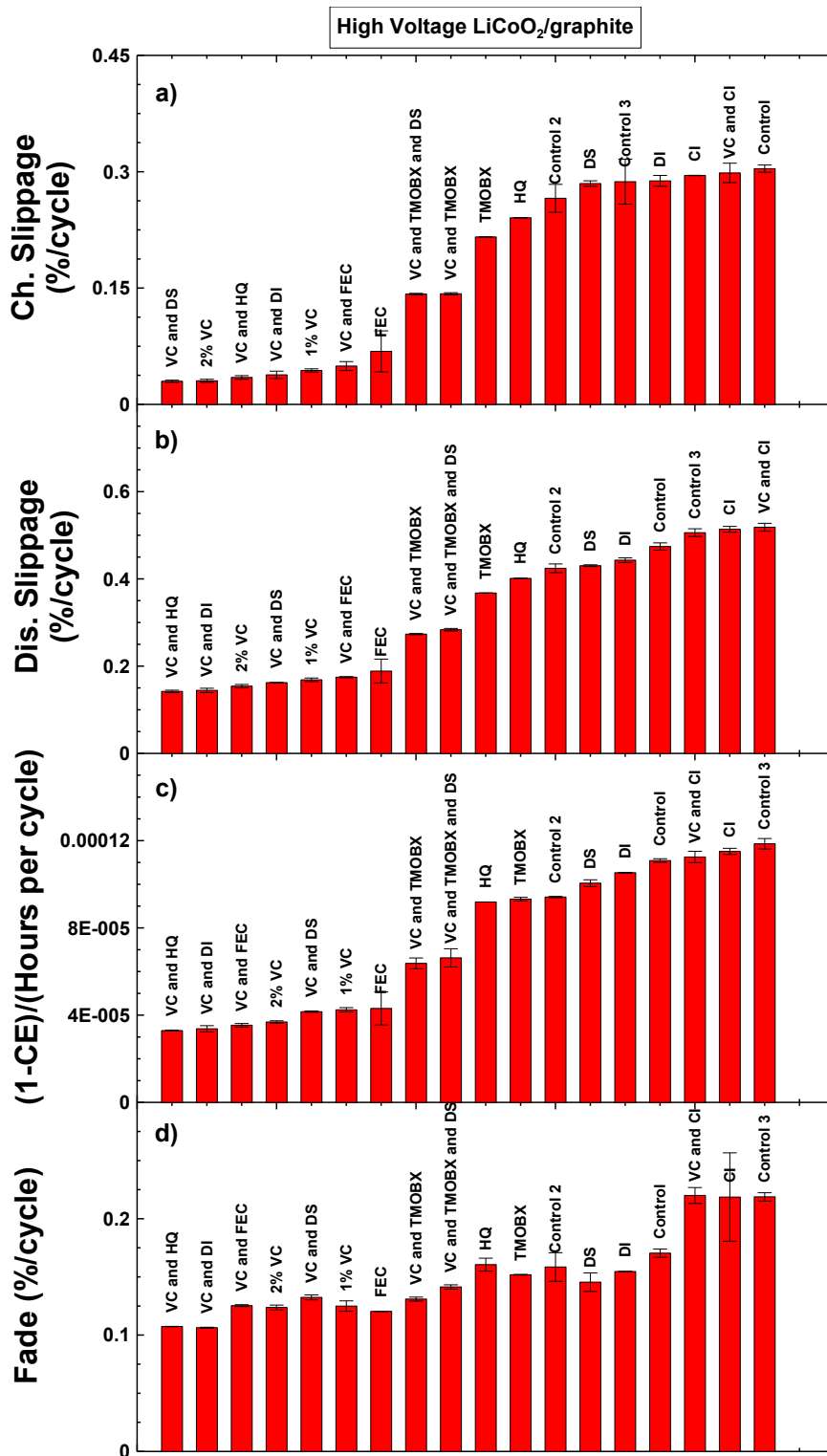


Figure 4.8 A summary of electrolytes tested in High Voltage LCO cells showing the fade rate, charge slippage, CIE/h and discharge slippage measured on the HPC. Note that panel d) is in the same order as panel c) to show the lack of a direct correlation between fade and coulombic efficiency. Error bars represent the spread in pair cells.

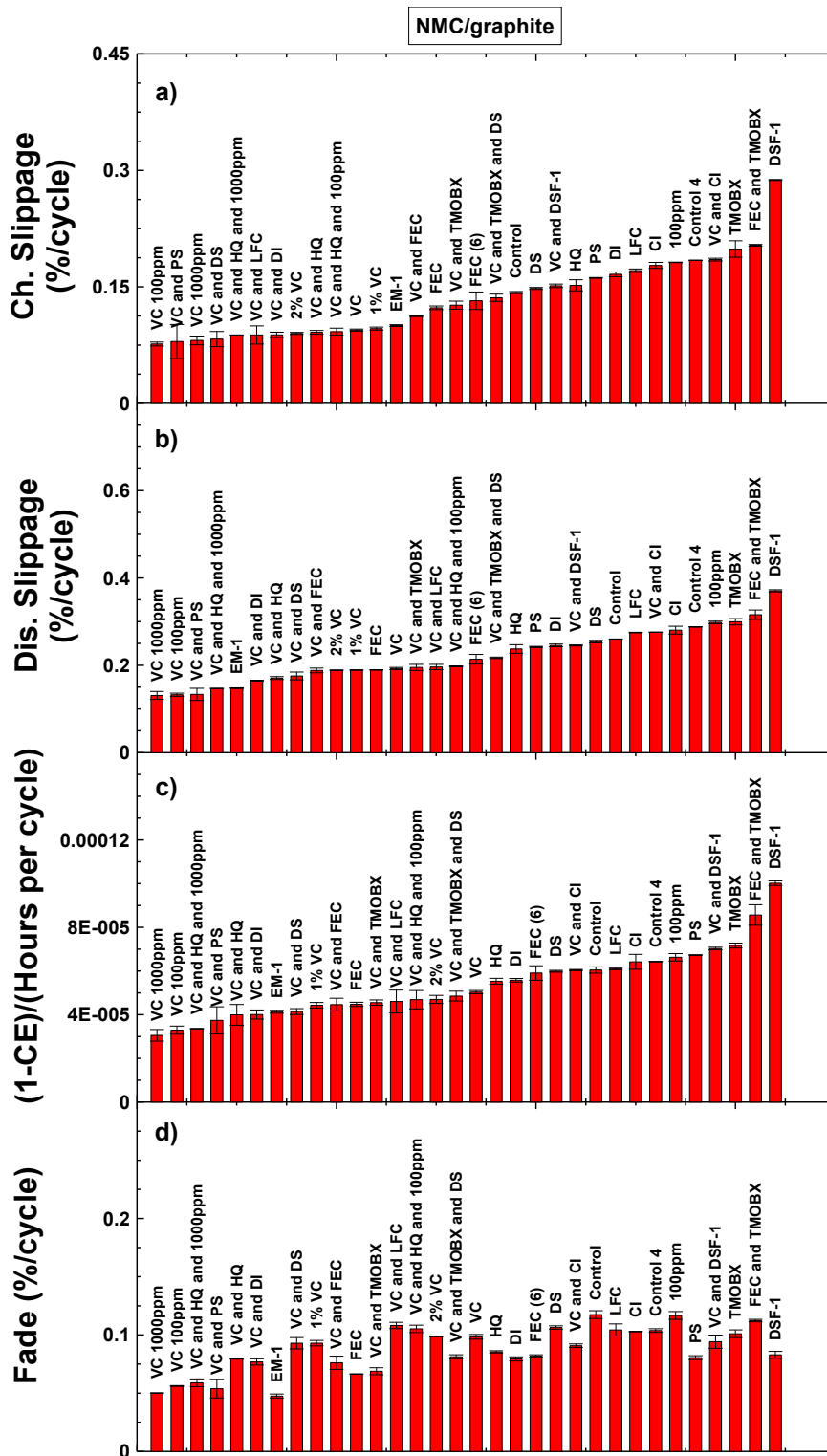


Figure 4.9 A summary of electrolytes tested in NMC cells showing the fade rate, charge slippage, CIE/h and discharge slippage measured on the HPC. Note that panel d) is in the same order as panel c) to show the lack of a direct correlation between fade and coulombic efficiency. Error bars represent the spread in pair cells.



through these studies, high precision coulometry has grown into an essential tool in screening the performance of different electrolyte additives in many recent publications [88,114,121–129]. While coulombic efficiency and charge slippage are certainly not the only metrics to be considered it does allow one to quickly evaluate the performance of an additive in terms of rate of parasitic reactions which will eventually limit the lifetime of a Li-ion cell.

#### **4.4 How Coulombic Efficiency Evolves with Cell Lifetime**

When work on the High Precision Charger project started, it was the first time that coulombic efficiencies could be measured accurately enough to differentiate very high performing cells from one another as well as detect the small deviations of the CE from 1.0000. Therefore, the question if a cell can ever actually have a coulombic efficiency of 1.0000 or how high the coulombic efficiency of a cell can be if it cannot reach exactly 1.0000 could be studied. (Note: the coulombic efficiency is highly dependent on rate [12] and therefore for the purposes of clarity this discussion is referring to the coulombic efficiency measured at a C/20 rate)

The coulombic efficiency data discussed in Section 4.2 show that as the cell continues to cycle the coulombic efficiency trends towards 1.0000. This is because as the parasitic reactions between the electrode and electrolyte occur, they continue to grow and thicken the surface films which slow the subsequent rate of reaction at the electrode surface. Therefore, as the cell ages and the surface films thicken, the coulombic efficiency increases towards 1.0000.

Previously aged cells that were cycled by the manufacturer were received for testing on the Ultra High Precision Charger. All cell testing and data analysis presented in this section was done by the author. Additional work was done in collaboration with Reza Fathi. Cells were manufactured by Medtronic. Cells were received in five different groups: 1) freshly made for this experiment, 2) cycled by the manufacturer for 1.5 y, 3) cycled by the manufacturer for ~6.5 y, 4) cycled by the manufacturer for ~11 y, and 5) used in an implanted medical device for ~6 y before being returned to the manufacturer. All cells were made with the same electrodes and electrolyte chemistry [130]. Figure

4.10 shows the capacity versus time collected by the manufacturer for groups 2 – 4. All cells show gradual capacity loss with time and only small differences between the groups. The green lines come from fit to the data using an SEI growth model. The model calculates the rate of the reaction between the electrode and electrolyte (and therefore the growth of the SEI) as inversely proportional to the SEI thickness [131]. Therefore, if the capacity loss is due to lithium consumption at the negative electrode associated with SEI growth, the capacity can be calculated as a function of time where  $x$  represents the SEI thickness,  $t$  is time and  $k$  is a constant related to the SEI growth rate.

$$\frac{dx}{dt} = \frac{k}{x} \quad 4.1$$

$$x = (2 k t)^{0.5} \quad 4.2$$

$$\frac{dx}{dt} = \left(\frac{k}{2}\right)^{0.5} t^{-0.5} \quad 4.3$$

Equation 4.3 gives a rate of growth which can be correlated to the capacity loss rate. Since  $x$  gives the thickness of the SEI which is directly proportional to capacity loss, the capacity of a cell ( $Q$ ) can be calculated as a function of time (where  $Q_0$  represents the initial capacity of the cell). Equation 4.4 shows this expression where  $A$  is a simplified constant from the coefficients in Equation 4.2.

$$Q(t) = Q_0(1 - A t^{0.5}) \quad 4.4$$

All three of these data sets fit the model well (considering the simplicity of the model) with only a slightly different value for the constant which could be due to slight differences introduced in the manufacturing process over 12 years.

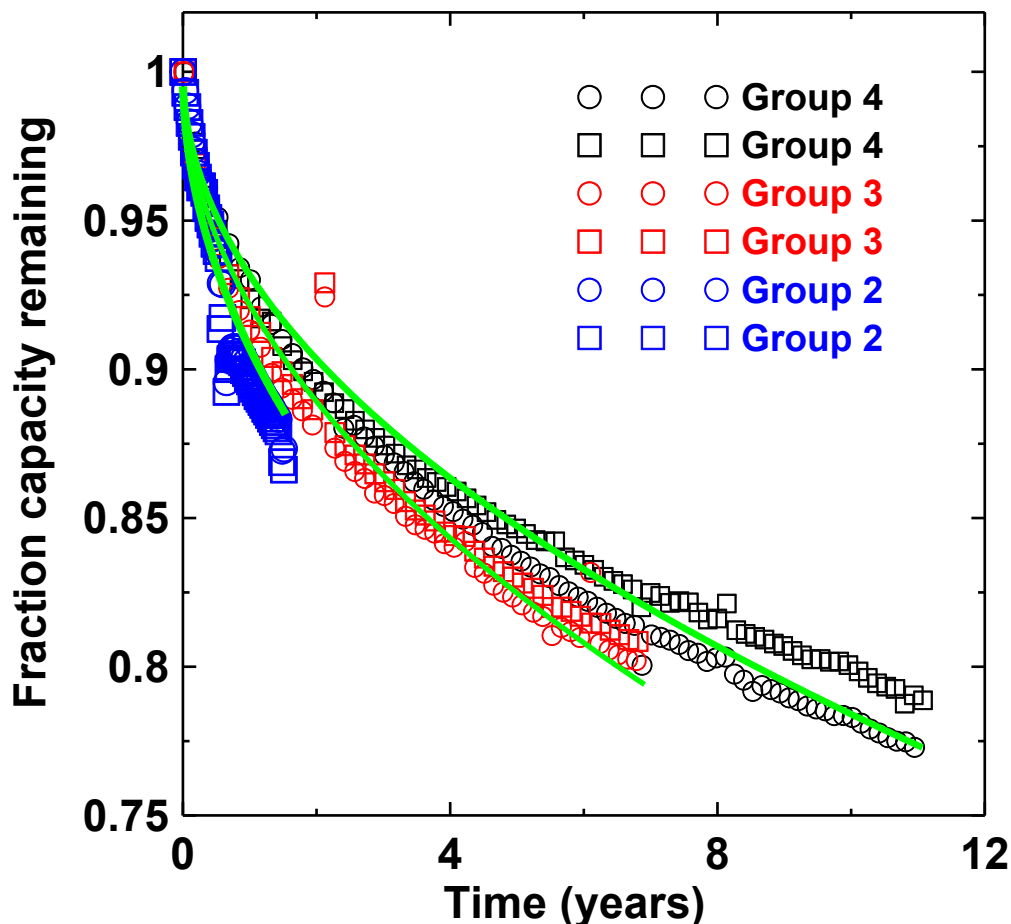


Figure 4.10 Long term cycling showing fractional capacity versus time for LCO/graphite cells cycling at 37°C. Green lines are calculated from a capacity loss model based on SEI growth. Reproduced by permission of The Electrochemical Society [130].

Cells were received and cycled on the Ultra High Precision Charger between the same voltage limits as their normal cycling (3.4 – 4.075 V) at 40°C at a rate of C/20. Figure 4.11 shows the data collected from the Ultra High Precision Charger as coulombic efficiency, capacity and charge endpoint capacity versus time (pair cells in blue). There was a power outage to the system after the cells were cycling for ~450 h and therefore cells were restarted and run for an additional ~450 h to collect enough data for interpretation. The left panel includes data from Group 1 which has very low efficiency and high charge slippage relative to the other groups as it is a fresh cell where the surface films have not had time to form and stabilize and therefore there is a high rate of reaction between the electrodes and electrolyte. The right panel zooms in to only show the aged cells to differentiate between the groups. The entire axis for the coulombic efficiency in

the right panel only spans 0.08% which is a scale that has never been accessible before as all previous data was lost to the noise level.

Generally speaking, as the cell age increases, the coulombic efficiency approaches 1.0000 and the charge slippage decreases. All of this is in agreement that as cells age the surface films become more stable and therefore the rate of parasitic reactions decrease. However, there is very little difference between the cells that are ~6 years old and those that are ~11 years old which shows that even though the films may have reached a very stable state, the coulombic efficiency is still not 1.0000 and the charge slippage is still measurable and not zero. Therefore despite the very stable performance of these cells after over a decade of cycling, there are still inefficiencies within the cells. Interestingly for the manufacturer, the cells that were implanted for ~6 years do not have as high a coulombic efficiency or as low a charge slippage rate and have a higher capacity compared to those cells that had been under controlled test for the same amount of time. This implies that that these cells actually have a lesser “effective age”. This could be due to the way the cells were used in the field in that they may not have been charged to 100% state of charge on each cycle and therefore had been operating at a lower average voltage which would limit electrolyte oxidation and age the cells at a lower rate than the full 0 – 100% state of charge cycles done by the manufacturer.

Using the data from Figure 4.11, Figure 4.12 shows a summary of the coulombic efficiency and charge slippage as a function of cell age. It shows that coulombic efficiency trends towards 1.0000 and charge slippage trends towards zero as the cells age, but neither reach those ideal levels. The data points in red represent the group 5 data from the implanted cells that fall off the trend of the other data points which reiterates the younger “effective age” of these cells although the exact cycling conditions of these cells is unknown as they were user controlled. The solid red line in the coulombic efficiency versus time plot comes from a calculated coulombic efficiency using the SEI growth model assuming the ONLY parasitic reaction is the growth of the SEI and no parasitic reactions at the positive electrode seen in Equation 4.5.

$$CE(t) = 1 - [A t^{-0.5} t_0] \quad 4.5$$

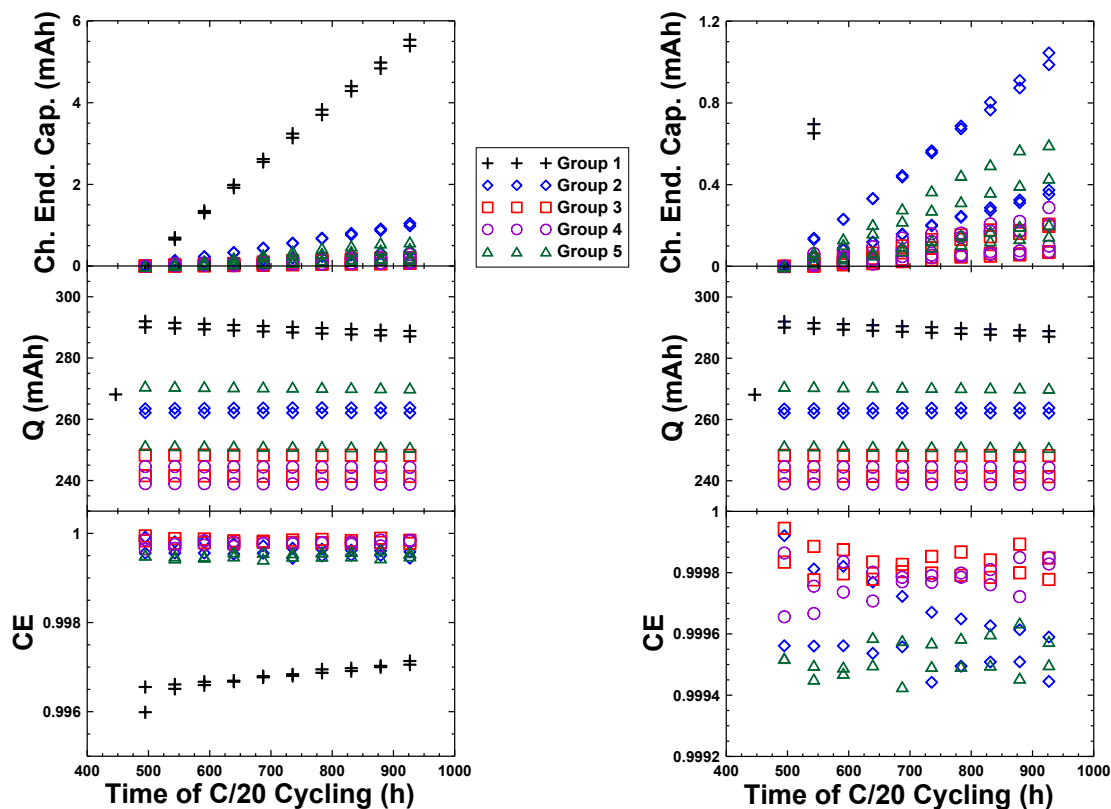


Figure 4.11 Charge endpoint capacity, discharge capacity and coulombic efficiency versus time collected on the UHPC system for cells after different amounts of cycling time. Right panels show a zoom of the left panels to only show the aged cells with high CE and low charge slippage.

It is clear that all coulombic efficiency data points fall well below this model line which means that there are more inefficiencies in the cell than just SEI growth at the negative electrode. Even small changes to the SEI growth model that would result in a better fit to the long term data would have a minimal impact on the calculated value of the coulombic efficiency as a function of time. These inefficiencies come from oxidation reactions that are captured by the charge slippage. The difference between the model line and the data points for each cell age is exactly equal to the inefficiency measured as the charge slippage. Therefore, while the SEI becomes very stable (the model line is almost exactly 1.0000) there are still parasitic reactions within the cell that do not manifest themselves in capacity loss. These reactions will eventually limit the lifetime of the cell as they are still consuming active electrolyte. Without the ability to measure charge slippage and coulombic efficiency at this high level of accuracy, these small inefficiencies which impact lifetime can easily be overlooked.

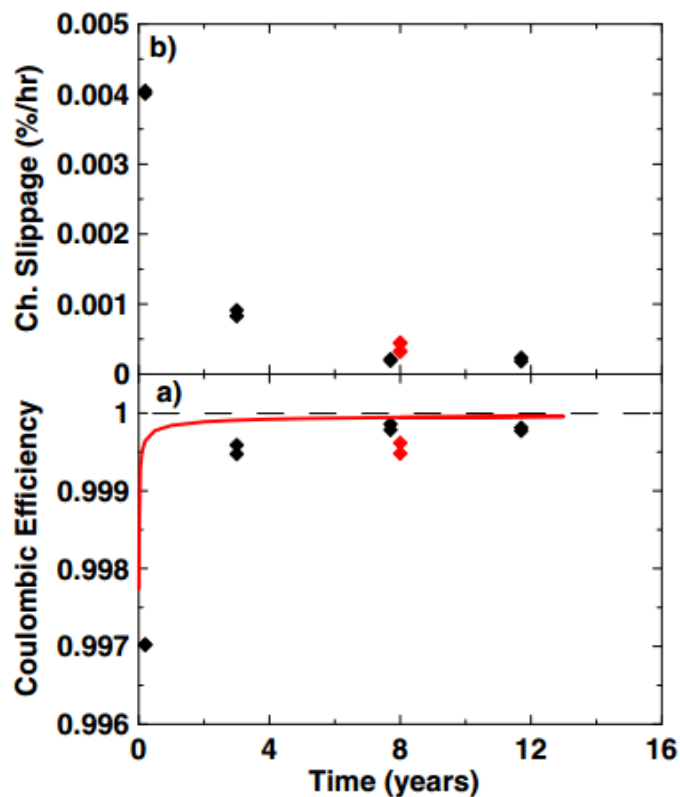


Figure 4.12 Summary of UHPC data showing the charge slippage rate and coulombic efficiency as a function of cell age in years. The red line is the calculated CE if the only parasitic reaction was SEI growth based on the SEI growth model fits seen in Figure 4.8. Reproduced by permission of The Electrochemical Society [130].

In addition to the high precision cycling data, impedance spectra of the cells were also collected. Figure 4.13 shows how the cell impedance evolved over time from Group 1 (fresh) to Group 4 (~11 year age). Group 5 shows a much smaller impedance spectra than expected based on the age which is likely related to the difference in cycling conditions as these cells did not undergo controlled cycling experiments. There is a significant variation between the pair cells of Groups 4 and 5 which can also be seen in the slight difference in capacity in Figure 4.10. This difference is likely from small differences during the manufacturing process which become more apparent over time. These impedance spectra split between two overlapping semicircular features attributed to both the negative electrode/electrolyte interphase and the positive electrode/electrolyte interphase. Generally speaking, the impedance grows over time. The contribution from the lower frequency semicircle increases significantly more than that of the higher

frequency feature. As previously mentioned this lower frequency semicircle is typically associated with the positive electrode [47,48]. The rise in impedance is due to the formation of passivation films on the electrode surfaces. These same passivation films, in turn slow the rate of parasitic reactions between the electrode and electrolyte. Therefore, it is not surprising that the cells with higher age have larger impedance and also have the higher measured coulombic efficiencies and lower charge slippage rates. Once again, the cells that were implanted have much smaller impedance spectra than the continually cycled cells of the same age, indicating a lesser “effective age”.

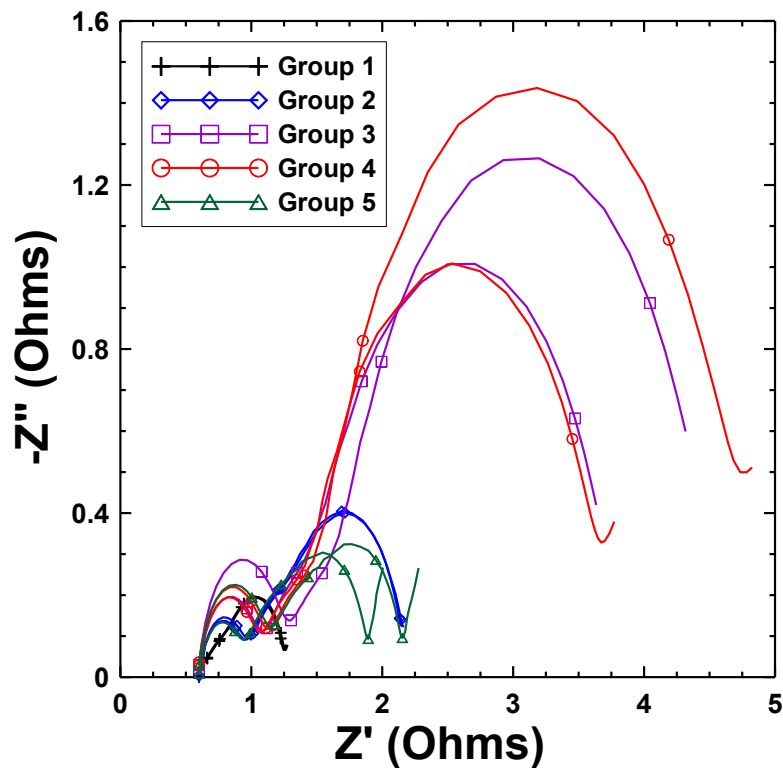


Figure 4.13 Impedance spectra presented in the form of a Nyquist plot of pair cells from each group collected at 3.9 V and 10°C after UHPC cycling tests. Reproduced by permission of The Electrochemical Society [130].

All of these results follow the trend that with continued use, cells degrade through the formation of passivation layers on the surface of the electrode. These passivation layers then limit the continued rate of parasitic reactions and cause impedance rise within the cell. However, the most important result is that despite the extremely long time these cells have been cycling (Li-ion cells were first invented 24 years ago and these cells have

been cycling for ~12 years), there are still measureable inefficiencies that continue to degrade the cell. These inefficiencies come from the continual oxidation of electrolyte at the positive electrode and can eventually lead to cell failure, this type of failure will be discussed more in section 5.2 and Chapter 7.



## Chapter 5 Impedance Reducing Additives

This chapter will present and discuss the detailed results from cells containing two different additives and discuss why they were selected as additives of interest for continued work moving forward. All cell testing and analysis except storage experiments were done by the author. Cell storage experiments were conducted in collaboration with Dr. Nupur Sinha. Cells were manufactured by Medtronic with HQ-115 being provided by 3M Company.

### 5.1 Impact of HQ-115 on Cell Performance

Lithium bis (trifluoromethanesulphonyl) imide ( $\text{LiN}(\text{CF}_3\text{SO}_2)_2$ , 3M Fluorad Lithium HQ-115) is a lithium salt that can be used as the primary salt in the electrolyte or as an electrolyte additive. HQ-115 has better thermal stability than  $\text{LiPF}_6$  due to the strong covalent bonding of the negative ion [37,132]; however it is not typically used as the primary salt due to corrosion of aluminum (used as the positive electrode current collector) above  $\sim 3.5$  V vs.  $\text{Li}/\text{Li}^+$  [133]. The use of even small amounts of  $\text{LiPF}_6$  in conjunction with HQ-115 can dramatically reduce corrosion of the current collector. In this study the impact of HQ-115 was studied at the 2 wt.% additive loading level with and without the presence of 2 wt.% VC in the electrolyte [50].

Figure 5.1 shows the cycling data for the HVC (a, d, g), LVC (b, e, h) and NMC cells (c, f, i) with pair cells shown in blue when available. As discussed in the previous chapter, when evaluating the performance of these additives for longest lifetime, it is ideal to have minimal change in charge endpoint capacity (such that there is a small charge slippage rate) and a coulombic efficiency close to 1.0000. Once again, all cells have comparable capacity loss rates over these early cycles and the cells with slightly less capacity loss are not necessarily those that also have high efficiency and low charge endpoint slippage so the fade rates will not be discussed in detail. In the cells with  $\text{LiCoO}_2$  positive electrodes, there is almost no difference in charge slippage or coulombic

efficiency when HQ-115 is added to either control or 2 wt.% VC-containing electrolyte except in the high voltage LiCoO<sub>2</sub> cells where there is a very slight improvement to adding HQ-115 to control electrolyte. In cells with an NMC positive electrode, when HQ-115 is added to control electrolyte, there is an increase in the charge slippage although almost no change the coulombic efficiency. When HQ-115 is added to the electrolyte containing VC, there is almost no change in either the coulombic efficiency or charge slippage rate. Therefore, the cycling data from the HPC suggests that the long term performance of cells with and without HQ-115 should be quite comparable and thus HQ-115 has little impact on long term performance in these cell chemistries.

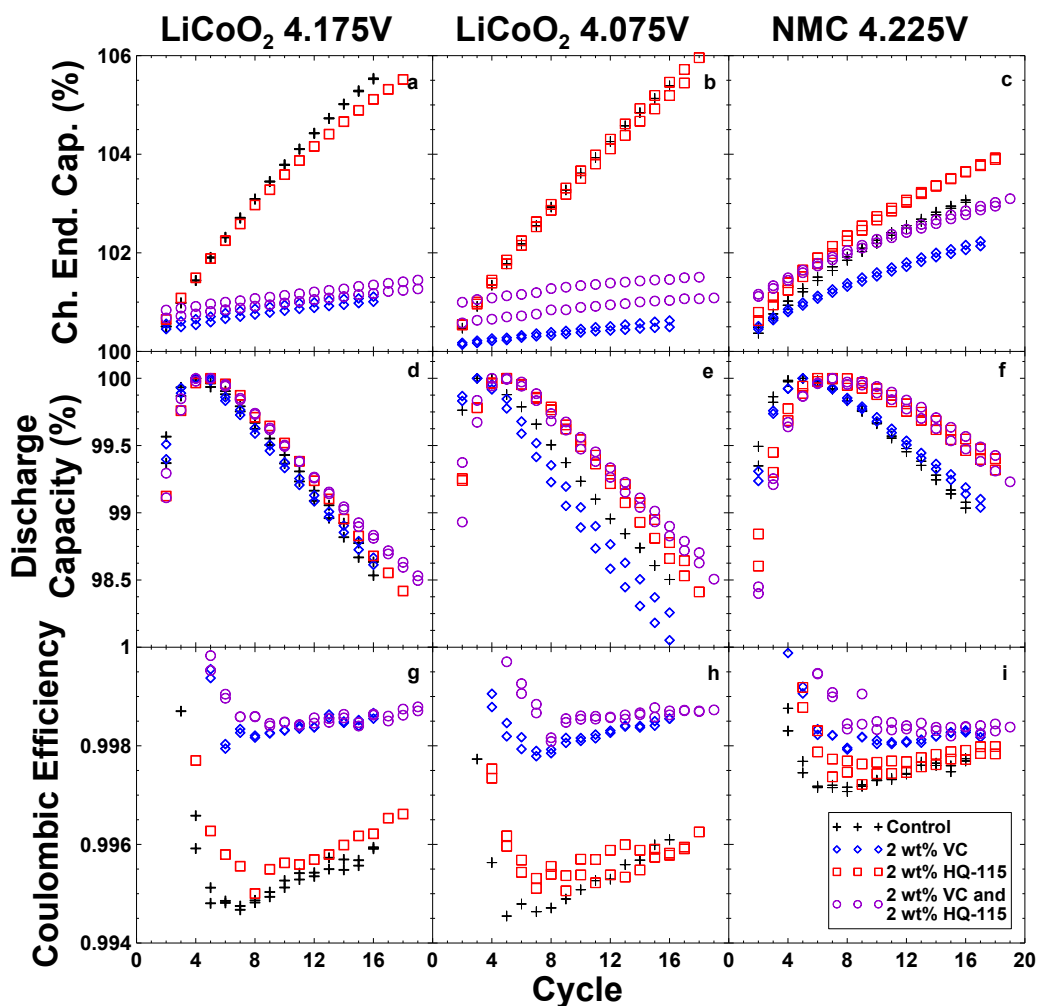


Figure 5.1 Charge endpoint capacity (a, b, c), discharge capacity (d, e, f) and coulombic efficiency (g, h, i) versus cycle number for High Voltage LCO (a, d, g), Low Voltage LCO (b, e, h) and NMC (c, f, i) cells cycling at C/20 at 40°C. Pair cells shown where available.

Figure 5.2 shows the voltage versus time plots during the open circuit storage segments of the cycling/storage procedure for the first (a, c, e) and second (b, d, f) storage periods. Pair cells are shown where available. For all storage plots, there is a noticeable decrease in open circuit voltage from the endpoint value due to the impedance within the cell. During charging there is an overpotential due to the internal resistance which depends on the current and therefore when the current is turned off such that the cells go into open circuit, this overpotential goes away and the voltage of the cell drops slightly. After the initial drop, all cells show very smoothly varying voltage versus time curves as the parasitic reactions within the cells cause self-discharge. Since the drop in open circuit voltage during storage is caused by the changing lithium content in the positive electrode, it is a measure of the oxidation-type parasitic reactions occurring at the positive electrode and should therefore agree well with the measurements of charge slippage. In most cases for both the first and second storage period, there is minimal difference in the voltage drop with or without the presence of HQ-115 beyond the level of certainty implied by the reproducibility of the pair cell measurements. Therefore, these measurements also suggest there should be minimal difference in the long term performance of the cells with and without HQ-115.

After ~600 hours of cycling on the HPC, impedance spectra were collected as described in the previous chapter. Figure 5.3 show these spectra with dashed black and blue lines for the comparisons to control and 2 wt.% VC, respectively. Interestingly, the use of HQ-115 in either control electrolyte or electrolyte containing 2 wt.% VC decreases the charge transfer impedance for all cell types. There are large differences in the shape of the impedance spectra for the cells with  $\text{LiCoO}_2$  positive electrodes compared to those with NMC electrodes due to the differences between the electrode/electrolyte interphases for the different cell chemistries. Despite these differences, HQ-115 decreases the cell impedance in both cell types which would allow for better capacity retention during higher rate cycling and allow for higher power. Therefore since HQ-115 appears to have no negative impact on cycling performance from the HPC testing and storage experiments but does decrease the cell impedance it can be a useful additive especially for cells made for higher power applications.

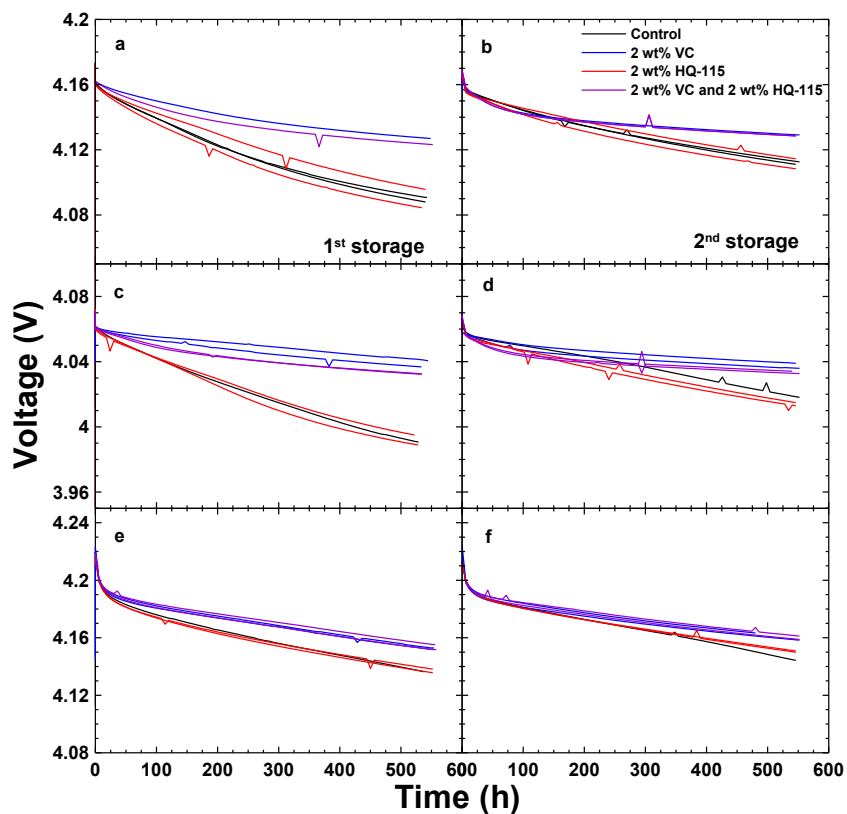


Figure 5.2 Cell voltage versus time during open circuit storage for High Voltage LCO (a, b), Low Voltage LCO (c, d) and NMC (e, f) cells at 40°C during a first (a, c, e) and second (b, d, f) storage period. Reproduced by permission of The Electrochemical Society [50].

In order to confirm the validity of using short term measurements of coulombic efficiency and charge endpoint capacity for predicting the long term performance of cells, these cells were moved to an older charger system to measure the longer term capacity loss. The cells were moved to a thermal chamber at 55°C to increase the rate of degradation and cycled with a 10 mA charge/discharge current between their respective voltage limits. The capacity was renormalized after the slight capacity fade during HPC cycling to the first cycle at 55°C. Figure 5.4 shows the capacity versus cycle number during this period and as predicted by the short term measurements, there is almost no difference in the capacity retention over ~150 cycles when HQ-115 is added to control or 2 wt.% VC containing electrolyte in any of the cell types. Since the 10 mA charge/discharge current is still a relatively low rate there is no improvement in capacity retention is seen that would be due to the decrease in impedance as a result of adding HQ-115 to the electrolyte.

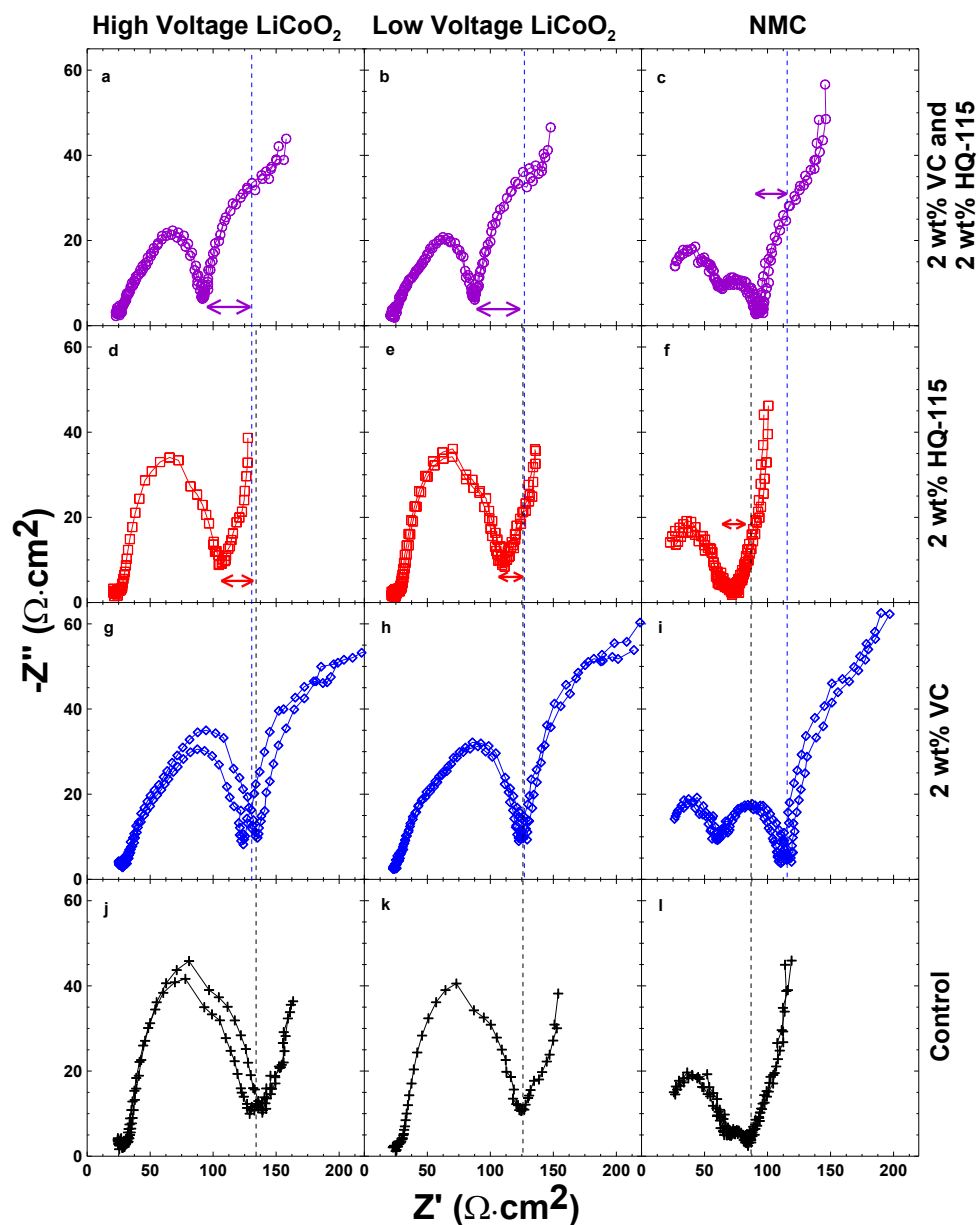


Figure 5.3 Impedance spectra in the form of Nyquist plots for High Voltage LCO (a, d, g, j), Low Voltage LCO (b, e, h, k) and NMC (c, f, i, l) cells containing control electrolyte with 2% VC + 2% HQ-115 (a, b, c), 2% HQ-115 (d, e, f), 2% VC (g, h, i) or no additives (j, k, l) after cycling on the HPC at C/20 at 40°C. Impedance spectra collected at room temperature. Pair cells shown where available.

The study of HQ-115 shows how the use of highly precise and accurate measurements of the coulombic efficiency and charge slippage can qualitatively predict the long term performance of the cells. Coupling this technique with impedance measurements is a good way to evaluate the performance of cells with varying electrolyte

additives much more quickly than traditional methods of cycling cells until appreciable differences in their capacity retention is measurable.

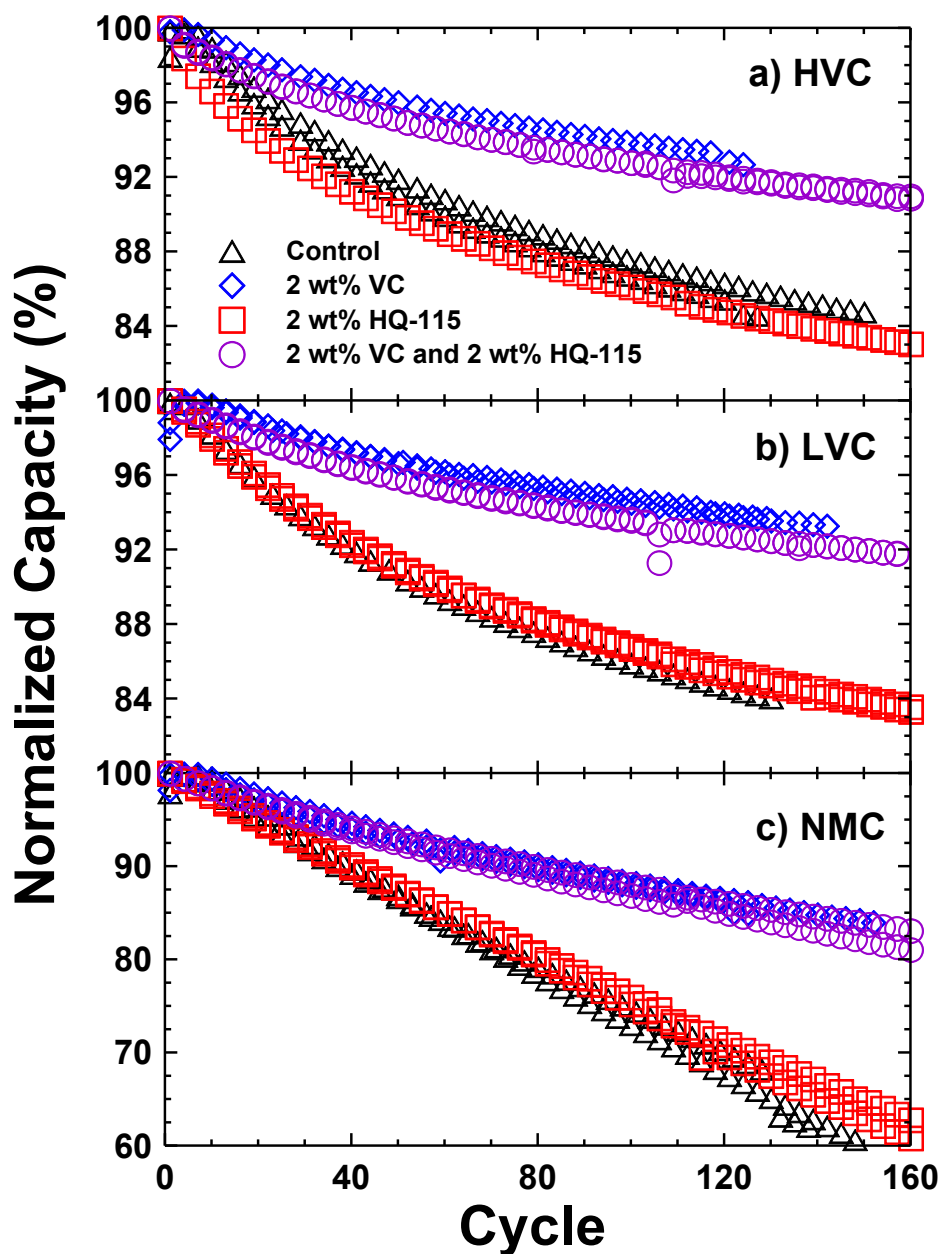


Figure 5.4 Normalized discharge capacity versus cycle number for High Voltage LCO (a), Low Voltage LCO (b) and NMC (c) cells cycling at  $C/10$  at  $55^{\circ}\text{C}$  after cycling on the HPC (capacity renormalized at first cycle  $55^{\circ}\text{C}$  cycling). Reproduced by permission of The Electrochemical Society [50].

## 5.2 Impact of Trimethoxyboroxine on Cell Performance

Another interesting additive studied with large improvements in cell impedance was trimethoxyboroxine ( $C_3H_9B_3O_6$ , called TMOBX). The performance of several additives with similar molecular structure to TMOBX (containing  $(BO)_3$  rings) were reported by Mao *et al.* [102] at low concentrations ( $< 1\%$ ) in  $LiCoO_2$ /graphite and  $LiMn_2O_4$ /graphite 18650-style cells. From the different boron ring based additives studied, TMOBX, with the three methoxy groups, led to cells with the best capacity retention during cycling. Other previous work [120] studied adding 0.3% TMOBX to  $LiCoO_2$ /graphite cells and  $LiCoO_2$ /LTO cells with and without the presence of VC. When TMOBX was added to control electrolyte in the graphite based cells the coulombic efficiency increased, but when added to VC-containing electrolyte the coulombic efficiency became worse at both 40 and 60°C. When added to the LTO based cells, the coulombic efficiency increased when used in control electrolyte at both temperatures as well as when used with VC-containing electrolyte at 40°C. When TMOBX was added to the VC-containing electrolyte at 60°C the coulombic efficiency decreased slightly. This study follows up on the impact of TMOBX in two types of  $LiCoO_2$  cells with different cut-off voltages and cells with NMC positive electrodes to better quantify the impact of the additive for Li-ion cells [49].

Figure 5.5 shows the high precision cycling data collected on cells containing control electrolyte and electrolyte with either 2 wt.% VC, 0.3 wt.% TMOBX or 2 wt.% VC + 0.3 wt.% TMOBX in the different cell types. The results for the  $LiCoO_2$  cells to both upper cut-off voltages agree well with the previous work in that the coulombic efficiency increases slightly when TMOBX is added to control electrolyte and the charge slippage is also slightly decreased. When added to VC-containing electrolyte in the  $LiCoO_2$  cells, TMOBX causes the coulombic efficiency to decrease and the charge slippage to increase. This indicates that the performance of the positive electrode is worse whenever TMOBX is added to the electrolyte. Again the capacity loss of the different cells is very similar and nothing discernible can be taken from the short term fade rate. In the previous section, the charge slippage and coulombic efficiency of the cells studied to characterize HQ-115 appears to be relatively independent of upper cut-off

voltage in the different  $\text{LiCoO}_2$  cells. However, in the cells with TMOBX the adverse effect of increasing the upper cut-off voltage is much more apparent. The coulombic efficiency remains relatively independent of upper cut-off voltage but the charge slippage of all cells (especially those containing TMOBX) increases when the cell is cycled to a higher voltage. This is due to the increased rate of electrolyte oxidation at the positive electrode which should ultimately limit the lifetime of the cells.

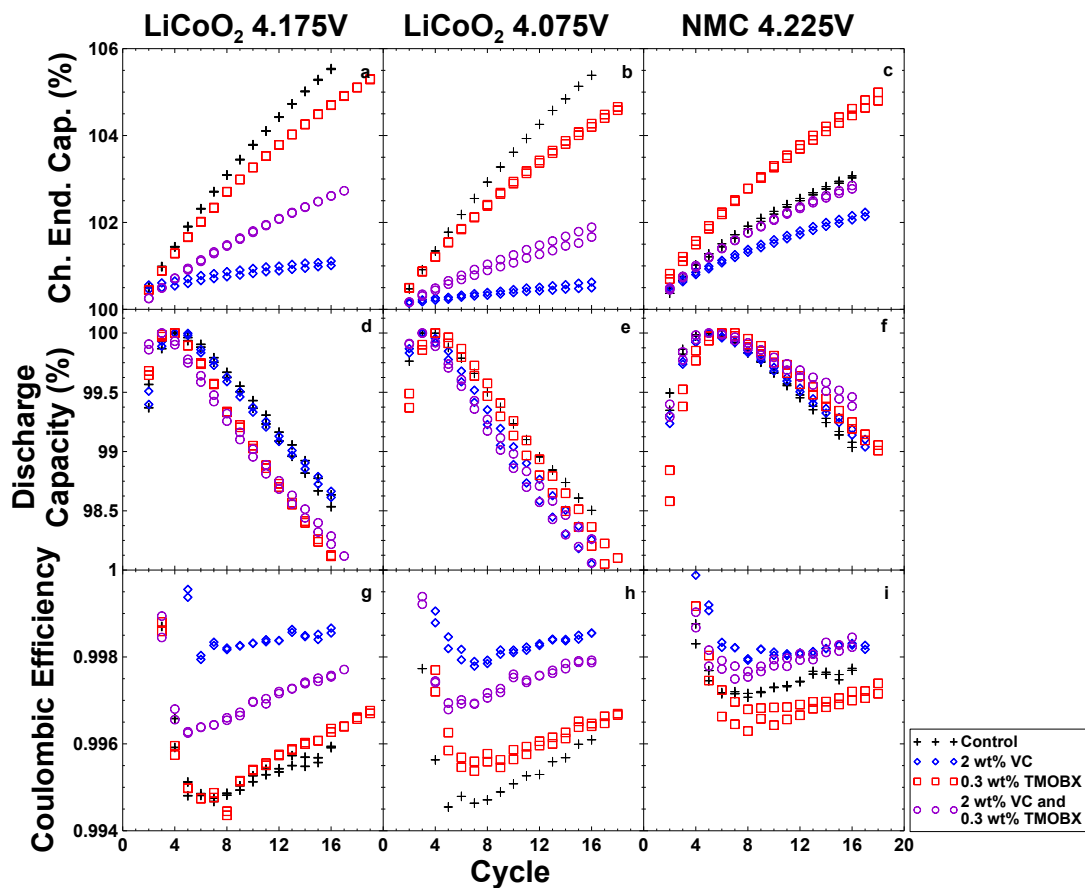


Figure 5.5 Charge Endpoint Capacity (a, b, c), discharge capacity (d, e, f) and coulombic efficiency (g, h, i) versus cycle number for High Voltage LCO (a, d, g), Low Voltage LCO (b, e, h) and NMC (c, f, i) cells cycling at C/20 at  $40^\circ\text{C}$ . Pair cells shown where available.

The cells with NMC positive electrodes show totally different impacts on the coulombic efficiency when TMOBX is added to control or VC-containing electrolyte. When TMOBX is used as the only additive it decreases the coulombic efficiency relative to control but when used with VC-containing electrolyte there is no change the coulombic efficiency. The charge slippage always becomes worse when TMOBX is



added to the electrolyte in the NMC cells. In fact, when TMOBX is added to VC-containing electrolyte, it almost completely negates the beneficial impact of VC in terms of charge slippage and becomes almost the same as control electrolyte. This indicates that the performance of TMOBX in cells is not only dependent on the other additives present but varies based on the electrodes used in the cell.

The results of the high precision cycling, specifically charge slippage, are again confirmed with measurements of the storage performance of the same cell types. Figure 5.6 shows that in LiCoO<sub>2</sub> cells going to either upper cut-off voltage, the addition of TMOBX increases the rate of self discharge leading to higher voltage drop during open circuit storage. This again indicates a higher rate of electrolyte oxidation in the cells with TMOBX present. This may be due to the oxidation of TMOBX itself or some impact that the presence of TMOBX has on the formation of a passivation film on the positive electrode that prevents electrolyte oxidation. Also as expected, the self discharge rates of all cells are higher when going to the higher upper cut-off voltage. The results between charge slippage and self discharge agree very well for the NMC cells as well even to the extent that the performance of VC + TMOBX is almost equivalent to control in charge slippage and voltage drop during storage. This reaffirms the direct relationship between charge slippage and voltage drop during storage as the quantitative results for the VC + TMOBX and control cells are identical in both even though there is a difference in the coulombic efficiency and thus the overall cell performance.

There appear to be no situations where the inclusion of TMOBX in the electrolyte leads to both an improvement in coulombic efficiency as well as a decrease in charge slippage and voltage drop during storage. Therefore TMOBX is not necessarily a beneficial additive for cycling performance and, unlike HQ-115 which was somewhat passive in the effect on cycling performance, actually can lead to adverse effects that may shorten cell lifetime. However, Figure 5.7 shows the benefit of TMOBX in terms of very large reductions to cell impedance when added to control or VC-containing electrolyte in all three cell types. This helps to explain the improved capacity retention seen by Mao *et al.* [102] because a high cycling rate was used during those experiments and therefore TMOBX help mitigate the increase of impedance within the cells which leads to capacity loss during high rate cycling.

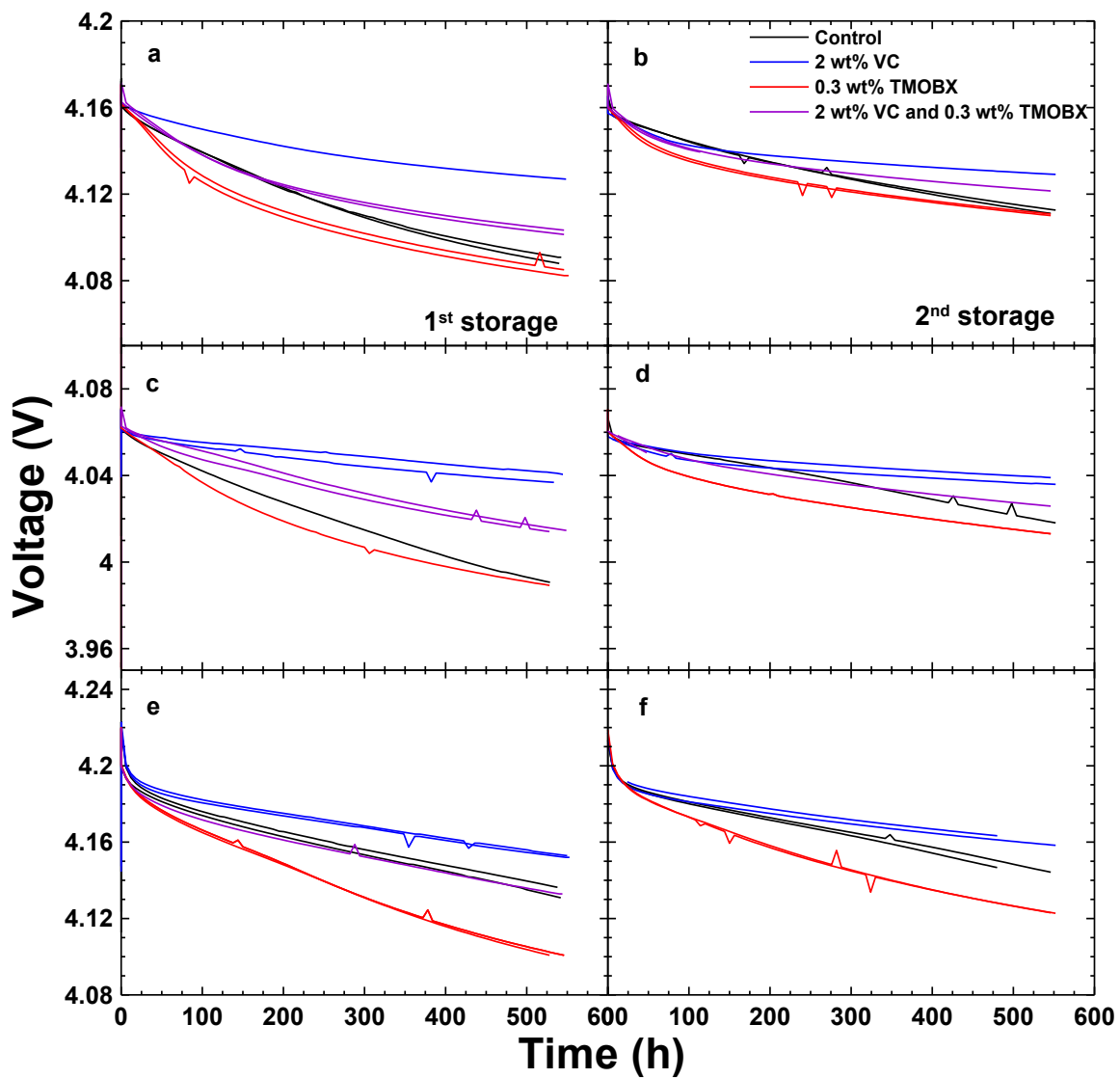


Figure 5.6 Cell voltage versus time during open circuit storage for High Voltage LCO (a, b), Low Voltage LCO (c, d) and NMC (e, f) cells at 40°C during a first (a, c, e) and second (b, d, f) storage period. Reproduced by permission of The Electrochemical Society [49].

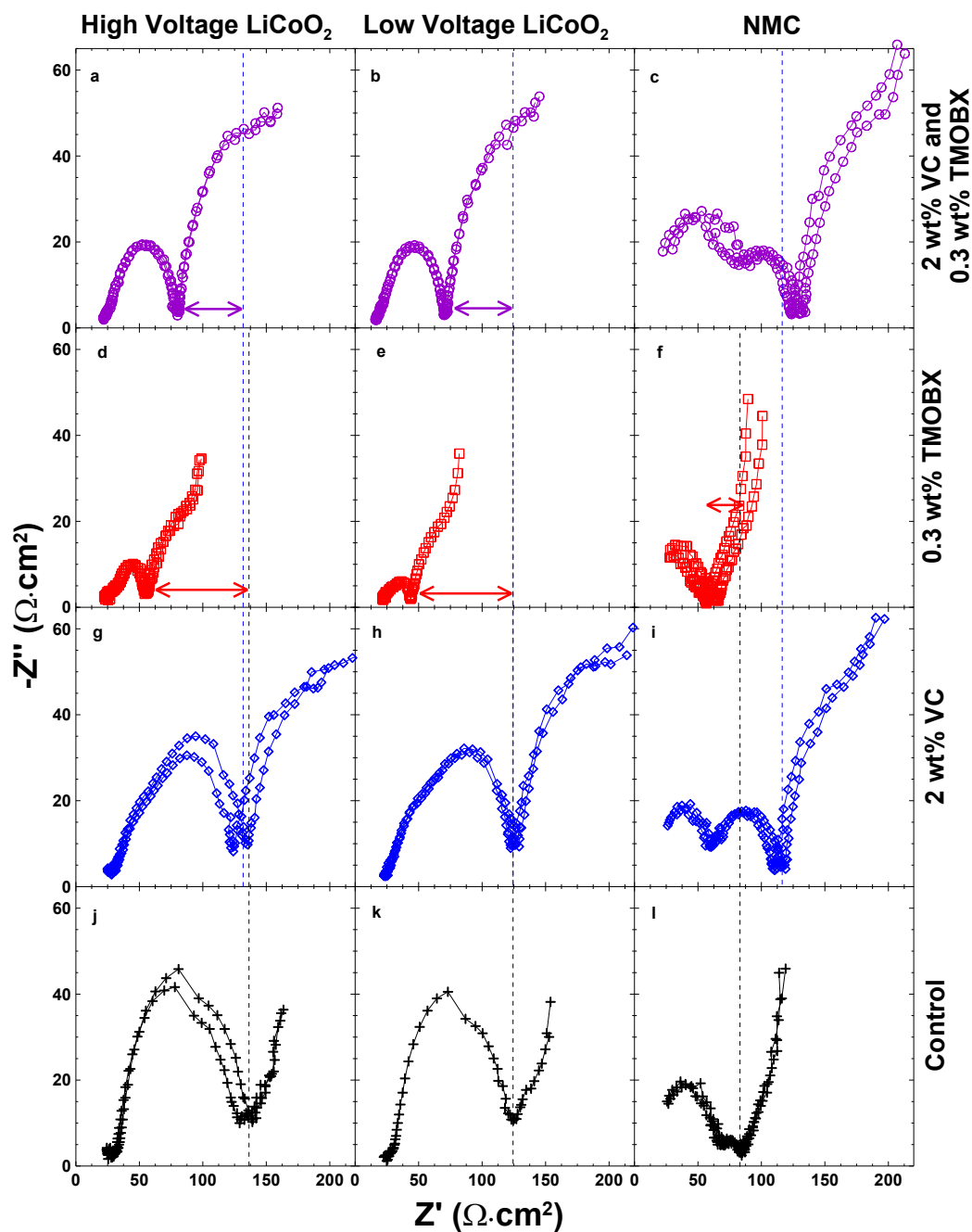


Figure 5.7 Impedance spectra in the form of Nyquist plots for High Voltage LCO (a, d, g, j), Low Voltage LCO (b, e, h, k) and NMC (c, f, i, l) cells containing control electrolyte with 2% VC + 0.3% TMOBX (a, b, c), 0.3% TMOBX (d, e, f), 2% VC (g, h, i) or no additives (j, k, l) after cycling on the HPC at C/20 at 40°C. Impedance spectra collected at room temperature. Pair cells shown where available.

This work indicates that TMOBX would be a beneficial additive for cells that need high rate performance but not necessarily a long lifetime as there was almost always an adverse effect to either the coulombic efficiency or charge slippage in the presence of TMOBX. The exception to these adverse effects are when TMOBX is added to control electrolyte in the LiCoO<sub>2</sub> cells going to either upper cut-off voltage where the coulombic efficiency and charge slippage are both improved and the cell impedance is decreased. However, while TMOBX may increase the lifetime of the control cells, the performance of those cells are still significantly worse than cells containing either VC + TMOBX or only VC. In order to validate the predictions made based on the short term measurements, the cells were again put on for long term cycling at 55°C at a cycling rate of ~C/10.

Figure 5.8 shows the (still on-going) results of the long term cycling performance. The results of the NMC cells do not necessarily agree well with the short term measurements as the use of TMOBX leads to better capacity retention compared to the corresponding cells without TMOBX. This again could be due to the difference in reactions that occur as a function of temperature with the NMC material. The performance of all the NMC cells is significantly worse than the LiCoO<sub>2</sub> cells at the higher temperature (note the scale change between panels). The results of the LiCoO<sub>2</sub> cells are very interesting given the results of the short term performance measurements. Unfortunately, the cell containing only VC cycling to 4.175 V was damaged during a power outage by the cycler and therefore was not able to be cycled after ~150 cycles. In the LiCoO<sub>2</sub> cells cycling to 4.175 V, the performance of the control and TMOBX-containing cells are very similar in terms of lifetime (depending on how end of life is defined but can typically be thought of as 80% initial capacity retention). This agrees with the similar performance in terms of coulombic efficiency and charge slippage in short term measurements. Both of these metrics were slightly better for the cell containing TMOBX which does achieve more cycles before showing a “roll-over” type failure mechanism where it begins to lose capacity very quickly starting around cycle 500 (note that this is over 1 year of cycling at elevated temperature until failure). This “roll-over” failure is believed to be caused by the products of electrolyte oxidation migrating to the negative electrode and forming an ionically insulating film which eventually prevents ion transport from the electrolyte to the electrode and leads to cell failure. This failure

mode will be discussed in more detail in Chapter 7. Unfortunately the comparison between the cell containing only VC and that containing VC + TMOBX cannot be made since one cell was damaged and had to be removed from cycling. Interestingly however, the cell containing VC + TMOBX shows the same “roll-over” type of failure mechanism after much higher capacity retention up to that point compared to the cell containing only TMOBX. Therefore, the increase of charge slippage compared to cells cycled to 4.075 V in both cell types manifests itself in a “roll-over” type failure mode.

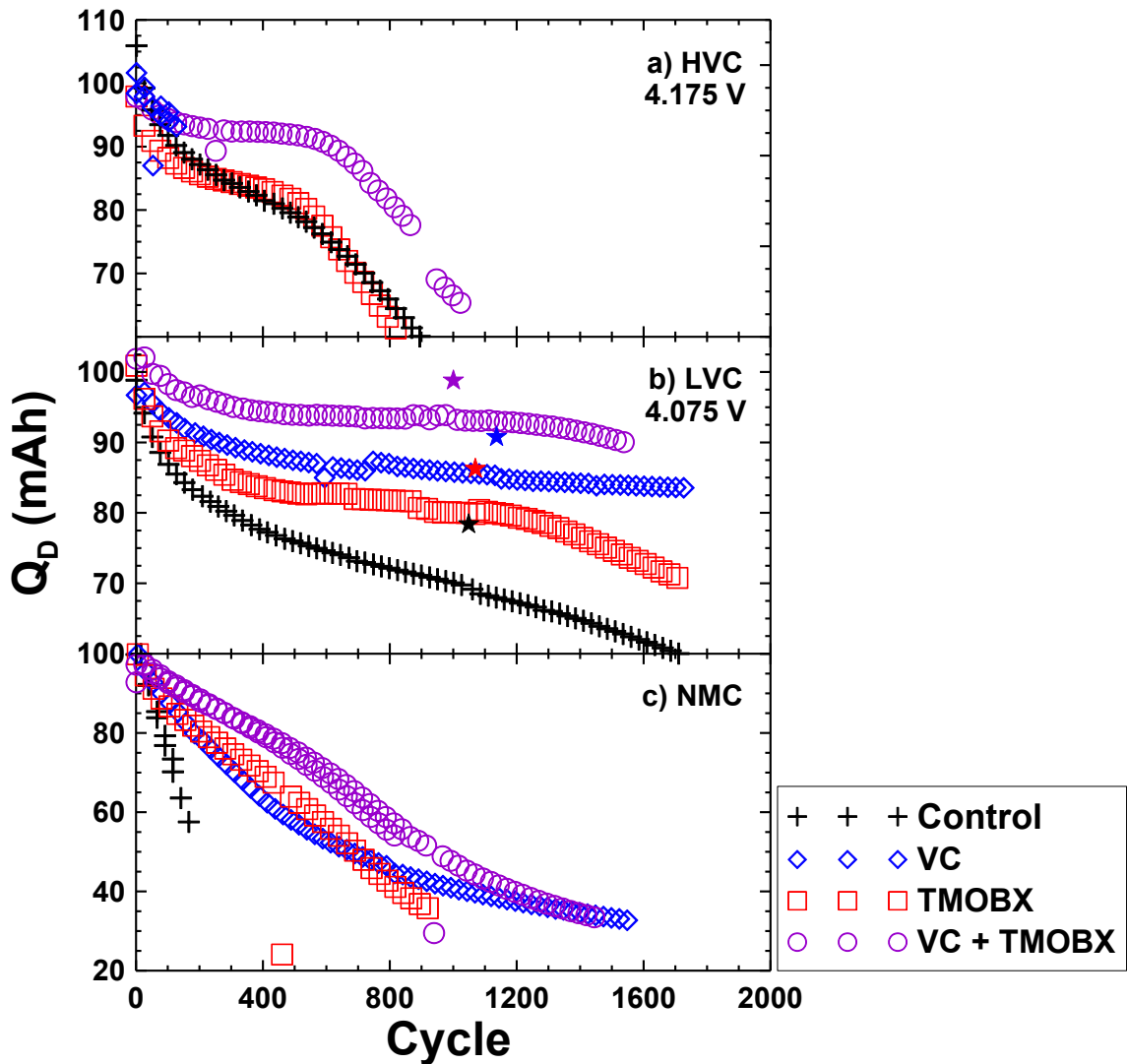


Figure 5.8 Normalized discharge capacity versus cycle number for High Voltage LCO (a), Low Voltage LCO (b) and NMC (c) cells cycling at C/10 at 55°C after cycling on the HPC. LVC cells have been cycled at 55°C for > 4 years including ~1500 hours of testing before beginning cycling at 55°C and therefore not shown in this figure.

The LiCoO<sub>2</sub> cells that are only cycled to 4.075 V show longer cycle lives than the corresponding cells cycling to 4.175 V. Upon closer inspection of the capacity loss curves, there is little difference in the capacity loss during the first several hundred cycles due to this difference in upper cut-off voltage which is understandable as the coulombic efficiency was independent of upper cut-off voltage. In these cells, the coulombic efficiency during the early cycles gives an indication of the amount of capacity loss mostly due to the SEI growth at the negative electrode, however as discussed in Chapter 4, when the SEI becomes very stable the cells reach a state where they cycle with very little capacity loss and the only inefficiency that remains in the cell is due to the oxidation of electrolyte (measured by charge slippage in the early cycles). Therefore, when comparing cells between the two upper cut-off voltages, they have similar fade curves except that the cells going to a higher voltage in Figure 5.8a show the “roll-over” failure at a much early cycle than the cells cycling to a lower cut-off voltage in Figure 5.8b because they have a worse charge slippage and therefore electrolyte oxidation rate. The fade rates are affected slightly by charge slippage since the fade is given by the difference between the discharge endpoint (directly related to coulombic efficiency) and charge endpoint slippage. Therefore, cells with higher charge slippage rates can maintain higher capacity retention despite an increase in parasitic reaction rates. If this is the case it should result in a shorter cycle life despite the cell having higher capacity during its lifetime.

The LiCoO<sub>2</sub> cells cycling to 4.075 V are an excellent example of how capacity fade cannot be used as the indicator for long term cycle life of cells and precise metrics such as coulombic efficiency and charge slippage are imperative to understanding and predicting cell lifetime. When comparing the control and TMOBX-containing cells in Figure 5.8b, the cells containing TMOBX have a slightly higher coulombic efficiency and lower charge slippage rate so, not surprisingly they show better capacity retention during long term cycling and achieve far more cycles before reaching an end of life criteria of ~80% compared to control cells. Eventually the “roll-over” failure is shown by the cell containing TMOBX but is less pronounced in the control cell as it has already lost significantly more capacity.

Since the cycling rate during long term cycling was still relatively low ( $\sim C/10$ ), the impact of the dramatic reduction in cell impedance associated with the use of TMOBX was assumed to not have a great impact on the capacity retention. In order to characterize this, after  $\sim 1000$  cycles the cells underwent a low rate,  $C/50$ , charge/discharge cycle. At this very low rate there should be virtually no impact on capacity caused by the overpotential due to impedance. The data points indicated with a star for each of the cells is the capacity during this low rate cycle. As expected, all cells show higher capacity at the low rate with the impact of impedance removed and the cells containing TMOBX show less of a difference between the low and higher rate capacity because their cell impedance is much smaller and therefore they have smaller over potentials compared to the cells without TMOBX.

The  $\text{LiCoO}_2$  cells cycling to 4.075 V containing VC or VC + TMOBX are more interesting because in the early cycles, the cell containing only VC showed slightly higher coulombic efficiency and significantly lower charge slippage compared to VC + TMOBX. Therefore it would be expected that the cell containing only VC should show greater capacity retention and a longer cycle life, but it actually shows a lower retained capacity once the cycling becomes very stable (cycle  $\sim 500$ ). However, this can be explained because the fade rate is kept small during the early cycles because the charge slippage is so much larger for the cell containing VC + TMOBX. Since the charge slippage is so high, the capacity fade can be small but it must have an adverse effect on the cycle life due to the increase in the rate of electrolyte oxidation. Therefore the cell containing VC + TMOBX should show the “roll-over” failure that the other  $\text{LiCoO}_2$  cells have exhibited at an earlier cycle compared to the cell containing only VC. Near cycle 1300, the VC + TMOBX cell appears to be beginning to slowly exhibit this “roll-over” failure while the cell containing only VC shows no indication of the on-set of this failure mode. Despite the higher retained capacity during cycling for the cell containing VC + TMOBX, the cell containing only VC which had higher coulombic efficiency and lower charge slippage is, in fact, the cell with the better long term performance as it should achieve more cycles before reaching the end of life criteria of 80%.

The short term measurements were able to be used to predict that the cell containing VC would have a longer lifetime than the cell containing VC+ TMOBX and it

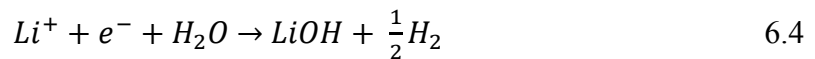
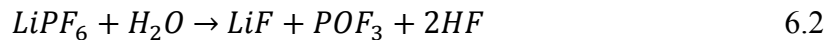
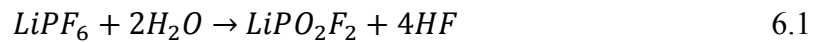
has taken > 3 years of continuous cycling at 55°C before it became apparent by only measuring capacity. If cells were not cycled until the “roll-over” failure was reached and the performance was compared based only on capacity retention, the cell containing VC + TMOBX would have been selected as the best performing cell but it would not have actually been the cell with the longest lifetime. This stresses why the use of high precision measurements of coulombic efficiency and charge slippage must be made in order to work on maximizing or predicting cycle life because they detect failure modes that are not always clearly manifested in only the capacity loss curves.



## Chapter 6      **Impact of Electrolyte Containing Intentionally Added Water**

### 6.1 Background

Lithium-ion cells are made in dry rooms or glove boxes to limit exposure of the electrodes and electrolyte to moisture as the presence of water in the electrolyte is believed to be detrimental to cell performance. For this reason manufacturing costs of cells and materials are driven up to ensure low moisture content. Typically moisture content in  $\text{LiPF}_6$  is  $< 20$  ppm and in the electrolyte solvents is  $< 15$  ppm. When water is present in a cell it can lead to numerous reactions that generate such things as HF,  $\text{POF}_3$  and hydrogen gas [35].



Despite the proposed mechanisms which result in potentially undesirable products, the performance of cells with intentionally added water in the electrolyte has not been extensively studied. Chen *et al.* [134] reported the results of maleimide used as an additive in combination with 100 ppm water that was able to mitigate any negative effects of water in the cells studied. In this work, the impact of up to 1000 ppm water was studied in cells with graphite negative electrodes and up to 2000 ppm water was studied in cells with LTO negative electrodes using the high precision charger and

associated techniques to evaluate cell performance and better understand the impact of the presence of water in the electrolyte on the long term performance of cells [135,136].

## 6.2 Cells with Graphite Negative Electrodes

The same ~120 mAh style prismatic cells were made for the study of intentionally added water as the cells used in the previous chapters except no high voltage LiCoO<sub>2</sub> cells were made for these experiments. The base electrolyte used was 1 M LiPF<sub>6</sub> in EC:EMC (3:7 by weight) with experimental groups containing either 100 ppm water, 2 wt.% VC, 2 wt.% VC + 100 ppm water, 2 wt.% VC + 1000 ppm water, 2 wt.% VC + 2 wt.% HQ-115 + 100 ppm and 2 wt.% VC + 2 wt.% HQ-115 + 1000 ppm water. Data from the cells containing 2 wt.% VC + 2 wt.% HQ-115 presented in the previous chapter will be used here for comparative purposes. Cells were made so that pairs were available for cycling on the high precision charger as well as for automated cycling/storage experiments. Impedance spectra for these cells were collected at 10°C on a Biologic VMP3 system at 3.900 V from 10 kHz – 10 mHz with a 10 mV amplitude drive signal collecting 10 points per decade. Impedance spectra were collected at low temperature to increase the cell impedance and therefore improve the signal to noise level in the data. All other cycling and storage conditions were the same as described in the previous chapters.

All cell testing and analysis except storage experiments were done by the author. Cell storage experiments were conducted in collaboration with Dr. Nupur Sinha. Cells were manufactured by Medtronic and formation data was collected at Medtronic.

Based on the previous results of the impact of water including the generation of excess gas in Li-ion cells, the first measurements made on cells with intentionally added water in the electrolyte was on swelling and irreversible capacity loss (IRC) during the formation cycling. Figure 6.1 shows the IRC (left) and swelling (right) as a function of water content for NMC/graphite (top) and LiCoO<sub>2</sub>/graphite cells (bottom) separated into groups based on additive content: no additives, VC or VC + HQ-115. IRC is plotted in mAh/g based on the positive electrode weight in the cell. Each point is an average of the

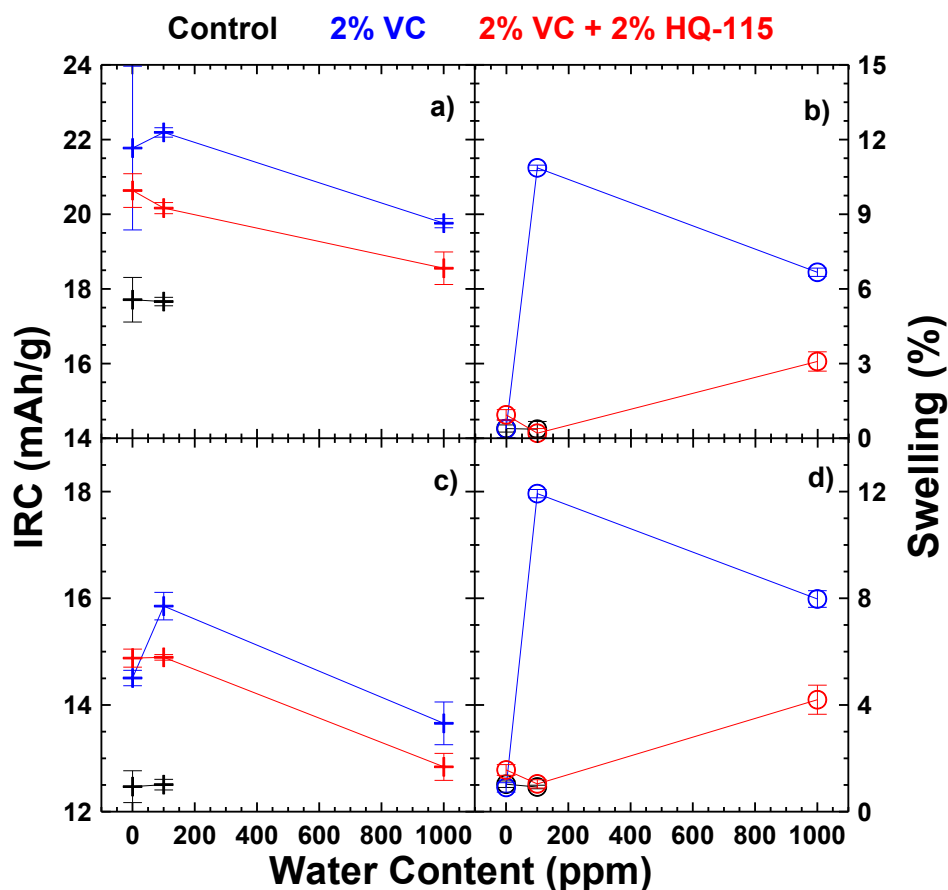


Figure 6.1 The first cycle irreversible capacity loss (a, c) and swelling (%) during first cycle (b, d) for NMC/graphite (a, b) and LiCoO<sub>2</sub>/graphite (c, d) cells as a function of water content in either control (black), VC-containing (blue) or VC + HQ-115-containing (red) electrolyte. Swelling was measured as the change in the thickness along the thin axis of the prismatic cells divided by the original thickness. These values represent an average of four cells each. Error bars represent the spread in the four cells.

four cells made in each group (two for cycling, two for storage). It is clear that the swelling and IRC depend heavily on the additives and water content but the trends are very similar whether the LiCoO<sub>2</sub> or NMC positive electrode is used. Despite the variability based on electrolyte, several key features can be observed. In almost all cases, the use of 2 wt.% VC increases the IRC and the addition of 2 wt.% HQ-115 to those electrolytes lowers the IRC. When there is no water in the electrolyte, there is minimal difference in swelling. When 100 ppm water is added to VC-containing electrolyte the swelling increases dramatically but when added to control or VC + HQ-115 containing electrolyte the swelling is not affected. The IRC is almost unchanged with 100 ppm is

added to control electrolyte (with neither VC nor HQ-115), but increases when added to the other electrolyte formulations. Interestingly, when the water content is increased to 1000 ppm in VC-containing electrolyte the swelling decreases even though when added to VC + HQ-115 containing electrolyte it increases. In all cases, the IRC is actually decreased at the 1000 ppm water level and in the cells with VC-containing electrolyte the IRC is actually lower than with no water in the electrolyte.

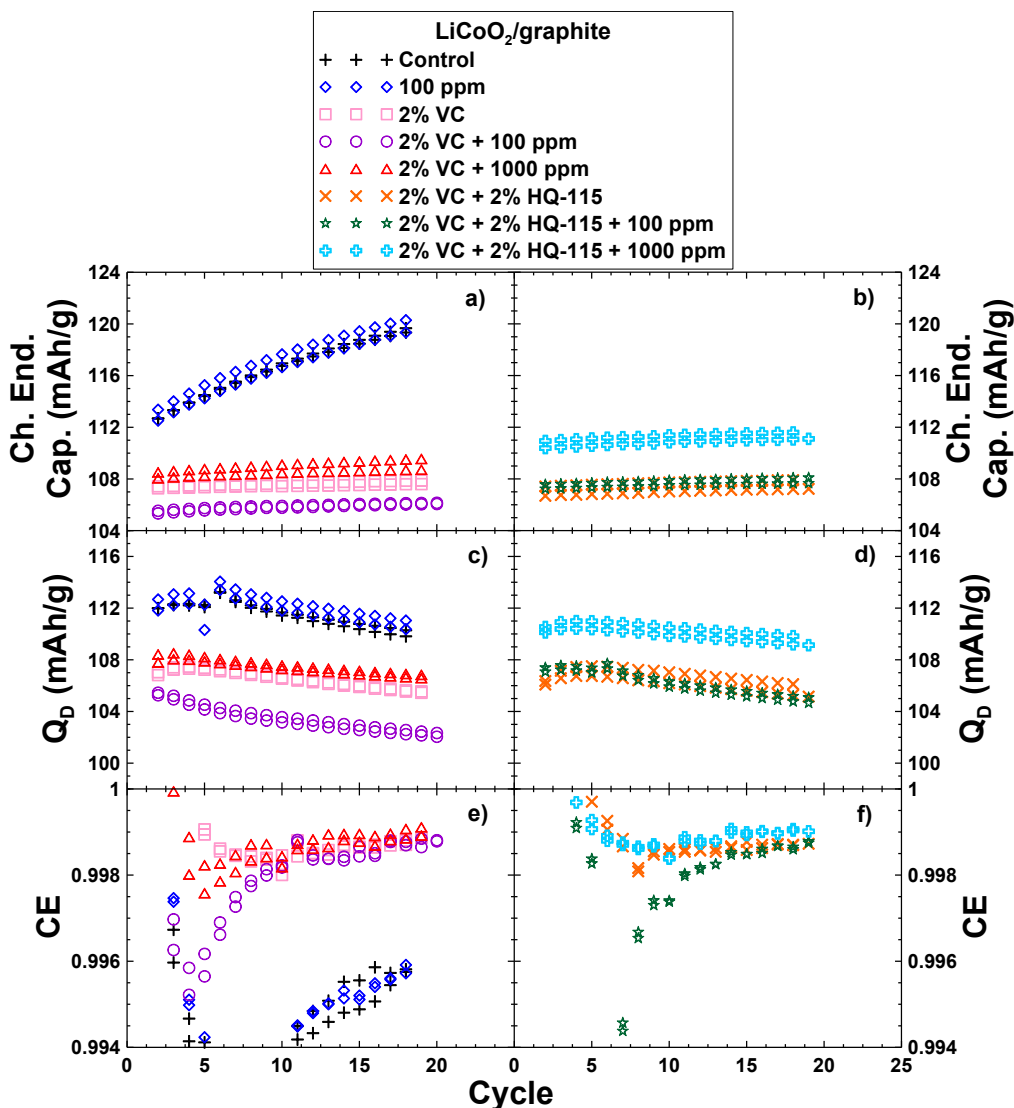


Figure 6.2 Cycling data collected from the HPC for  $\text{LiCoO}_2/\text{graphite}$  cells with constant current charge and discharge ( $\sim C/20$ ) at  $40^\circ\text{C}$ . Shown are the charge end point capacity (a, b), discharge capacity (c, d) and coulombic efficiency (e, f) as a function of cycle number. The VC + HQ-115-containing electrolytes are plotted in the right panels for clarity. Pair cells are shown where available.

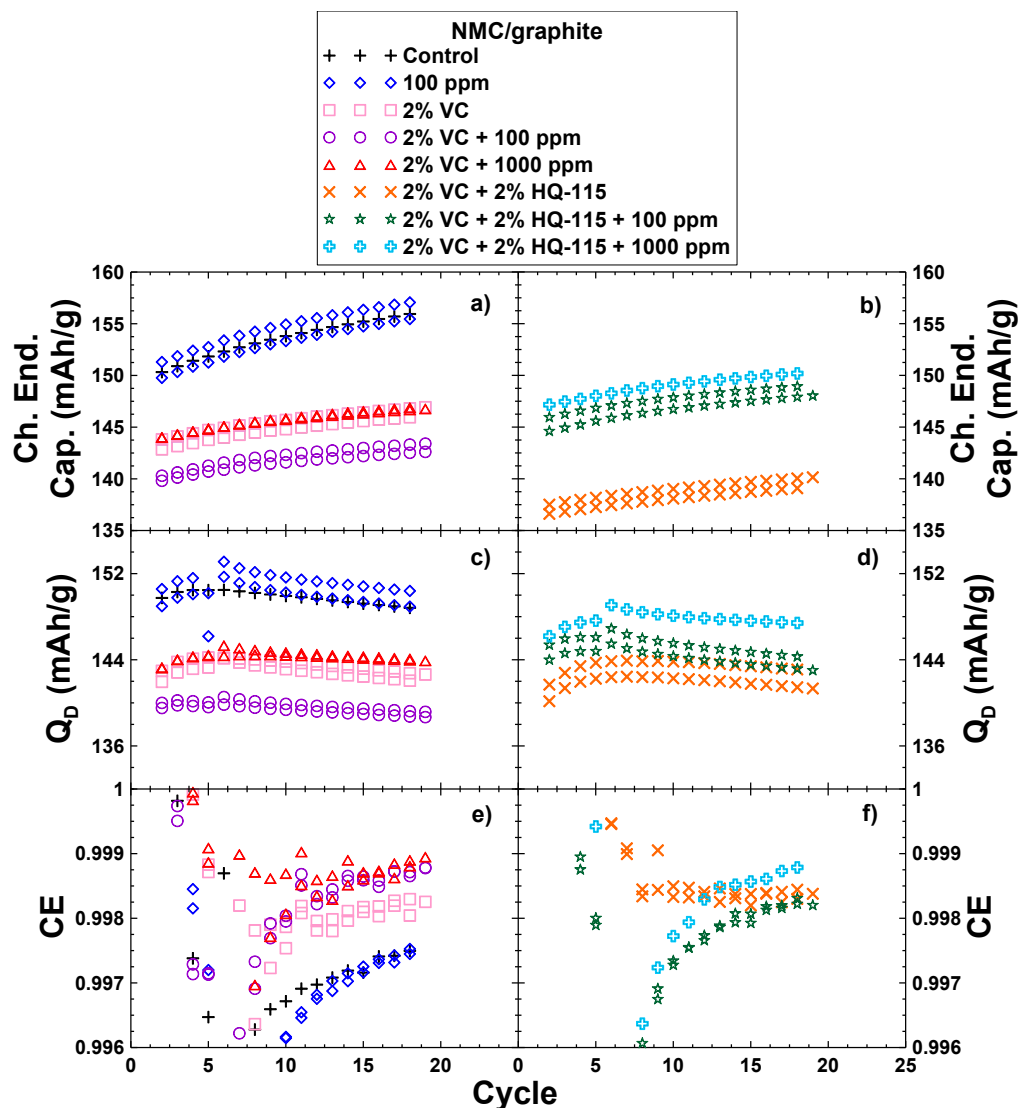


Figure 6.3 Cycling data collected from the HPC for NMC/graphite cells with constant current charge and discharge ( $\sim C/20$ ) at  $40^\circ\text{C}$ . Shown are the charge end point capacity (a, b), discharge capacity (c, d) and coulombic efficiency (e, f) as a function of cycle number. The VC + HQ-115-containing electrolytes are plotted in the right panels for clarity. Pair cells are shown where available.

Figures 6.2 and 6.3 show the cycling data for the  $\text{LiCoO}_2$  and NMC cells, respectively. In both plots the cells containing VC + HQ-115 and varying water content are shown on the right panel for clarity. To evaluate the cycling performance, the charge endpoint capacity (a, b), discharge capacity (c, d) and coulombic efficiency (e, f) are examined during cycling at  $C/20$  for  $\sim 600$  hours. There was a power outage that affected the system and some of the cells at cycle 5. This caused the efficiency of some cells to

drop quickly and then rise back to expected values. A “glitch” is seen in the discharge capacity curves for the affected cells. Duplicate cells show high levels of reproducibility and there is minimal difference in the capacity loss during the cycling on the High Precision Charger. Despite no difference in the fade rates, there are still measurable differences in the coulombic efficiency and charge endpoint slippage. The differences between the cells with and without VC in the electrolyte are clear from this plot but the performance of the remaining cells is very similar. This means that the addition of 100 or 1000 ppm water to the electrolyte does not have a dramatic impact on the cycling performance of the cells. In both the LiCoO<sub>2</sub> and NMC cells, the electrolyte formulation that leads to the highest measured coulombic efficiencies are actually those containing 1000 ppm water with either VC or VC + HQ-115, respectively.

Figure 6.4 and 6.5 show the results of the high precision cycling data in the form of a bar chart for more clarity. Instead of coulombic efficiency,  $1 - CE$  is shown so that lower bars indicate better performance. The coulombic efficiency was calculated as an average of the final three cycles and the charge slippage was calculated from the slope of a linear fit to the final five data points in the charge endpoint capacity versus cycle number plot. In addition to the data from the High Precision Charger, the results of storage and impedance measurements made after cycling on the HPC are also shown through the voltage drop and charge transfer resistance ( $R_{CT}$ ), respectively. All data points come from an average of the two cells for each experiment when available. In each panel, the data is shown in ascending order with the best performance being shown in the smaller bars.

For the cells with LiCoO<sub>2</sub> positive electrodes shown in Figure 6.4, the electrolyte formulation containing VC + HQ-115 + 1000 water shows the best performance in each category except charge slippage where many of the cells have extremely similar, high performance. This is surprising since it is typically believed that trace amounts of water in the electrolyte can lead to very poor cell performance but, in fact, as much as 0.1% water can be added to the electrolyte in many cases and not lead to adverse effects. The added water actually appears to be beneficial in some aspects. Even when 100 ppm water is added to only control electrolyte, the performance becomes only slightly worse in terms of impedance but is virtually unchanged in the other metrics. In most situations,

the addition of HQ-115 to the VC + water electrolytes improves the performance which could indicate an additional benefit of HQ-115 beyond the reduction in impedance shown in the previous chapter.

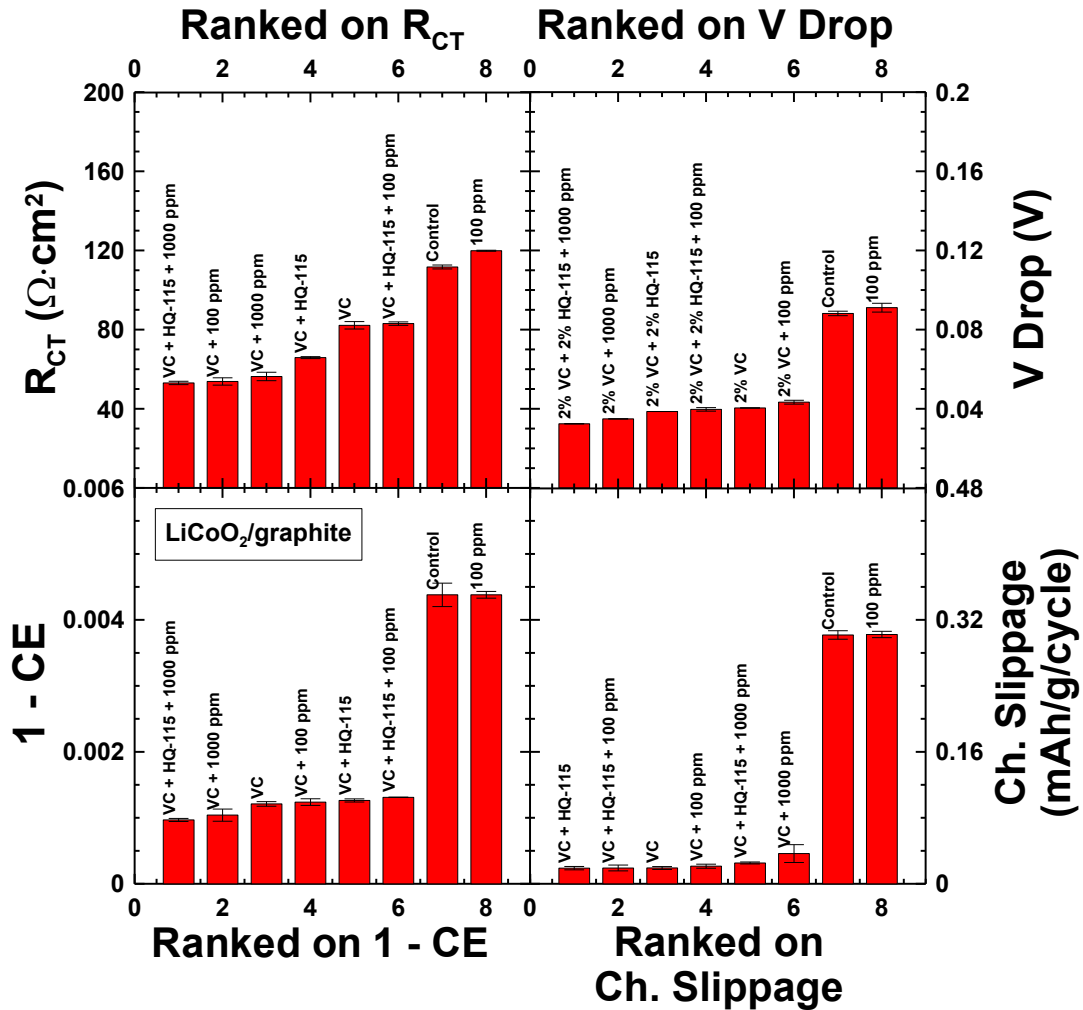


Figure 6.4 A summary of data collected for LiCoO<sub>2</sub>/graphite cells showing the coulombic inefficiency ( $1 - \text{CE}$ ), charge slippage rate, voltage drop during storage (V drop), and charge transfer resistance ( $R_{CT}$ ) for each electrolyte formulation. The data is presented such that lower values in each respective panel represent better performance in that category and each panel is ordered from best to worst for comparative purposes. Data is an average of pair cells where applicable and error bars represent the spread in pair cells.

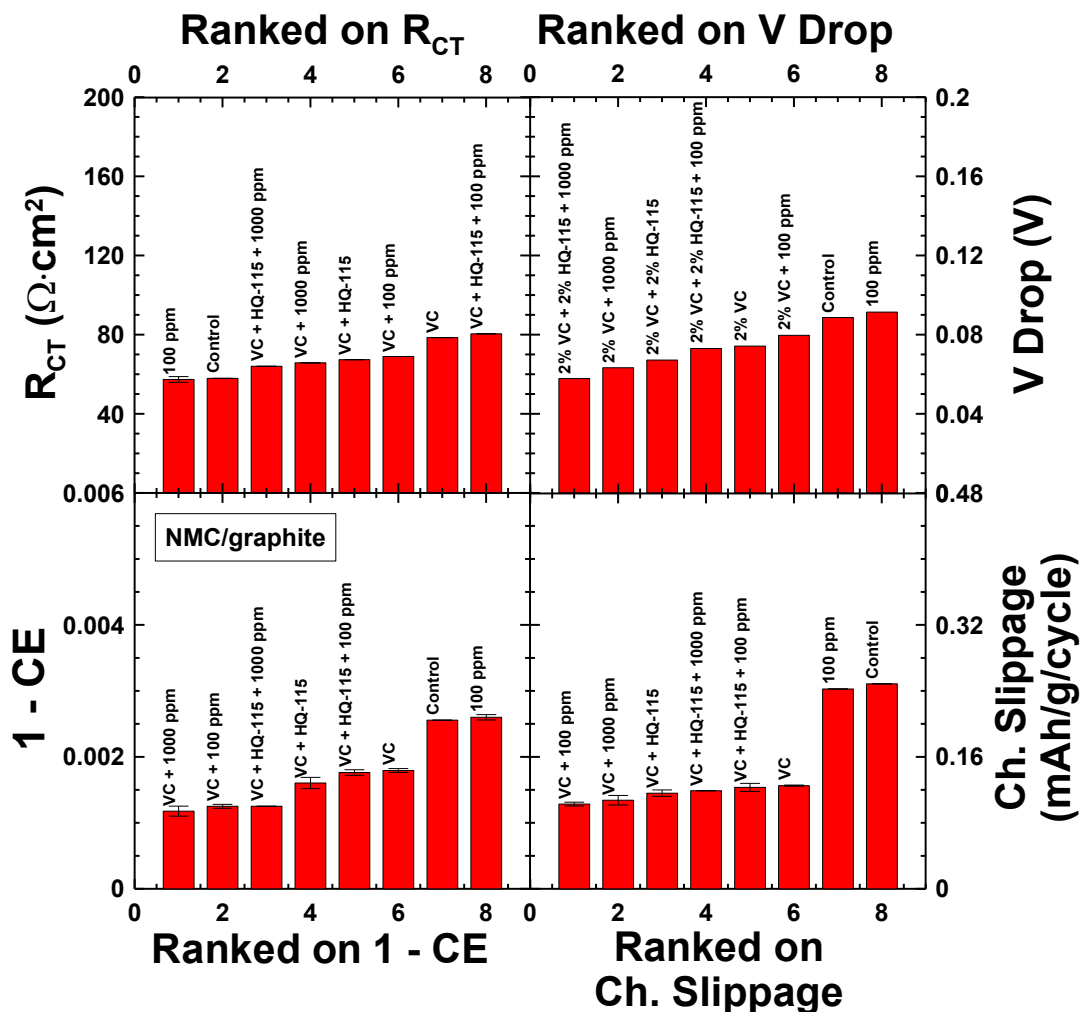


Figure 6.5 A summary of data collected for NMC/graphite cells showing the coulombic inefficiency ( $1 - CE$ ), charge slippage rate, voltage drop during storage ( $V$  drop), and charge transfer resistance ( $R_{CT}$ ) for each electrolyte formulation. The data is presented such that lower values in each respective panel represent better performance in that category and each panel is ordered from best to worst for comparative purposes. Data is an average of pair cells where applicable and error bars represent the spread in pair cells.

For the cells with NMC positive electrodes shown in Figure 6.5, an electrolyte formulation containing water is again the best in each category. Interestingly, the addition of 100 ppm water to control electrolyte leads to the lowest cell impedance. As shown in the previous chapter, the addition of HQ-115 to VC-containing electrolyte reduces the impedance and here it is seen that the addition of 1000 ppm water to VC + HQ-115 containing electrolyte further reduces the impedance. All of these metrics again



suggest that the addition of water to these electrolytes do not have a significant negative impact cell performance but in fact in most cases resulted in better performance.

After cells were cycled on the HPC and the impedance spectra collected, they were cycled through a different voltage window which is not presented here. After that cycling experiment, the cells were put on an older system for long term cycling at  $\sim C/10$  and pair cells were split between 40 and 55°C. If only one cell was available for long term cycling, it was put at 40°C so it would be at the same temperature as the cycling on the HPC. Figure 6.6 shows the capacity versus cycle number during the long term cycling. The capacities in Figure 6.6 do not exactly match those in Figures 6.2 and 6.3 because of capacity loss during the additional cycling between those tests. In addition to the cells tested on the HPC, cells with 1000 ppm water in control electrolyte were made for only the long term cycling experiments based on the results of the short term performance testing. Long term cycling data for the VC + HQ-115 cells was only available at 55°C as it was previously collected from the experiments presented in the previous chapter.

The long term cycling of the cells with LiCoO<sub>2</sub> positive electrodes show minimal difference in fade rates for most cells at 40°C (panel a). As expected, there is high fade rate for those cells without VC in the electrolyte compared to those cells with VC in the electrolyte. Apart from the cell containing VC + 100 ppm water in the electrolyte which shows more capacity loss, the remaining cells show very comparable and small fade rates. At 55°C (panel b) the fade rates for all electrolyte formulations become worse due to the elevated temperature. Again the cell with VC + 100 ppm water in the electrolyte shows the most capacity loss but none of the other cells containing water in the electrolyte show significantly more fade than the non-water containing counterparts. At the elevated temperature, it is possible that any parasitic reactions that could be associated with the addition of water to the electrolyte are more significant even though they did not appear to impact the cycling at 40°C in either the short or long term tests.

The cells with NMC positive electrodes all show greater capacity loss rates than the cells with LiCoO<sub>2</sub> positive electrodes, but many of the same trends emerge. At 40°C (panel c) the cells without VC in the electrolyte show significantly more loss than the cells containing VC. However, when VC is present in the electrolyte there are only small

differences in the fade rate between cells as expected by the similar performance during the short term experiments. There is no evidence that the addition of water to these electrolytes cause any increased degradation rate as was previously believed. At 55°C (panel d) the cells show significantly more capacity loss (note the scale change) but again the cells with water in the electrolyte do not perform worse than the same formulations without the additional water.

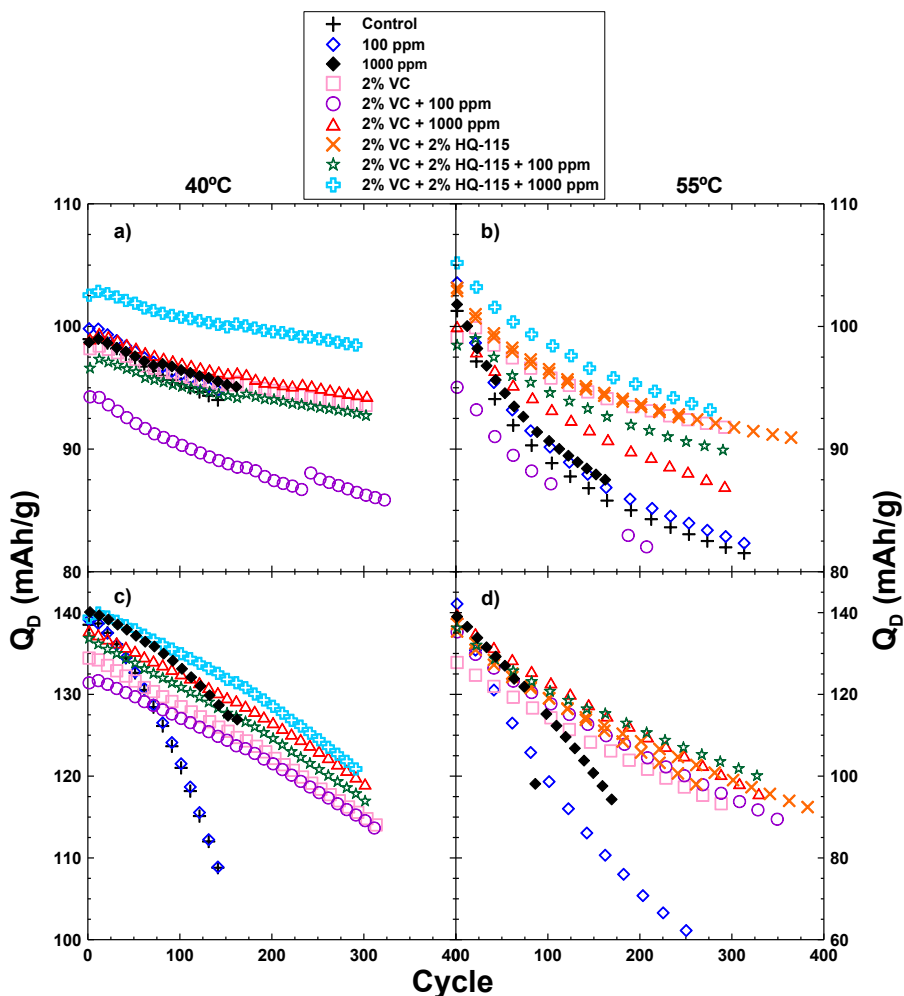


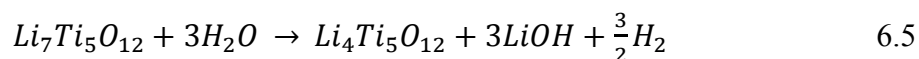
Figure 6.6 Long term cycling of the  $\text{LiCoO}_2/\text{graphite}$  (a, b) and  $\text{NMC}/\text{graphite}$  (c, d) cells at  $\sim C/10$  that were initially cycled on the HPC as well as cells containing 1000 ppm water in control electrolyte that were not cycled on the HPC. Pair cells were split between 40 (a, c) and 55°C (b, d) and if only one cell was available it was put at 40°C so that long term data was collected at the same temperature as initial HPC measurements. Note the scale change between (c) and (d) for the  $\text{NMC}/\text{graphite}$  cells based on the temperature of cycling. Reproduced by permission of The Electrochemical Society [135].

All of the short term metrics showed that water should have no negative impact on the cell performance in terms of cycle life or cell impedance. Surprisingly, many of the high performance cells were those containing at least 100 ppm, often 1000 ppm, water added to the electrolyte. The only negative impact of water in the electrolyte was on the swelling and first cycle IRC which depended on electrolyte formulation. The long term cycling confirmed the results anticipated by the high precision cycling and showed that the impact of water had little detrimental effect on the cycling performance of the cells. Most cells show almost little impact on cycling from additional water in the electrolyte, but the cells with  $\text{LiCoO}_2$  cycling at  $55^\circ\text{C}$  show slightly higher capacity loss rates with increasing water content. In most cases, the use of HQ-115 when water was present in the electrolyte lead to increased performance compared to cells with only VC and intentionally added water. These results suggest that perhaps it is possible to lessen the tight water tolerance allowed in materials and production for Li-ion cells which could lead to lower cost cells with the same performance.

### **6.3 Cells with Lithium Titanate Negative Electrodes**

In addition to studying the impact of water in the electrolyte for cells with graphite negative electrodes, cells with  $\text{LiCoO}_2/\text{LTO}$  electrodes were also studied with water contents up to 2000 ppm. These cells were manufactured for cycling and storage experiments at  $\sim C/20$  with voltage limits of 1.9 – 2.8 V in the same format as the previously studied prismatic cells. The base electrolyte used was again 1 M  $\text{LiPF}_6$  in EC:EMC (3:7 by weight) with experimental groups containing either 200, 1000 or 2000 ppm water. Enough cells were made for HPC cycling as well as cycling/storage experiments at 30, 40, 50 and  $60^\circ\text{C}$ . Based on the electrode configuration, to be discussed in detail surrounding Figure 6.8, the storage experiments were conducted so that the cells went into open circuit storage at  $\sim 90\%$  state of charge, or 2.460 V. Impedance spectra were collected at 2.350 V and  $10^\circ\text{C}$  on a Biologic VMP3 system between 10 kHz – 10 mHz with a 10mV amplitude drive signal collecting 10 points per decade both before storage, to serve as “fresh” cell data, and after HPC cycling.

The first measurements made were on cell swelling through the formation cycle. As seen in the results shown for the graphite based cells, the addition of water results in increased swelling. Without the use of any electrolyte additives in LTO based cells, as more water is added to the electrolyte the amount of swelling from gas production also increases. The cause of this gas is likely from the LTO electrode producing  $H_2$  through a reaction with water [137,138].



The swelling gradually increases as up to 1000 ppm water is included (from ~0.5% up to ~3%) and then increases significantly (~10%) when the water content is increased to 2000 ppm.

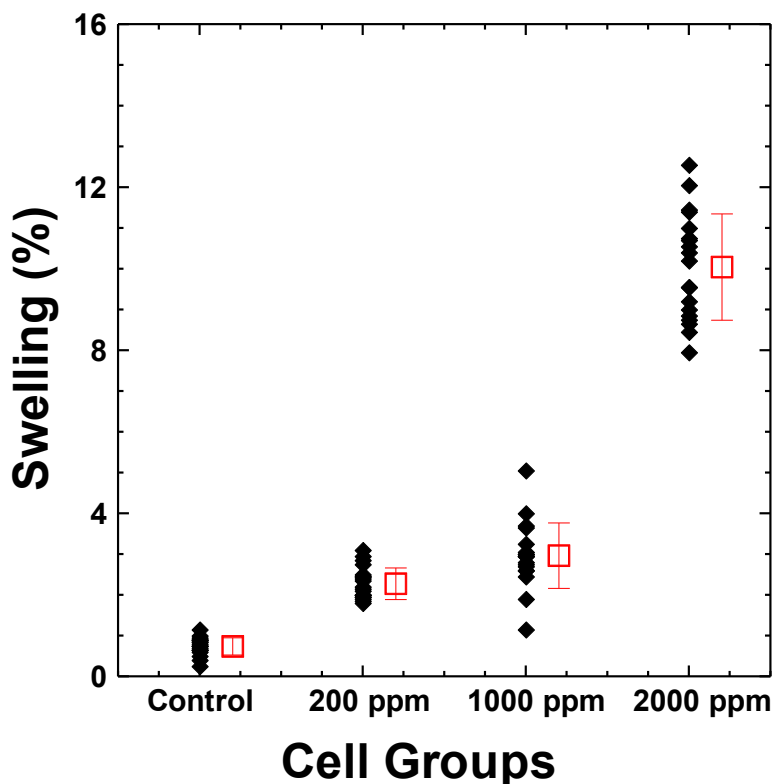


Figure 6.7 The swelling of the prismatic cell case during the formation cycle as a function of the amount of intentionally added water to the electrolyte. An average (red square) with standard deviation error bars for cells with different amounts of water added to the electrolyte is shown next to the data points. Reproduced by permission of The Electrochemical Society [136].

Figure 6.8 shows the voltage profile of a full  $\text{LiCoO}_2/\text{LTO}$  cell in panel (b) (plotted versus specific capacity of the LTO electrode) along with a schematic of the positive and negative electrode voltage versus absolute capacity curves for an early cycle (solid line) and later cycle (dashed line) to show what happens as the cell ages. The voltage profiles used in this schematic are from the same electrodes used in the full cells and were collected in half cells versus lithium metal. These cells were made such that both electrodes are limited by the state of charge of the LTO electrode. In graphite based cells, the fully discharged state is reached when the graphite electrode is fully delithiated and the charged state is reached when the positive electrode reaches a certain amount of delithiation. However, for the LTO cells, the discharge is reached when the LTO becomes fully delithiated and the charged state is reached with the LTO is fully lithiated so that each endpoint is reached with a steep voltage versus capacity curve and the entire capacity of the LTO electrode is utilized.

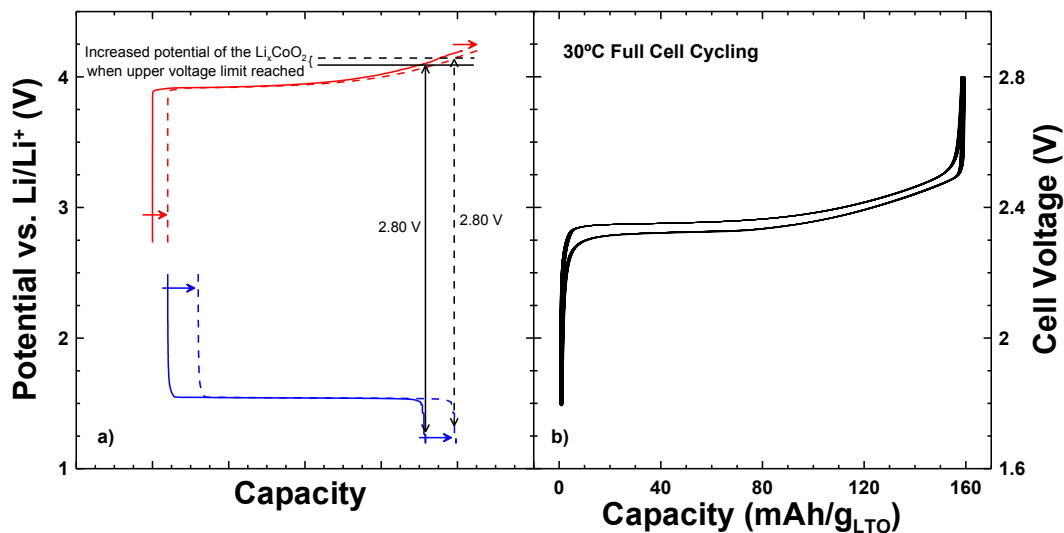


Figure 6.8 Panel a) shows a schematic of the potential-capacity curves for the electrodes of a LTO-limited LCO/LTO cell. The location of each curve on the capacity axis was determined based on the first cycle irreversible capacity difference between the electrodes. The arrows indicate the rate of slippage of each electrode to the right (moving from solid to dashed curves) with cycling from parasitic reactions. This causes the positive electrode to be charged to higher potentials later in cycling as shown by the horizontal solid and dashed lines. Panel b) shows voltage versus specific capacity of the LTO electrode for a full LCO/LTO cell at 30°C demonstrating the charge and discharge voltages seen from the schematic in panel a). Reproduced by permission of The Electrochemical Society [136].

The schematic in panel (a) shows what happens as the cell ages and the electrodes slip to higher absolute capacity, as indicated by the arrow, from the solid lines to the dashed lines. Based on previous long term data, the LTO electrode must slip at a higher rate than the LiCoO<sub>2</sub> electrode or a change in the discharge endpoint would be seen when the cell reached a state where the LiCoO<sub>2</sub> electrode becomes fully lithiated before the LTO electrode becomes fully delithiated during discharge. Therefore, as the LTO electrode slips to the right, it forces the LiCoO<sub>2</sub> electrode to higher relative states of charge before the fully charge state is reached. To compensate for the changes to the state of charge of the LiCoO<sub>2</sub> electrode, the LTO does not reach as low a potential when fully charged but the difference is negligible due to already reaching the point of the steeply varying voltage versus capacity curve. However, this does impact the cell as it causes the average voltage during charge to increase as the LTO electrode remains the same but the positive electrode is driven to higher voltage as described. This should be a measurable change over time to confirm that this is in fact the way that the cell is aging.

Figure 6.9 shows the average charge voltage (top) and average voltage hysteresis, or delta V, (bottom) for cells cycled on the HPC at 30 (left) and 60°C (right). The cells cycled at 40 and 50°C are not shown but fall in the logical trend of decreasing performance (manifested in a more quickly increasing average charge voltage and delta V) as the temperature increases. As expected, the average charge voltage increases with time and at an accelerated rate when cycled at elevated temperature. The voltage hysteresis is relatively flat at 30°C (despite a small decrease in the early cycles) but increases steadily at 60°C. A single cell from the control and 2000 ppm water groups were left on for longer cycling to monitor these trends and there is minimal appreciable difference between the rates of change for the two groups but the average charge voltage is higher for cells containing 2000 ppm water which also leads to a greater value for delta V. Since the rate of change of average charge voltage should be directly related to the electrode slippage within the cell, just the slight difference between the water-containing electrolyte and the control electrolyte from this data indicates that there should be minimal difference in the cycling performance.

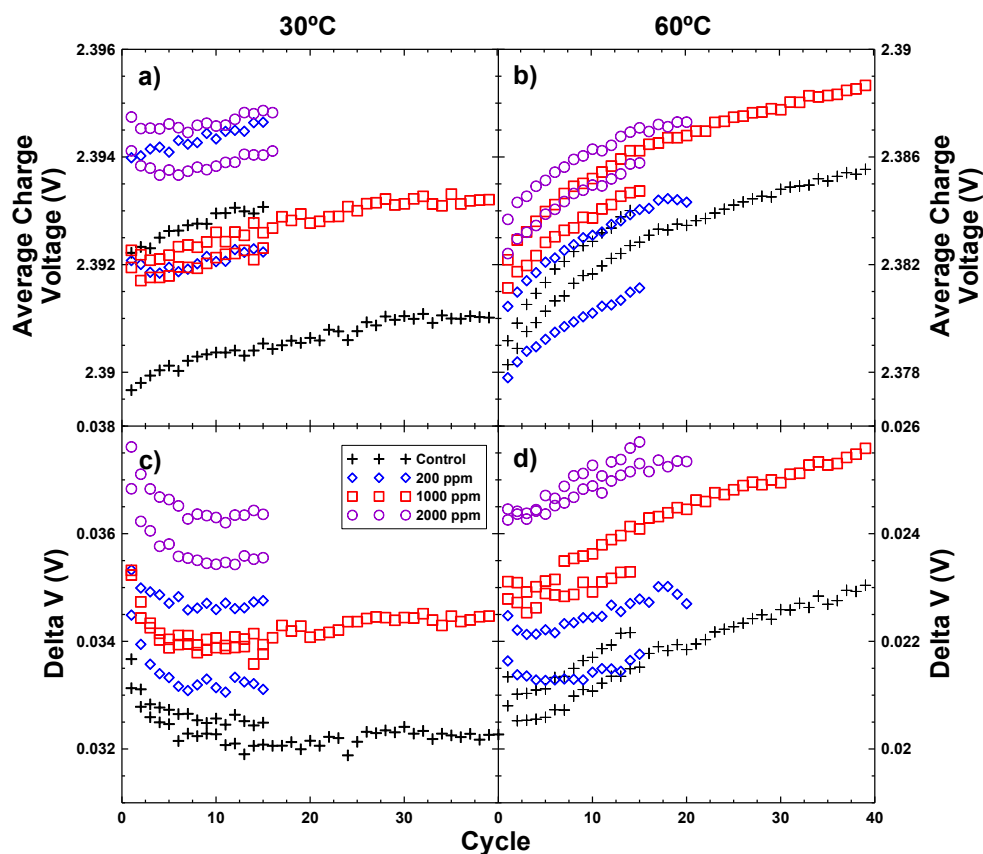


Figure 6.9 Cycling data collected using the HPC for LCO/LTO cells with constant current charge and discharge ( $\sim C/20$ ) at 30 (a, c) and 60°C (b, d). Shown is the average charge voltage (a, b) and difference between the average charge and discharge voltage (referred to as delta V) (c, d) as a function of cycle number for cells with different amounts of water added to the electrolyte. Pair cells are shown where available.

The difference in rates of average charge voltage increase is reflected in the other cycling data collected with the high precision charger. Figure 6.10 shows the charge endpoint capacity, discharge capacity and coulombic efficiency for cells cycled at 30 and 60°C (the same cells as Figure 6.9). It is first worth noting that the coulombic efficiency of cells with LTO negative electrodes is much higher than that of cells with graphite negative electrodes. At 40°C and a  $C/20$  cycling rate, cells with control electrolyte and LTO negative electrodes have a coulombic efficiency of  $\sim 0.9987$  (seen in Figure 6.15) while those with control electrolyte and graphite negative electrodes have a coulombic efficiency of  $\sim 0.9960$  (seen in the previous section). This large difference in efficiency reflects the much lower rate of parasitic side reactions associated with an LTO electrode relative to a graphite electrode that leads to cells with much longer cycle life. Figure 6.10

shows that at 30°C the cycling performance of cells is actually improved by adding 1000 ppm water in terms of a higher coulombic efficiency and smaller charge slippage rate. Interestingly, at 60°C there is almost no difference between the control cell and that containing 1000 ppm water. The largest difference between cells is the difference in reversible capacity (plotted normalized to the active mass of the LTO electrode) which decreases as increasing water content is added to the electrolyte. It is difficult to distinguish the results of the cells containing 200 and 2000 ppm water so those results will be summarized more clearly in Figure 6.15. Therefore the initial results of adding water to the cells with LTO electrodes again indicate that the cell performance does not decrease significantly when water is present in the electrolyte.

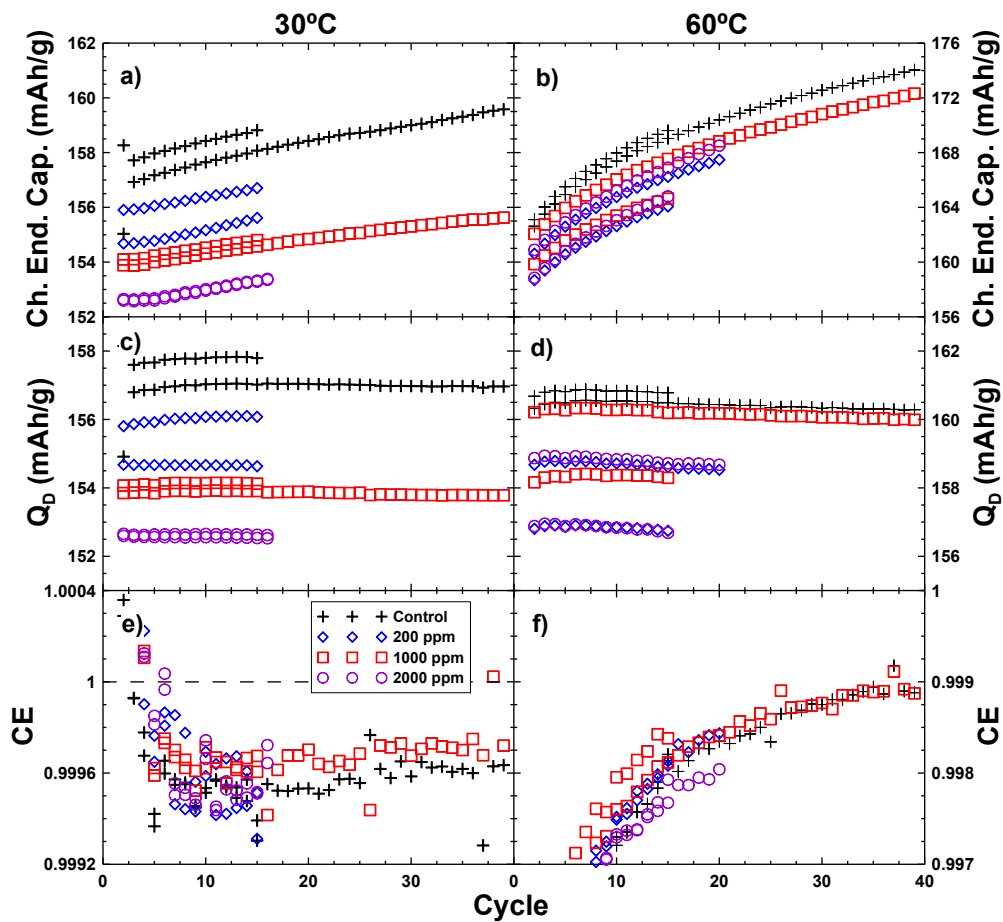


Figure 6.10 Cycling data collected from the HPC for LCO/LTO cells with constant current charge and discharge ( $\sim C/20$ ) at 30 (a, c, e) and 60°C (b, d, f). Shown is the charge end point capacity (a, b), specific discharge capacity (c, d) and coulombic efficiency (e, f) for cells with different amounts of water added to the electrolyte. Pair cells are shown where available.



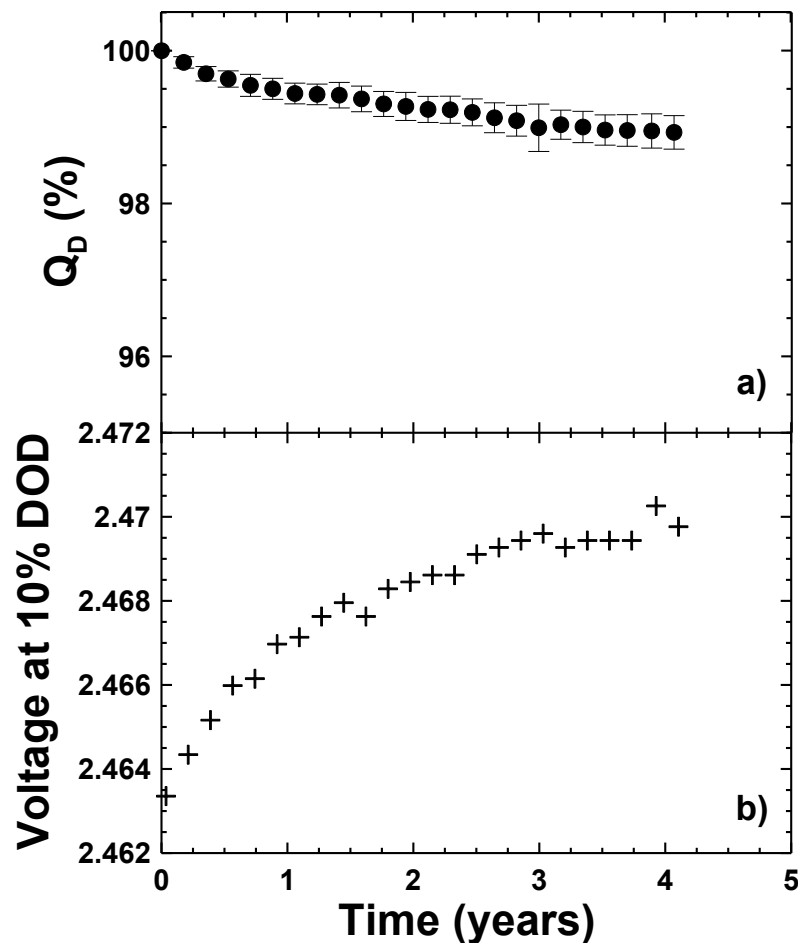


Figure 6.11 Long term (4 years) cycling data from the manufacturer showing the normalized (%) (based on first cycle capacity) discharge capacity (with error bars based on the standard deviation of six cells) (a) and discharge voltage at 10% depth of discharge (b). The data shown in this figure corresponds to control cells.

Figure 6.11 shows data provided by the manufacturer for the same format cells with control electrolyte cycled for over 4 years at 37°C. This cycling was performed over the same voltage limits but with a 2C charge and a discharge at C/168. The data points show the average (standard deviation as error bars) of six cells under test in this experiment. Panel (a) shows the long term performance of these cells with only ~1% capacity loss over 4 years of continued cycling while in Chapter 4 it was shown that the cells with graphite based electrodes lost almost 15% after 4 years of cycling. This is expected based on the much higher coulombic efficiency of the LTO based cells. Panel (b) shows the voltage at 10% depth of discharge (DOD) every 10 cycles. The voltage is increasing over time corresponding to the slippage of the LTO electrode relative to the

LiCoO<sub>2</sub> electrode forcing the positive electrode to higher potentials versus Li/Li<sup>+</sup> and increasing the average voltage. Some contribution to the average charge voltage increase over time could be impedance rise within the cell causing a larger overpotential during charge. Interestingly, this increase in voltage appears to begin leveling off around year 3. This could be because as the positive electrode is taken to higher potentials, its relative slippage rate increases. Therefore if the rate of slippage of the positive electrode matches that of the negative electrode there would no longer be a rise in average cell voltage over time.

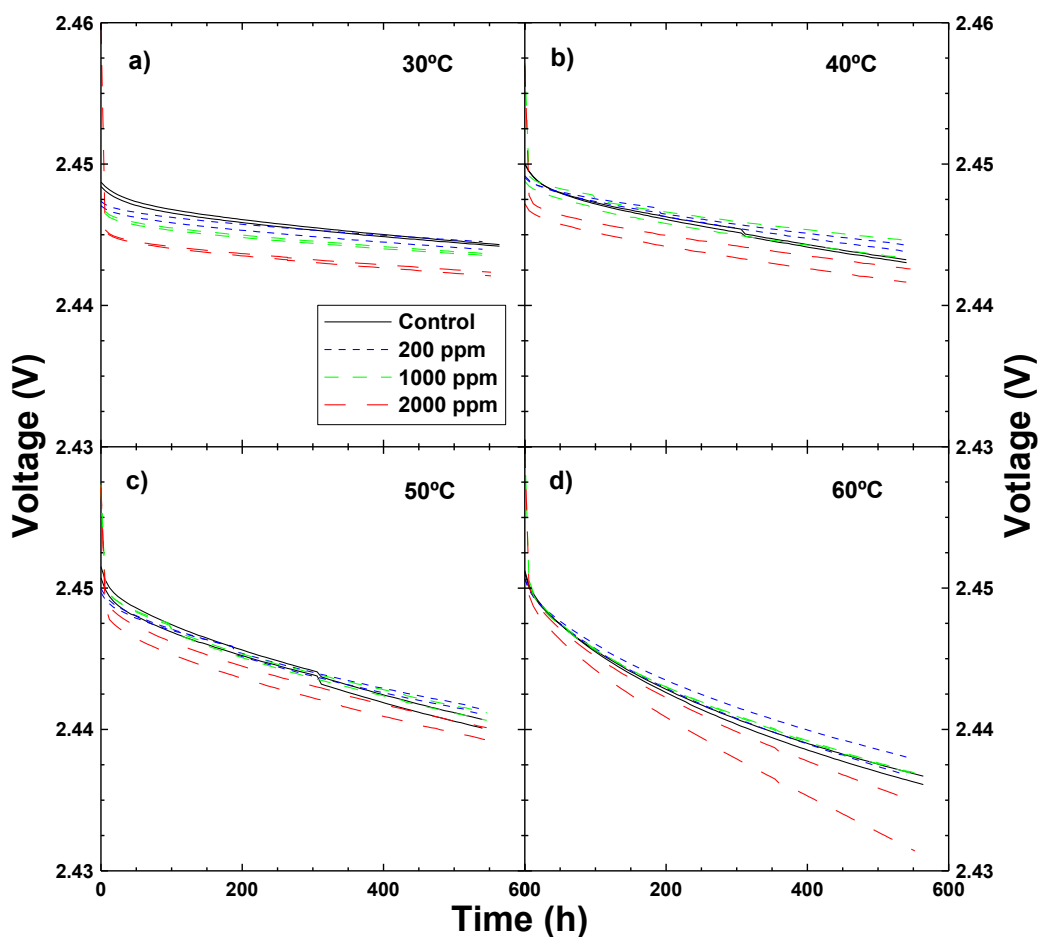


Figure 6.12 Open circuit voltage versus time during storage at 30 (a), 40 (b), 50 (c), and 60°C (d) for cells with different amounts of water added to the electrolyte. The cells were charged to 2.460 V before going into open circuit storage. Pair cells are shown for each group. Reproduced by permission of The Electrochemical Society [136].

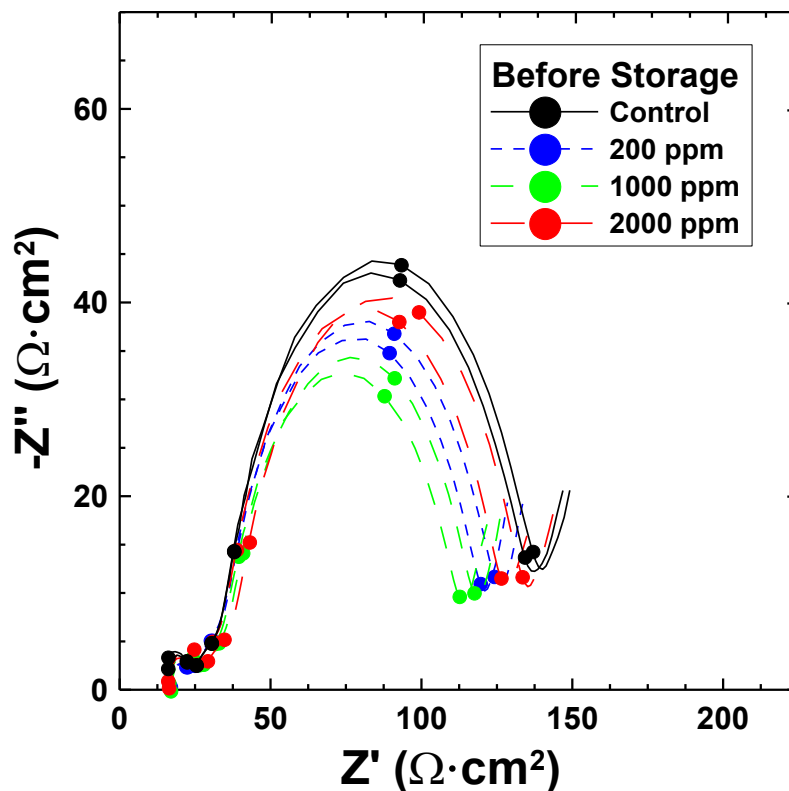


Figure 6.13 Area specific impedance spectra presented as Nyquist plot for data collected at 10°C for cells with different amounts of water added to the electrolyte before storage experiments. The cells were at 2.350 V for these measurements and pair cells are shown. Data points in each set represent 10 kHz, 1 kHz, 100 Hz, 10 Hz, 1 Hz and 100 mHz. Reproduced by permission of The Electrochemical Society [136].

In addition to cycling experiments, automated cycling/storage experiments were also conducted on cells with the same electrolyte formulations. Cycling was done at C/20 with a storage period of ~560 hours. However, instead of storage at 100% state of charge, these cells were stored at 2.460 V (~90% state of charge). This was done so that the storage experiments were representative of the positive electrode performance as the negative electrode must be at a state of charge where the voltage does not change with lithium content. For LTO electrodes, this is the majority of the state of charge window but the endpoints where the voltage changes rapidly with state of charge must be avoided. For cells tested at a given temperature there are only small differences between the rates of voltage drop with the varying water content. In many cases (except at 60°C), the electrolyte formulation with the largest voltage drop is actually the control electrolyte and the addition of water shows lower voltage decay during storage. However, at 60°C the

cells with 2000 ppm water perform quite poorly which may indicate that at high temperature the addition of such high water contents may decrease storage performance. It is also clear that as the water content increases the actual voltage during storage decreases. This is likely due to difference in cell impedance, causing a difference in the overpotential while charging to 2.46 V, which results in the cells quickly relaxing to different voltages. With the exception of high temperature and large water content, the storage performance of cells is not hindered by the addition of water to the electrolyte.

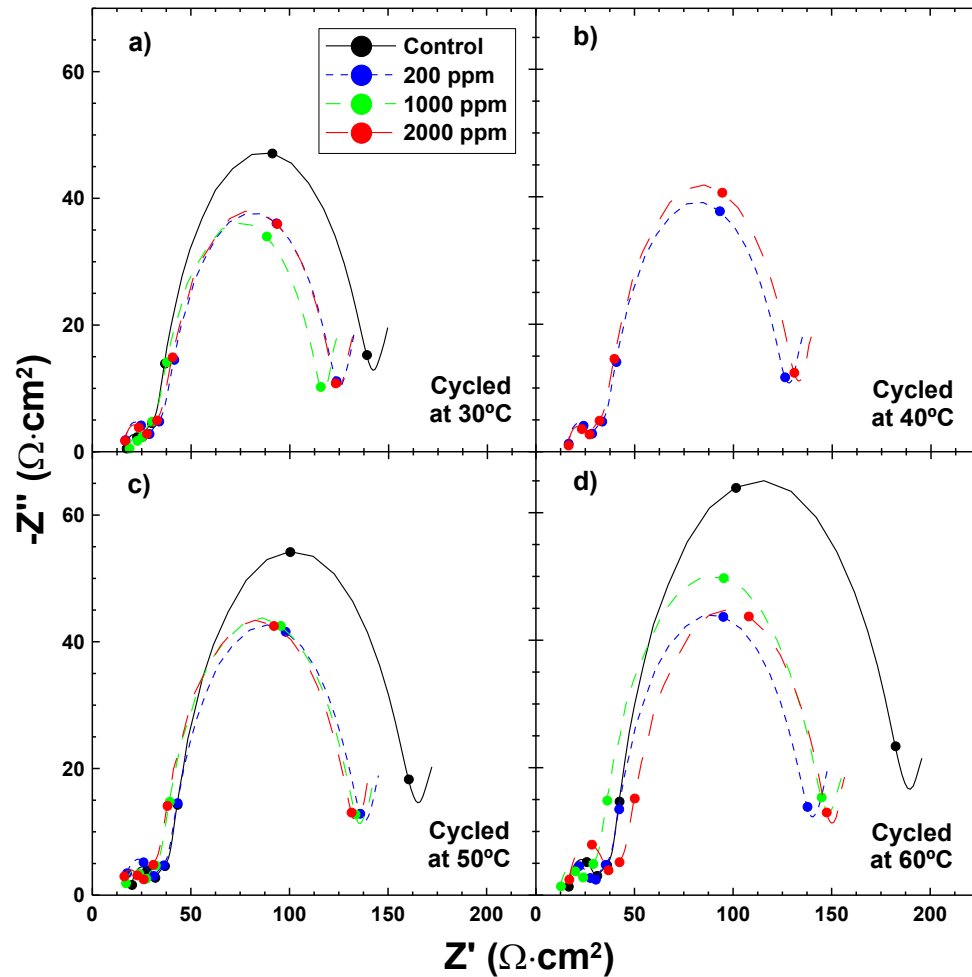


Figure 6.14 Area specific impedance spectra presented as Nyquist plots for data collected at 10°C after cells were cycled on the HPC at 30 (a), 40 (b), 50 (c), and 60°C (d). The cells were at 2.350 V for these measurements and only one cell for each condition is shown as the pair cell was subjected to further cycling. The control and 1000 ppm cell are not shown as the cells were discharged by a faulty scanner card in the EIS system. Data points in each set represent 10 kHz, 1 kHz, 100 Hz, 10 Hz, 1 Hz and 100 mHz. Reproduced by permission of The Electrochemical Society [136].

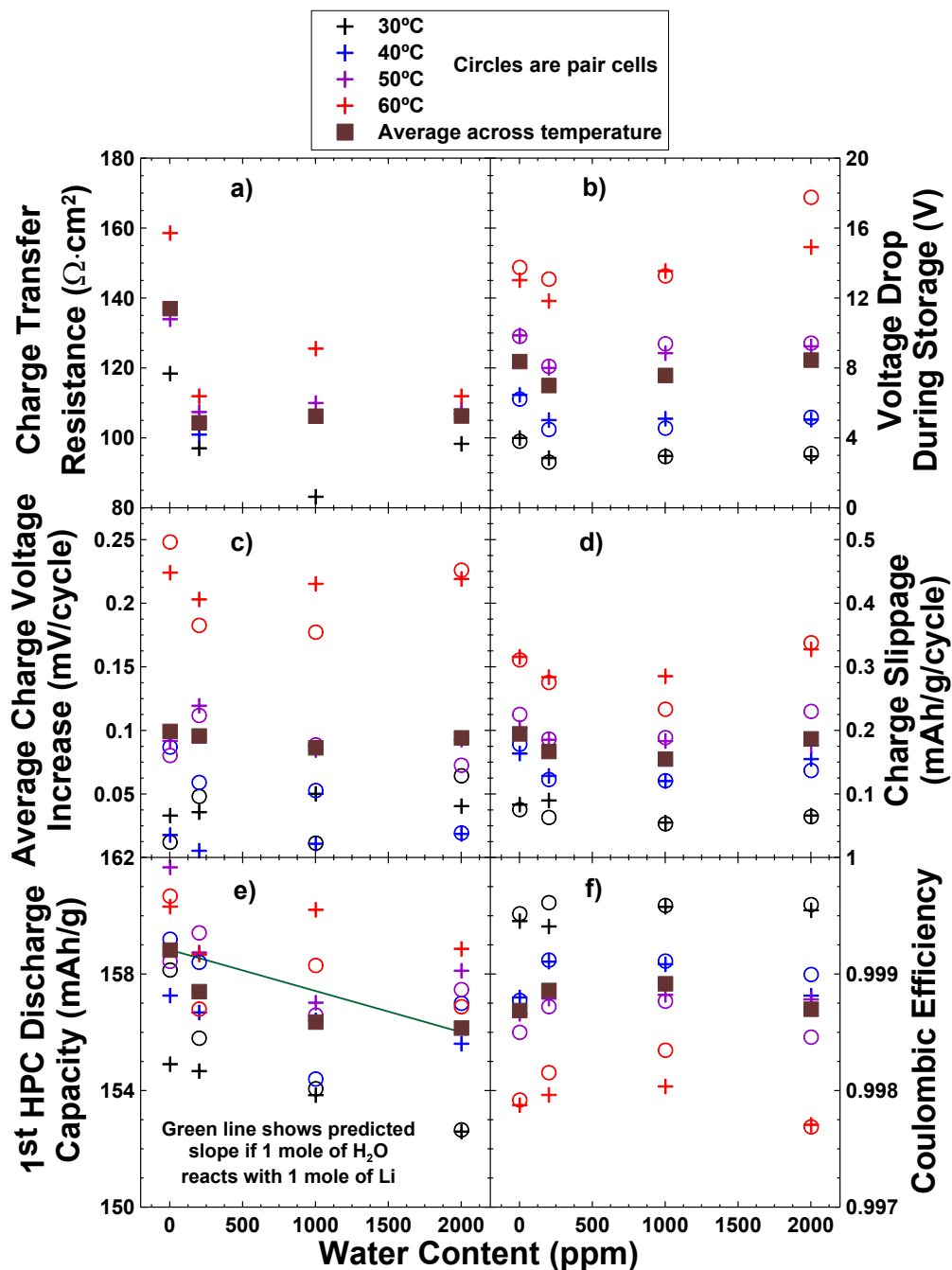


Figure 6.15 A summary of all measured parameters in HPC cycling, storage and impedance measurements as a function of the amount of water added to the electrolyte for each temperature. Shown is the charge transfer resistance (a), voltage drop during storage (b), average charge voltage increase (c), charge slippage rate (d), the discharge capacity of the first cycle measured on the HPC (e) and the coulombic efficiency (f). Both cells are shown, where applicable, for 30 (black), 40 (blue), 50 (purple) and 60°C (red) and averages (over all temperatures) of all cells with a given amount of water added to the electrolyte are shown in brown squares. Reproduced by permission of The Electrochemical Society [136].

The impedance spectra of cells was measured at 10°C both before any testing was conducted and then after cycling at the different temperatures. Unfortunately there was an issue with the equipment that did not measure the spectra for the control and 1000 ppm water cells that had been cycled at 40°C. Figure 6.13 shows the impedance spectra after only formation where the addition of water decreased the charge transfer resistance of the cells. The cell with lowest charge transfer resistance is actually the cell containing 1000 ppm water but when 2000 ppm water is added to the electrolyte, the charge transfer resistance increases. Figure 6.14 shows that regardless of the temperature that cells were cycled at the cells containing water in the electrolyte retain lower charge transfer resistance relative to control electrolyte. The impedance spectra grow after cycling and those cells cycled at a higher temperature show a larger increase in charge transfer resistance compared to lower temperatures. This is likely due to the higher rate of reactions forming thicker passivation films on the electrodes at elevated temperature. While the cells with 1000 ppm water do not always have the lowest charge transfer resistance after cycling, the differences between the charge transfer resistances of cells containing any water is quite small and are all significantly less than the control electrolyte.

In an attempt to quantify the full impact of water concentration on cell performance, Figure 6.15 shows a summary of all metrics as a function of water content. Each panel shows pair cells (when available) for each temperature in a cross and circle. The brown squares represent an average across pair cells at all temperatures for a given added water concentration in the electrolyte to look for general trends in each metric. The green line in panel (e) represents the slope of a line that would result from a reaction of one mole of lithium with one mole of added water to the electrolyte which would lead to a decrease in capacity after formation. In all panels except that related to the first discharge capacity measured on the HPC, the highest performing cells at all temperatures contain some added water to the electrolyte. In several instances it appears that the addition of 2000 ppm water at 60°C testing leads to poorer performance than control electrolyte but all other concentrations and temperatures tend to be better or comparable to the performance of control electrolyte.

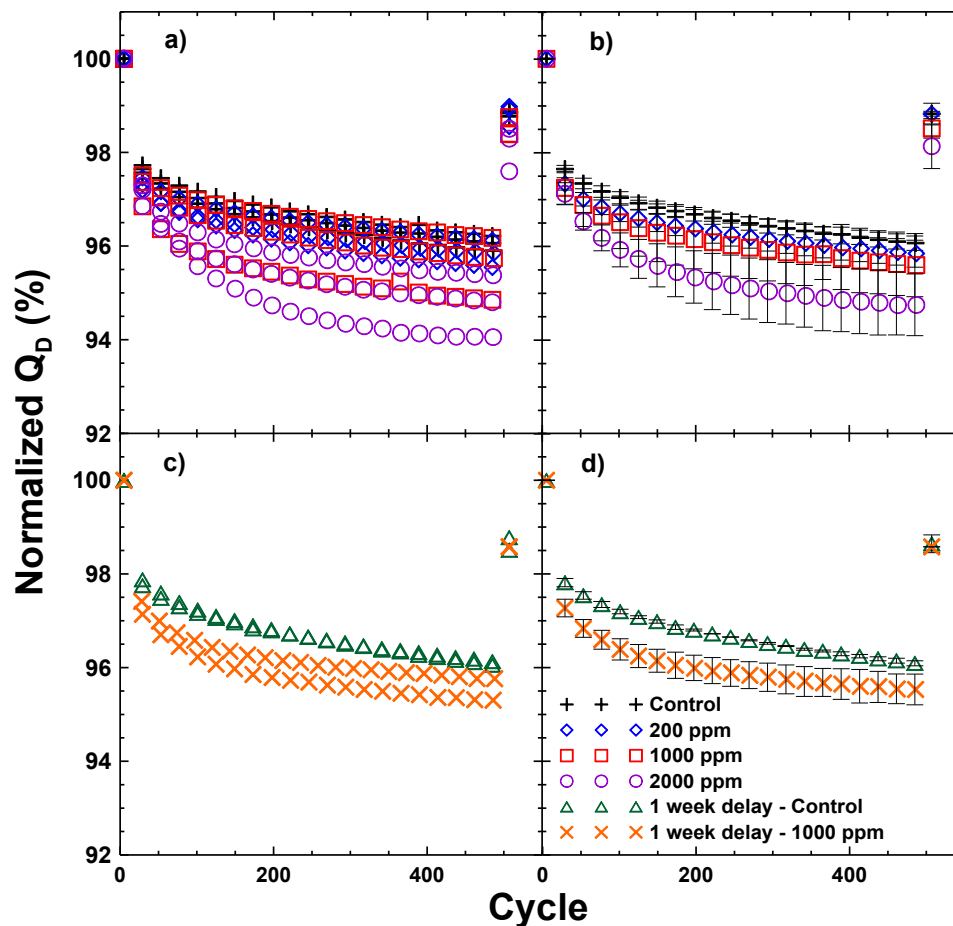


Figure 6.16 Normalized capacity (%) versus cycle number for three cells with control electrolyte and electrolyte containing 200, 1000 and 2000 ppm water (a) and the average for those cells with standard deviation error bars (b). Also shown in the normalized capacity versus cycle number for pairs of control cells and cells containing 1000 ppm water that were formed one week after being filled with electrolyte (c) and the averages for the two cells (d). Slow rate discharges ( $C/168 - 1$  week) were conducted at the beginning of cycling and again after 500 cycles. Except for the two slow rate discharges, the cells were all cycled with a 2C charge and C-rate discharge.

In addition to the cells made for the short term HPC and storage studies, the manufacturer cycled the same electrolyte formulations at 37°C. Figure 6.16 shows the cycling data measured with a 2C charge and C-rate discharge except at the beginning and end (at 500 cycles) where a  $C/168$  discharge cycle was conducted. The right hand panels show an average and standard deviation error bar for the set of cells made with each electrolyte formulation. These results show that the added water has minimal impact on long term performance at high or low rates in terms of capacity retention except for the

cells containing 2000 ppm water which show slightly higher capacity loss. The bottom panels show results for cells that had electrolyte added to cells that were then stored for one week before the formation cycle. Only control cells and cells with 1000 ppm water in the electrolyte were made for this study. These results show that the additional water leads to slightly higher loss during high rate cycling but show minimal to no impact on the low rate discharge capacity after 500 cycles. Without knowing the impedance of these cells it is difficult to gauge the impact of the delayed formation in the presence of water but the long term capacity retention is better compared with the low rate cycle that shows no impact from the addition of water.

This chapter has presented the impact of relatively high concentrations of water added to the electrolyte in both cells with graphite and LTO negative electrodes. Despite conventional wisdom in the industry, the results show that in most cases the addition of water shows benefits in short term performance metrics such as coulombic efficiency, charge slippage and charge transfer resistance. The one notable exception is the addition of 2000 ppm water in the cells with LTO negative electrodes when tested at 60°C. The long term cycling data collected confirm that there are no major detrimental impacts to adding water to the electrolyte in terms of cycle life and in some cases the cells that showed the best long term cycling performance contained water in the electrolyte. These results suggest that there may be potential cost savings in the manufacturing of both materials and cells where currently the allowable tolerance on water concentrations is very low (typically < 20 ppm). These tolerances may be raised without impacting the long term performance of the cells.



## Chapter 7      Electrolyte Additive Testing in “Zero-Fade” Cells

The previous chapters have shown that short term measurements of the coulombic efficiency and endpoint slippage rates of cells can be used as a good predictor of lifetime, especially when comparing between cells where the only variation is the electrolyte formulation. However, most of these cells (all but the cells with LTO negative electrodes) show steady capacity loss over time during cycling due to continual loss of active lithium to the growth of the SEI layer on the negative electrode. Figure 7.1a shows the general capacity loss of such cells plotting the normalized capacity versus cycle number. Through traditional cycling, estimates of capacity loss rates can be made from the capacity versus cycle number plots in order to estimate lifetime (recall that cells can eventually still show “roll-over” failure after gradual capacity loss as shown in Figure 5.8b).

Li-ion cells can also be made in such a way that there is almost no capacity loss during cycling before they reaching a point where rapid capacity loss and failure occur very quickly. Figure 7.1b shows an example of two cells that show this “roll-over” failure mode but have identical capacity loss rates before failure. It is virtually impossible to distinguish between the performance of cells that show this failure mode unless they are cycled until failure which takes too long for developing new cell chemistries geared towards long life (10+ years) applications. However, these cells must still have inefficiencies that eventually manifest in this failure mode. These inefficiencies should therefore still be detectable through high precision coulometry where the cells with higher coulombic efficiency, and therefore lower rate of parasitic reactions, should achieve more cycles before showing this rapid failure. In order to not lose capacity with cycling, the dominant side reaction within the cell must not be growth and formation of the SEI but rather a reaction that is balanced by slippage of the positive electrode. If the slippage rates of both the positive and negative electrode are the same due to an equal amount of parasitic side reactions occurring at each electrode, a cell can cycle without capacity loss but the coulombic efficiency would not be equal to 1.0000 [11].

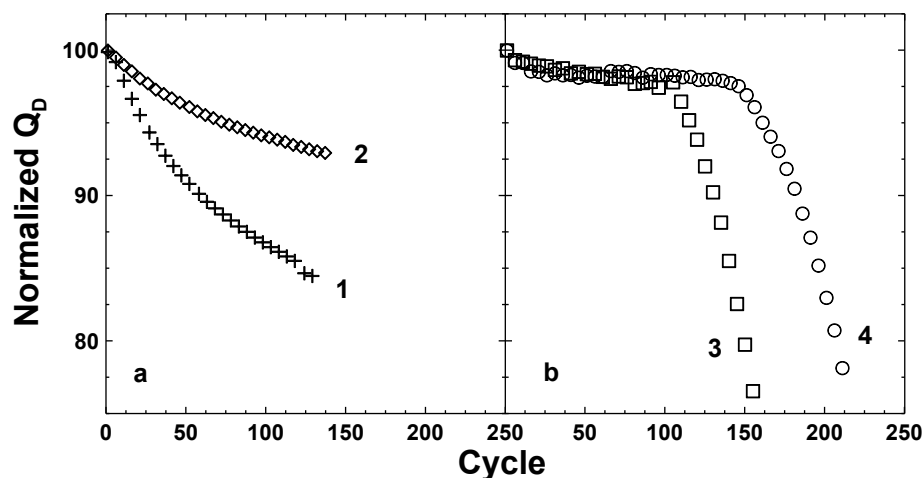


Figure 7.1 Normalized discharge capacity (%) versus cycle number showing examples of gradual capacity loss (cells 1 and 2 in panel a)) and rapid “roll-over” capacity loss (cells 3 and 4 in panel b)). Reproduced by permission of The Electrochemical Society [44].

## 7.1 Experimental Details

In order to study this type of “roll-over” failure mechanism, one hundred and sixty 18650 style  $\text{Li}[\text{Ni}_{1/3}\text{Mn}_{1/3}\text{Co}_{1/3}]\text{O}_2/\text{graphite}$  cells with a nominal 2.0 Ah capacity that were known to exhibit this type of failure were made by E-One Moli Energy [44]. The manufacturer stated that the cycle life of the cells could, to an extent, be controlled by the porosity of the negative electrode. Highly compacted negative electrodes with low porosity would lead to cells with much shorter cycle lives than cells with highly porous graphite electrodes. Therefore, the cells made for this study had highly compressed negative electrodes so that the experiment could be completed in a reasonable length of time. The base electrolyte for all cells is proprietary but different electrolyte additives were added at 1.5 wt.%. Nine electrolyte additives were studied singly and in different combinations. Four of the additives, vinylene carbonate (VC), fluoroethylene carbonate (FEC), vinylethylene carbonate (VEC) and 1-3 propane sultone (PS), are commonly known additives. The other five additives were proprietary to the manufacturer. The cells with known additives were labeled by the additives present while the cells with proprietary additives were labeled with a three character code such as 3UA indicating

blend A with three unknown additives, or 2UE which indicates blend E with two unknown additives. Pair cells were made for both HPC cycling and automated cycling/storage experiments.

Cycling of cells on the HPC or during cycling/storage experiments was done at 30°C between 2.5 – 4.2 V at a charge/discharge rate of C/20. After cells were cycled on the HPC, the impedance spectra were collected at 10°C using a Biologic VMP3 from 100 kHz – 10 MHz collecting ten points per decade. Then all the cells were sent back to the manufacturer for long term cycling. The extended cycling at the manufacturer was done at room temperature. The charge consisted of a 2 A constant current step until 4.2 V when the cell was switched to a constant voltage step to hold at 4.2 V until the current decreased to 100 mA. The discharge used a constant current of 2 A to 2.5 V (a nominal 1C discharge rate). Storage experiments were conducted with two 550 hour storage periods with a discharge, one full cycle and recharge between the two storage periods. The storage experiments will not be presented here but trends agreed well with the HPC results.

The set of known electrolytes was decided by the author and Dr. Jeff Dahn. All cell testing and analysis was done by the author. Long term cycling data was collected by E-One Moli Energy.

## 7.2 Results

Figure 7.2 shows several interesting results of the entire experiment in a short summary with results from 5 different electrolyte formulations. Panel a) shows the first 50 cycles conducted by the manufacturer AFTER cycling on the HPC (~650 hours). Apart from the cells containing VC + FEC which appear to have a higher rate of capacity loss over the first fifty cycles, the rest of the cells shown are fairly similar. If one was to attempt to rank the performance of the cells from these first cycles it appears that the cells containing VC or FEC are quite good, cells containing 2UB or VC + VEC + FEC + PS are slightly worse and the cells containing VC + FEC would be considered the worst. Figure 7.2c shows all of the cycles collected by the manufacturer until failure. Cell

failure was defined when the capacity reached 1.6 Ah (80% of the nominal 2 Ah rating). From shortest to longest cycle life the cells are: FEC, VC, VC + FEC, 2UB, and VC + VEC + FEC + PS. This is not the order expected by examining the capacity loss rates in the first 50 cycles. In fact, with the ability to only measure cell capacity it would be impossible to reliably know the long term performance of these cells without cycling all cells until failure.

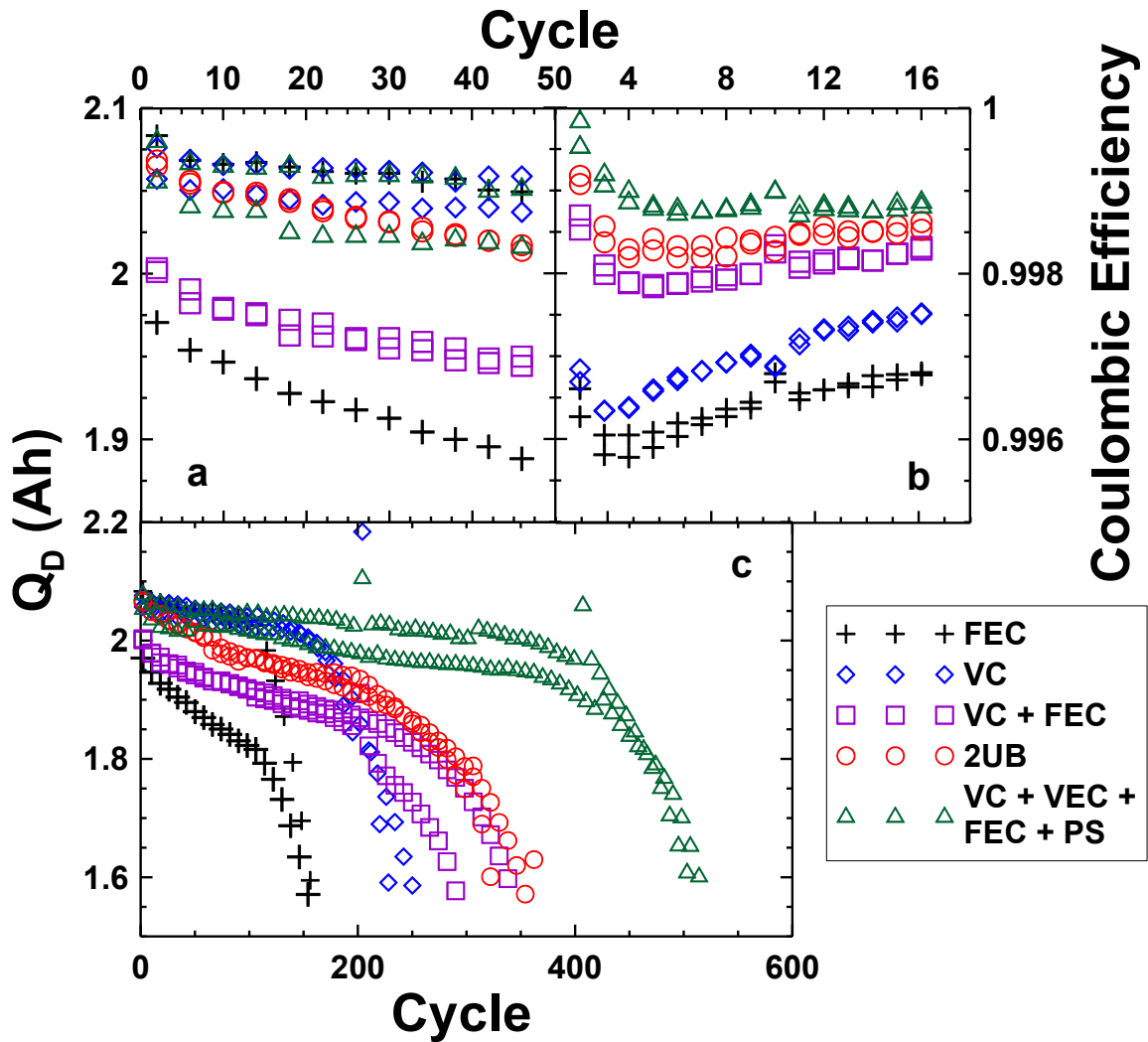


Figure 7.2 a) Capacity versus cycle number for the first 50 1C cycles, after low rate HPC cycling, of the NMC/graphite 18650 cells with the additives listed in the legend; b) coulombic efficiency for the same cells as a) measured during the first 16 C/20 cycles after formation using the high precision charger and c) capacity versus cycle number for the same cells as a) showing all 1C long term cycling data until failure at 1.6 Ah.

Figure 7.2b shows the measurements of coulombic efficiency made on the HPC before the cells were sent for long term cycling at the manufacturer. Despite negligible differences in the capacity loss rates, there are clear differences in the coulombic efficiencies. Therefore, using coulombic efficiency as a predictor for long term performance, it would be expected that the cells would fail in order from low to high efficiency which is exactly the same order that the cells reach 1.6 Ah in the long term experiments. This means that these slight differences in cell performance can be detected by coulombic efficiency despite showing minimal difference in capacity loss rates until failure.

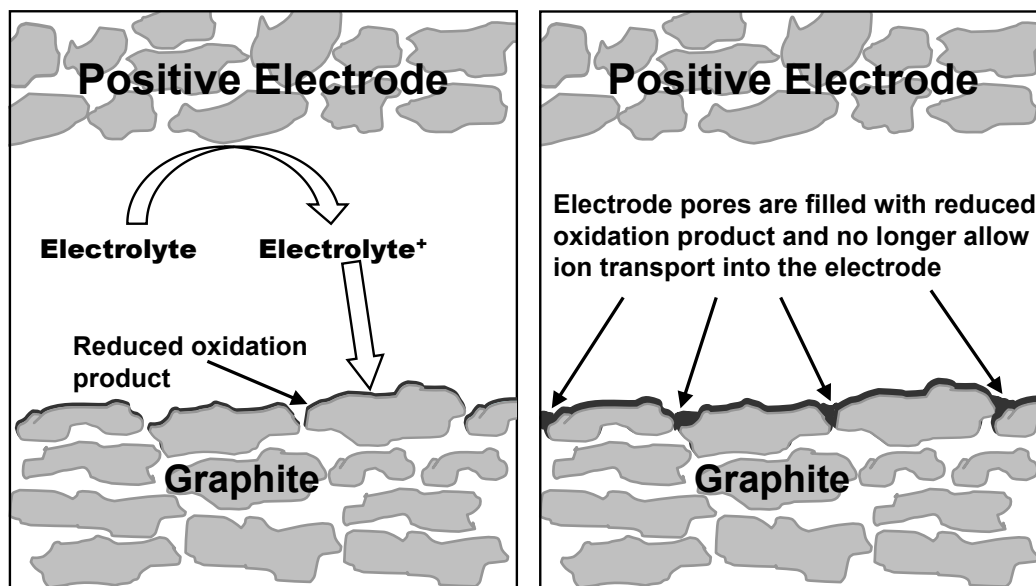


Figure 7.3 Schematic model of a process that could cause “roll-over” failure in Li-ion cells with highly compressed negative electrodes after a sufficient number of charge-discharge cycles. Reproduced by permission of The Electrochemical Society [44].

Since the coulombic efficiency is not 1.0000, there must be parasitic reactions occurring that do not lead to the consumption of active lithium within the cell as that would manifest as capacity loss. If no lithium is consumed but the coulombic efficiency is not 1.0000 then there may be a shuttle type reaction where electrolyte is oxidized at the positive electrode and the oxidized species is then reduced at the negative electrode which transfers charge within the cell that is not associated with  $\text{Li}^+$  intercalation/deintercalation leading to a lower coulombic efficiency [11]. Such

electrode-electrode interactions have been proposed previously [139–141]. Figure 7.3 illustrates how this type of reaction could lead to the deposition of an inactive layer on the negative electrode that eventually clogs the pores and does not allow lithium transport from the electrolyte into the electrode during the charging process. This proposed reaction mechanism explains why the porosity of the negative electrode can be used to extend the cell lifetime because with a more porous negative electrode, the pores would simply take longer to become completely clogged and therefore the cell could function for more cycles until the “roll-over” failure is reached.

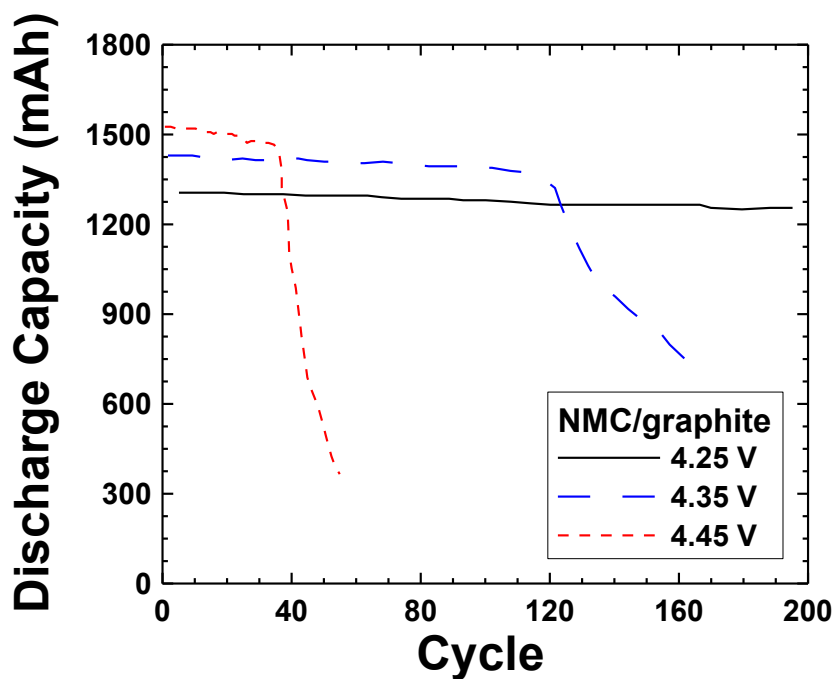


Figure 7.4 Capacity versus cycle number for NMC/graphite cells cycling to different upper cut-off limits to illustrate the impact of high voltage on “roll-over” failure. Note: these are not the same style cells as the rest of the cells presented in this chapter.

It is possible that this type of shuttle reaction could begin with electrolyte reduction at the negative electrode and the reduced species could migrate to the positive electrode where it is oxidized to form an inactive layer at the positive electrode. Figure 7.4 shows the cycling performance of a different set of NMC/graphite 18650 cells cycling to different upper cut-off voltages that also show “roll-over” failure after extended cycling. The three cells were all balanced to be cycled to 4.45 V but one was only

charged to 4.25 V and another to 4.35 V. There is a strong dependence on the cycle life of these cells depending on the upper cut-off voltage where the higher voltages cause cell failure much sooner. This implies that the parasitic reaction causing failure is rate limited by the positive electrode as it is accelerated (causing earlier cell failure) by increasing the cell voltage. If the parasitic process began with electrolyte reduction at the negative electrode, it would probably be independent of the upper cut-off voltage of the cell as the potential of the graphite is constant at high states of charge and therefore the change in cell voltage comes entirely from the positive electrode at high state of charge.

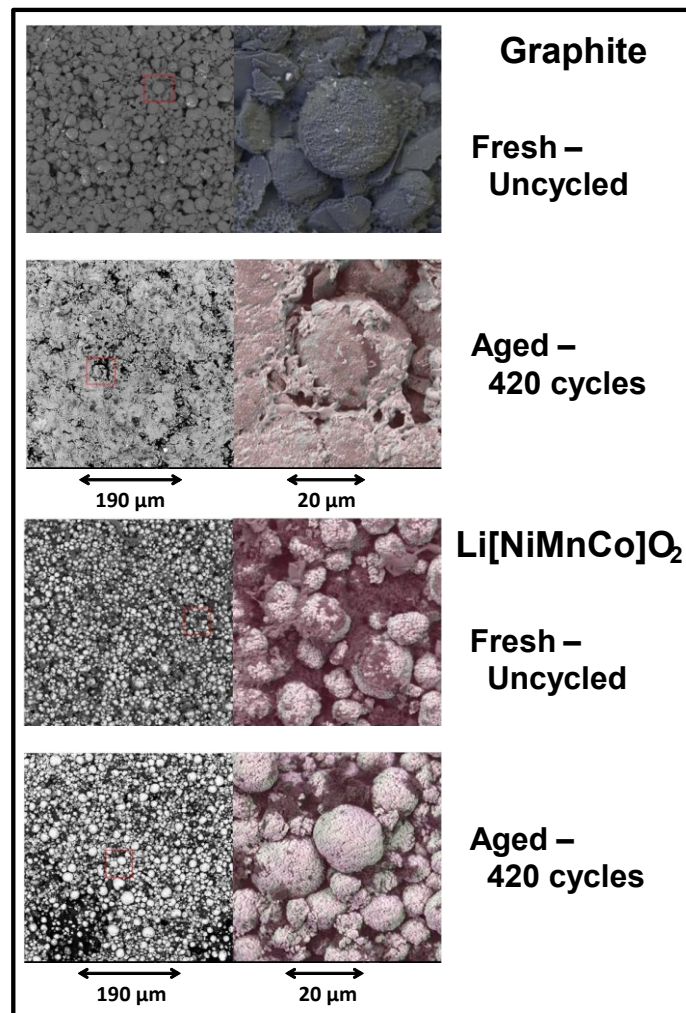


Figure 7.5 SEM micrographs of uncycled electrodes and cycle electrodes from cells with VC + VEC + FEC electrolyte additives. The negative electrode surface has been covered with a film of unwanted reaction products while the positive electrode appears totally unchanged. Reproduced by permission of The Electrochemical Society [44].

Since the proposed mechanism for cell failure is the clogging of the porosity in the negative electrode, this should be visible upon inspection of aged electrodes. Figure 7.5 shows SEM images of electrodes taken from cells after failure. Cells were discharged to 0 V before opening in a glovebox and transferring to the SEM for imaging. For comparative purposes, a fresh cell was also disassembled for inspection. When imaging the fresh negative electrode, the spherical graphite particles are clearly visible. There is also binder and conductive carbon that can be seen in addition to the graphite particles. Images of the aged negative electrode show a layer of material on the top surface of the electrode making it difficult to even distinguish the graphite particles. This material is the proposed inactive layer that leads to the clogging of pores and eventual cell failure. In contrast to the negative electrode, the fresh and cycled positive electrodes look almost identical. This further confirms the premise that the parasitic reaction begins with electrolyte oxidation but results in a layer of inactive material on the graphite electrode that leads to kinetic hindrance and eventually causes failure.

The coulombic efficiency is a measure of the efficiency of lithium intercalation and deintercalation during charge and discharge and therefore the difference between unity and the measured coulombic efficiency is a measure of the charge transferred by parasitic reactions during a full cycle. In these cells, the dominant parasitic reaction must be the shuttle of oxidized electrolyte to the negative electrode where it is reduced since there is no appreciable capacity loss during the early cycles. Therefore  $1 - CE$  is a measure of the rate of this reaction and should be related to the amount of inactive material forming on the negative electrode each cycle. Since all cells manufactured for this experiment have the same negative electrode porosity, after a certain amount of inactive material has been deposited on the negative electrode it should cause failure in any of the cells. This allows for a quantitative prediction of the onset of rapid failure to be made using the coulombic efficiency.

$$(1 - CE) * (\textit{Cycles until failure}) = (\textit{Constant}) \quad 7.1$$

$$(\textit{Cycles until failure}) = (\textit{Constant}) / (1 - CE) \quad 7.2$$





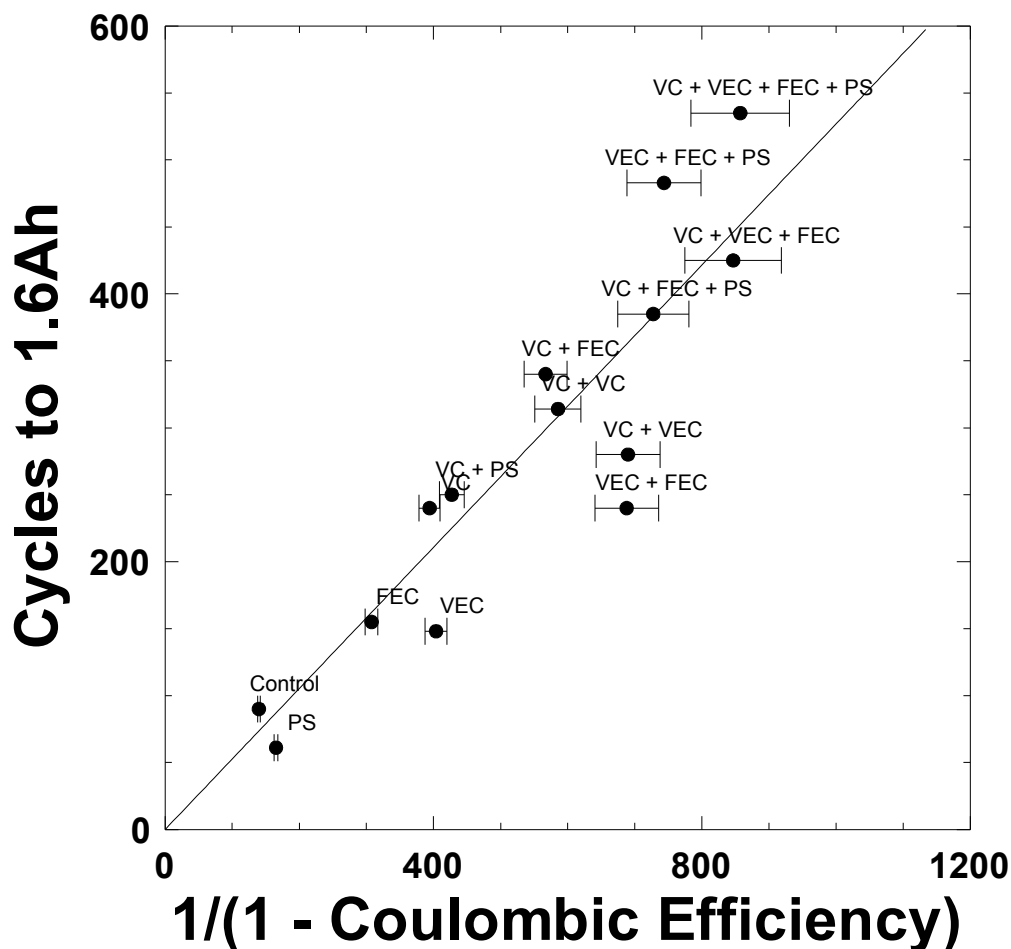


Figure 7.7 The number of cycle until failure (capacity reaching 1.6 Ah) versus  $1/(1 - CE)$  for the cells with known electrolyte compositions. This data is a subset of the data seen in Figure 7.6 but shown here for clarity. The solid line is the same fit seen in Figure 7.6.

Since there is negligible fade in these cells (especially during the early cycles on the HPC), the coulombic efficiency is driven away from unity due to the charge slippage. In earlier discussions, it was brought up that charge endpoint capacity slippage is a measure of the oxidation rate of electrolyte and thus seemingly should be used in this prediction. However, Figure 7.6a shows the direct relationship between the charge slippage and the coulombic efficiency for all cells tested. There is a strong linear relationship and thus the inverse of charge slippage could replace  $1 - CE$  in Equations 7.1 and 7.2 and it would change the calculated constant but not the trend.

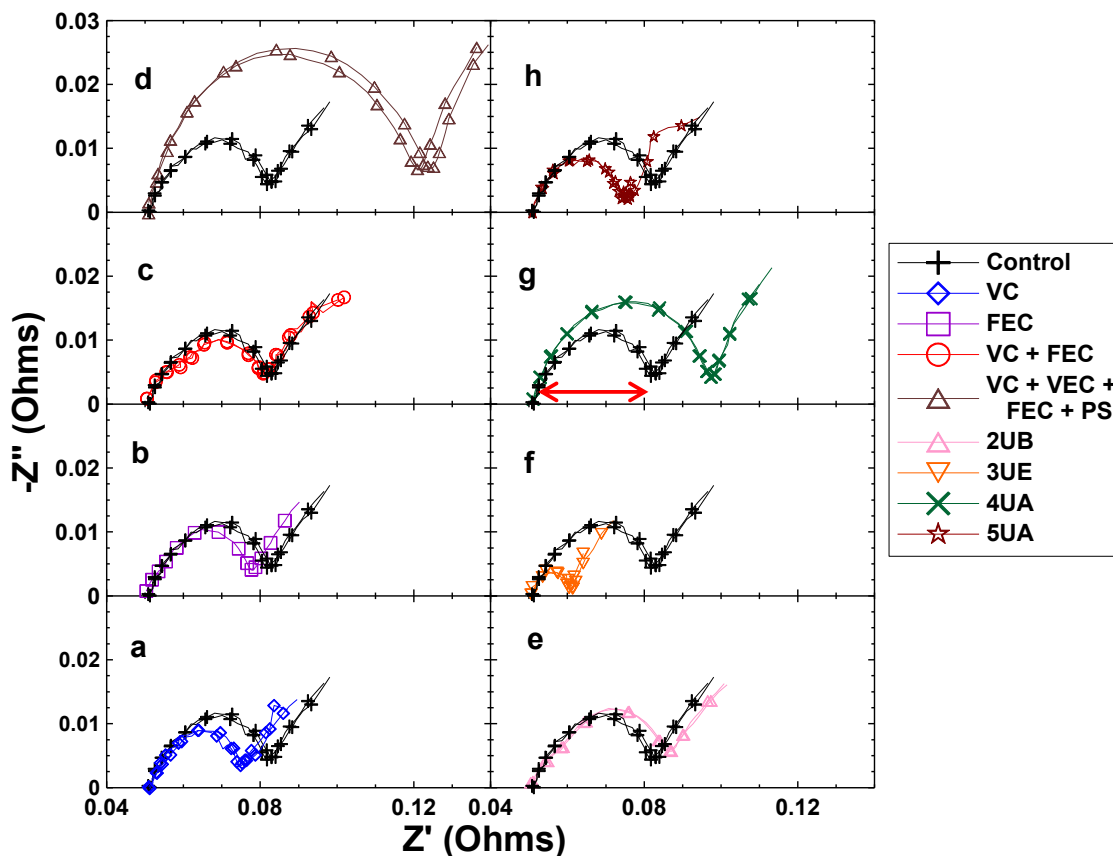


Figure 7.8 Impedance spectra presented in Nyquist plots collected on cells after cycling on the HPC. The cells shown are (a) 1.5 wt.% VC, (b) FEC, (c) VC + FEC, (d) VC + VEC + FEC + PS, (e) 2UB, (f) 3UE, (g) 4UA and (h) 5UA. The results for the control electrolyte are shown in every panel for reference. Reproduced by permission of The Electrochemical Society [44].

Figure 7.6b shows the relationship expressed in Equation 7.2 with the constant calculated from only the cells with known electrolyte compositions. Figure 7.7 shows only the data points for the cells with known electrolyte which show a good fit almost passing through all error bars with  $R^2 = 0.802$  and the linear constant = 0.524. This leads to a two-tailed P value of less than 0.0001 indicating a very high degree probability of correlation between the short term and long term measurements. However it is clear that many of the unknown additive blends result in much longer cycle life than expected by this simple model of cell failure. For example, 3UE has a mid-range coulombic efficiency but is able to achieve about 1700 cycles until failure. Additionally, while 4UA fits the model line quite well, the addition of a single additive (resulting in 5UA) does not affect the coulombic efficiency but increases the cycle life from 500 to 2000 cycles. The

single additive used in 5UA that is not present in 4UA does not increase the cycle life dramatically for all cells in which it is used. Therefore it is the combination of this additive with the other additives that leads to this huge benefit in cycle life.

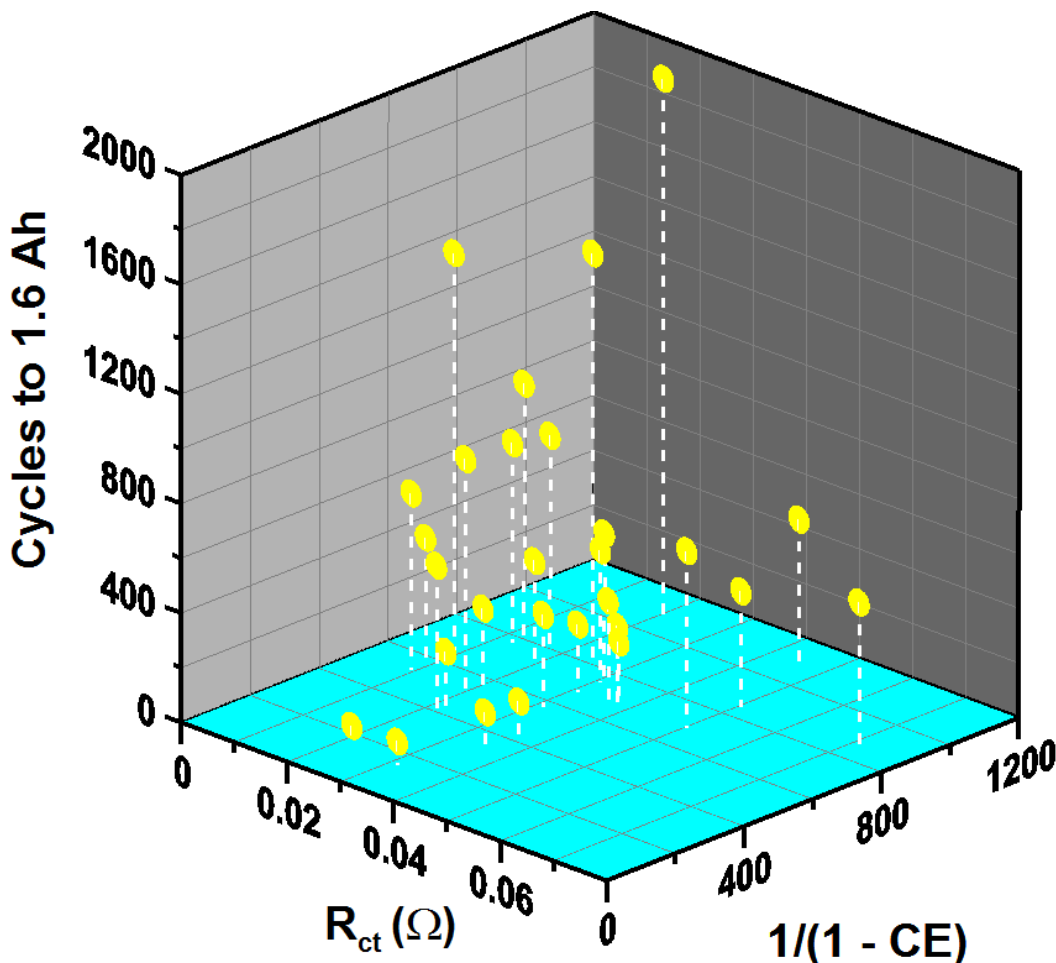


Figure 7.9 Number of cycles to failure at 1.6 Ah (cycling at 1C) plotted as a function of both  $1/(1 - CE)$  and charge transfer resistance ( $R_{CT}$ ) [ $\Omega$ ]. Reproduced by permission of The Electrochemical Society [44].

It is clear that the coulombic efficiency does not predict the cycle life of all cells in this experiment well. Since the failure mode is due to the build-up of an inactive layer on the graphite electrode that leads to kinetic hindrance and prevents the transport of  $\text{Li}^+$  into the electrode understanding how these additives impact the impedance of the cells should also be a key element in determining their failure. Figure 7.8 shows the impedance spectra for eight of the experimental groups including the control cell plotted

in each panel for comparison. The arrow in panel (g) shows how the charge transfer resistance ( $R_{CT}$ ) is calculated for each cell. There are several interesting results evident in these impedance spectra. All of the known additive blends had relatively small impacts on impedance reduction and the blend that lead to the longest life VC + VEC + FEC + PS has a significantly larger  $R_{CT}$  value than control, but also had a much higher coulombic efficiency and therefore achieved a cycle life of about 500 cycles. When comparing 4UA and 5UA, while the cells had almost identical coulombic efficiencies, 5UA has a significantly lower  $R_{CT}$ . Therefore it is possible that the products of the reduction reaction at the negative electrode are soluble or allow better  $Li^+$  transport which does not lead to impedance rise. Even though the same amount of charge is being transferred by parasitic reactions with each cycle, it will not lead to the same kinetic hindrance as early a cycle due to different reaction products. However, without more quantitative chemical analysis of the cells after failure it is not possible to know with certainty the differences formed from reactions occurring with cells containing different electrolytes. Similarly, the impedance spectra of 3UA shows a much lower  $R_{CT}$  compared to the cell containing control electrolyte which could explain why it is able to achieve such a long cycle life despite not having a high coulombic efficiency. The charge transfer resistance of 2UB is very similar to control and fits the model line quite well in Figure 7.6b. Therefore, including the charge transfer resistance in the prediction of cycle life should account for those cells that fall well above the model line.

Figures 7.9 and 7.10 show the dependence of cycles until failure on both the charge transfer resistance and coulombic efficiency in a 3D figure and contour plot, respectively. These figures show a relatively smooth relationship between cycle life and both  $R_{CT}$  and CE. The combination of low cell resistance and high coulombic efficiencies leads to the highest cycle life. For a given coulombic efficiency, additive blends with lower charge transfer resistance can achieve longer cycle lives. Similarly for cells with the same charge transfer resistance, the cell with higher coulombic efficiency will have a longer cycle life. This result shows that it is possible to draw a strong relationship to short term measurements (both the CE and  $R_{CT}$  were collected after about ~650 h of cycling) and the long term performance. Without precision measurements of the coulombic efficiency the only way to know the long term performance of the cells

would have been to cycle until failure which becomes unrealistic in an R&D program to develop cells with very long lifetimes.

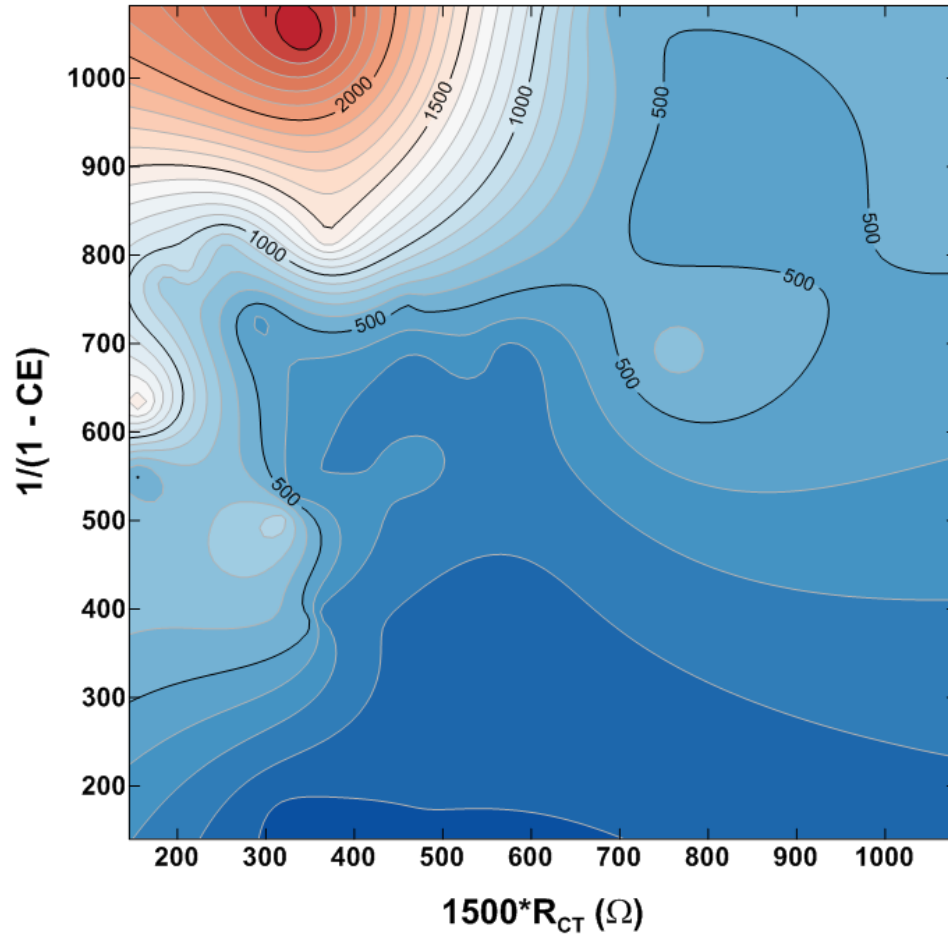


Figure 7.10 Number of cycles to failure at 1.6 Ah (cycling at 1C) plotted as a function of both  $1/(1 - CE)$  and  $1500 \times$  charge transfer resistance ( $1500 * R_{CT}$ ) as a contour plot. The x-axis scale was selected for ease of viewing with the graphics software.

Many researchers attempt to shorten these long term cycling experiments by elevating the cell temperature to induce cell failure sooner. However, this is not a reliable way to predict cycle life as different reactions can be the dominant failure mode at different temperatures. Figure 7.11 shows that for these cells, if the cycling temperature is elevated to  $60^{\circ}\text{C}$  the cells no longer show no capacity loss until failure but rather show gradual capacity loss with continued cycling. At the elevated temperature, the rate of growth of the SEI must be increased leading to continual loss of active lithium

(and therefore capacity loss). In addition, the impact of any kinetic hindrance at the negative electrode would be lessened at elevated temperatures. This shows why low rate cycling and precise measurements of the coulombic efficiency are the best method for reliably comparing cell performance as it can be done at the appropriate temperature and voltage range without exposing the cell to more aggressive cycling conditions than expected during normal use.

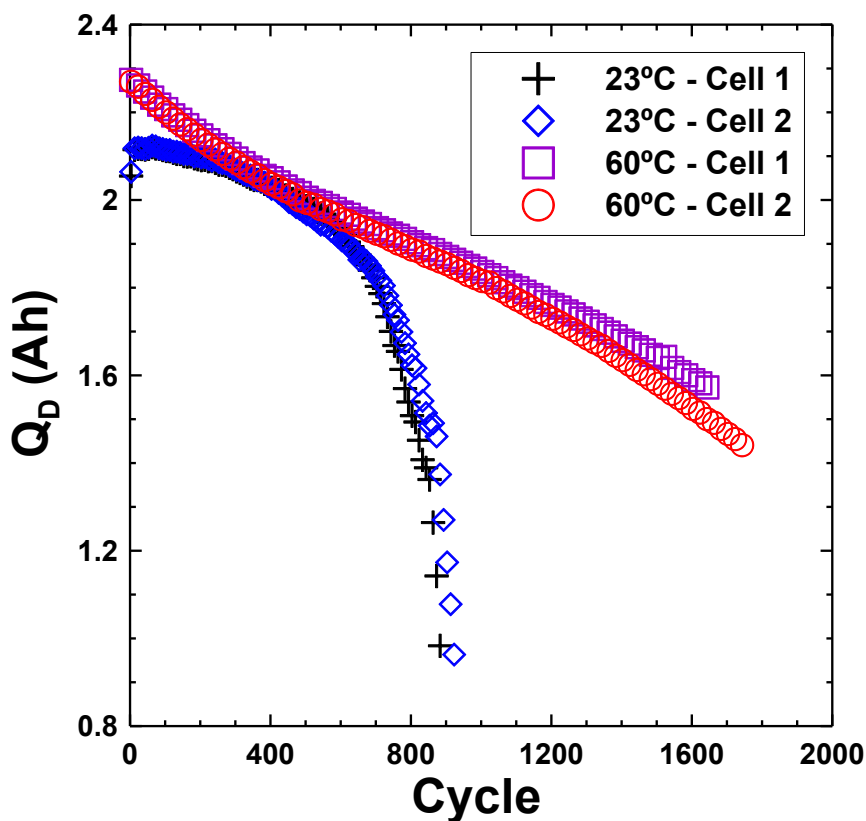


Figure 7.11 Capacity versus cycle number for NMC/graphite 18650 cells with a proprietary set of electrolyte additives cycled at 2A currents at 23°C and at 60°C. Reproduced by permission of The Electrochemical Society [44].

## Chapter 8      Application-Based Performance Testing

### 8.1 Uses of High Precision Coulometry for Battery Management

All of the work discussed thus far has shown that precise measurements of the coulombic efficiency and charge endpoint slippage collected during low rate cycling can provide insight into the long term performance of cells. This method works very well as during low rate cycling the coulombic efficiency is a probe of the stability of the cell chemistry and the failure mode is always due to these parasitic reactions consuming active lithium in the cell, depleting the electrolyte or developing inactive surface films that can lead to failure. These parasitic electrochemical reactions occur with time and the rate is primarily determined by temperature and electrode potentials. Smith *et al.* [12] showed that in commercial cells with different electrode chemistries, the rate of cell degradation was independent of cycling rate, when cycling at low rate, but rather depended only on temperature (for cells within a given group cycled through the same voltage window). Therefore, by normalizing the coulombic efficiency for cycling time, the CIE/h was identical for all cells of a given chemistry at each temperature regardless of cycling rate. This rate independent degradation was then confirmed in further work as cells cycled at three different cycling rates all failed after the same amount of time despite having significantly different cycle counts [142].

$$\frac{CIE}{h} = \frac{(1-CE)}{(time\ per\ cycle)} \quad 8.1$$

While parasitic reactions limit the lifetime of cells under low rate conditions, it is possible to have cycle (or cycling condition) dependent failure as well. Examples of cycle dependent failure include particle fracturing [143–146] and lithium plating during high rate charge [147–151]. Stable chemistry is crucial for achieving long cycle life, but cells must also meet the demands of applications and therefore testing under application



conditions is equally important. These types of cycle dependent failure should also impact the coulombic efficiency if a shortened cycle life occurs. Therefore, coulombic efficiency measurements should not only be able to be used as measures of the stability of cell chemistry at low rates but also to probe failure mechanisms during application-driven cycling conditions. In this study, the impact of high charge rates and thus the potential onset of lithium plating on the degradation rate of Li-ion cells was studied [152].

## 8.2 Impact of Charge Rate on Performance

All data presented in this section on the impact of charging rate on performance was decided upon and conducted by the author. The general concepts for this experiment were discussed after initial studies of cells cycling at low rates with Dr. Aaron Smith and Dr. Jeff Dahn.

Charging Li-ion cells at high rates can lead to the deposition of metallic lithium on the negative electrode if the electrode potential is driven below 0 V vs.  $\text{Li/Li}^+$  due to impedance. The presence of metallic lithium on the negative electrode can lead to issues with both cell performance, due to its low efficiency of plating/stripping, and safety, due to the reactivity of metallic lithium with the electrolyte. The most obvious way to detect lithium plating is with a three electrode cell by monitoring the potential of the negative electrode relative to a lithium potential and if it drops below 0 V then lithium plating must be occurring [147,148]. However, this methodology is not practical in commercial cells as a reference electrode is not present in commercial cells. Differential voltage and capacity plots can be used to detect large amounts of lithium plating [150] and isothermal microcalorimetry can be used to detect even small amounts of lithium plating [149]. Downie *et al.* [149] used microcalorimetry to measure the efficiency of lithium plating/stripping on  $\text{Li}_x\text{C}_6$  particles and found it to be ~97-98% depending on the graphite material. Therefore, since this efficiency is far below that of the intercalation/deintercalation process (> 99.5%), small amounts of lithium plating should decrease the coulombic efficiency due to significantly lower plating/stripping efficiency of that process, which should be detectable with the High Precision Charger.

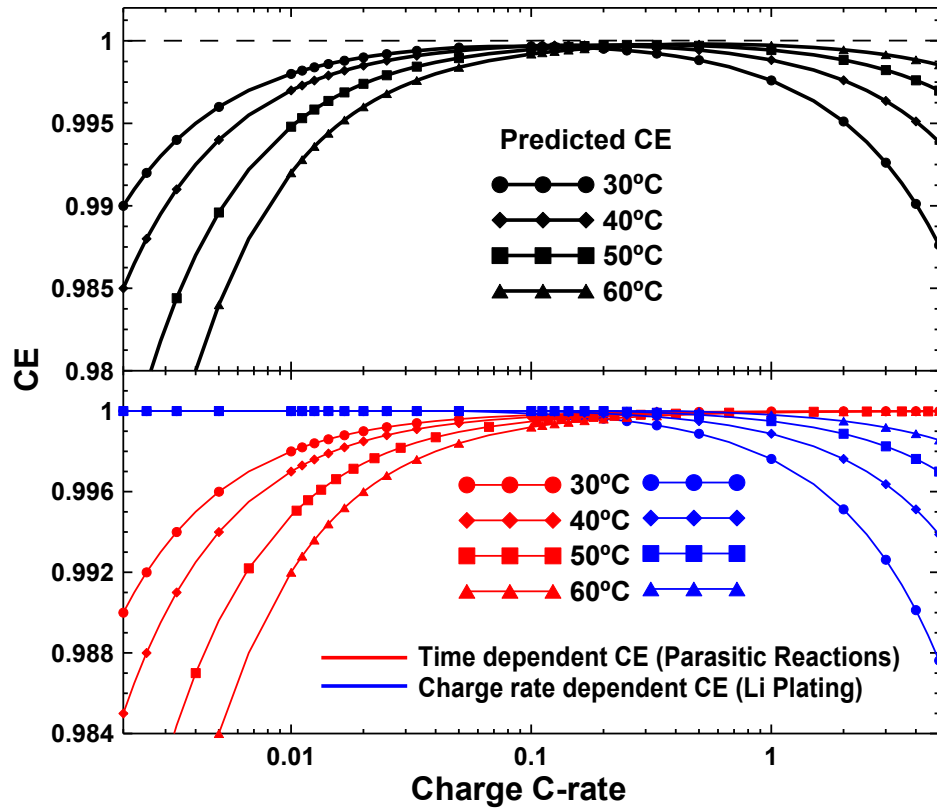


Figure 8.1 Schematic of coulombic efficiency versus charge rate with both the time dependent and charge rate dependent resolved curves (bottom) and the resulting CE versus rate curve (top) at different temperature.

Figure 8.1 shows the anticipated dependency of coulombic efficiency on charging rate. The inefficiencies within the cell are separated to “time” or “charge rate” dependent. The time dependent curve comes from the work of Smith *et al.* [12] which showed that the CIE/h is constant for cells at a given temperature despite cycling at different rates. The coulombic efficiency versus charge rate curves show that at low rates there is no contribution to the inefficiency in the cell from rate dependent processes. However, at high rates the coulombic efficiency decreases as more capacity is delivered from the plating and stripping of lithium at a much lower coulombic efficiency than the intercalation and deintercalation of lithium. The “hump” shaped curves in the top panel come from the combination of the two curves from the bottom panel. These humps shift to the right with increasing temperature as the low rate performance gets worse due to an increase in the parasitic reaction rates at elevated temperature during each cycle but the improved kinetics at higher temperature delay the onset of lithium plating until higher

charge rates. Therefore, with a high precision charger, these curves can be measured as a function of charge rate and the charge rates at which lithium plating occurs can be identified from the CE data alone.

In order to measure this predicted the onset of lithium plating during high rate charge, 220 mAh wound Li[Ni<sub>1/3</sub>Mn<sub>1/3</sub>Co<sub>1/3</sub>]O<sub>2</sub>/graphite 402035-size pouch cells from Li-Fun Technology were cycled with different charge rates to measure the coulombic efficiency as a function of charge rate. The positive electrodes were 96.2% active material, 1.8% carbon black and 2.0% polyvinylidene fluoride (PVDF) binder. The positive electrode had a total thickness of 105 μm with a single side coating of 47.5 μm compressed to 3.55 g/cc and an areal density of 16 mg/cm<sup>2</sup>. The negative electrodes were 95.4% active material, 1.3% carbon black, 1.1% carboxymethyl cellulose (CMC) and 2.2% styrene-butadiene rubber (SBR) as the binder. The negative electrodes had a total thickness of 110 μm with a single side coating of 51 μm compressed to 1.55 g/cc and an areal density of 9.5 mg/cm<sup>2</sup>. The positive electrodes were 26 mm x 200 mm and the negative electrodes were 28 mm x 204 mm. The electrodes were coated on both sides except for small regions at the end of the electrode which resulted in an active area of approximately 100 cm<sup>2</sup>.

The “dry” (no electrolyte) pouch cells were all dried under vacuum at 100°C overnight before being transferred into an argon-filled glove box where electrolyte was added to the cells. The cells were vacuum filled with 0.9 g of 1 M LiPF<sub>6</sub> ethylene carbonate:ethyl methyl carbonate (3/7 by weight, BASF) + 2% VC (BASF, 99.97%) electrolyte and sealed (MTI Corporation, MSK-115A). The formation process consisted of a 1.5 V hold for 24 hours followed by a C/20 charge to 3.5 V at 40°C. After formation, the cells were transferred inside an argon-filled glove box, cut open to release any gas generated during the formation process and resealed. The cells then were put at 12, 30 or 50°C and the first charge to 4.2 V was completed along with the first discharge at C/20 before beginning to cycle at various charge rates for ~600 hours. The cycling consisted of variable charge rates from C/50 up to 5C with the discharge step always conducted at C/10 between 2.8 – 4.2 V. In an attempt to minimize noise in the coulombic efficiency data, some cells underwent a two stage charge/discharge process. During charge the current was reduced to C/30 at 4.19 V and during discharge the current was reduced to

C/30 at 2.85 V. After cycling, cells were disassembled within an argon-filled glovebox at ~50% state of charge to look for lithium plating.

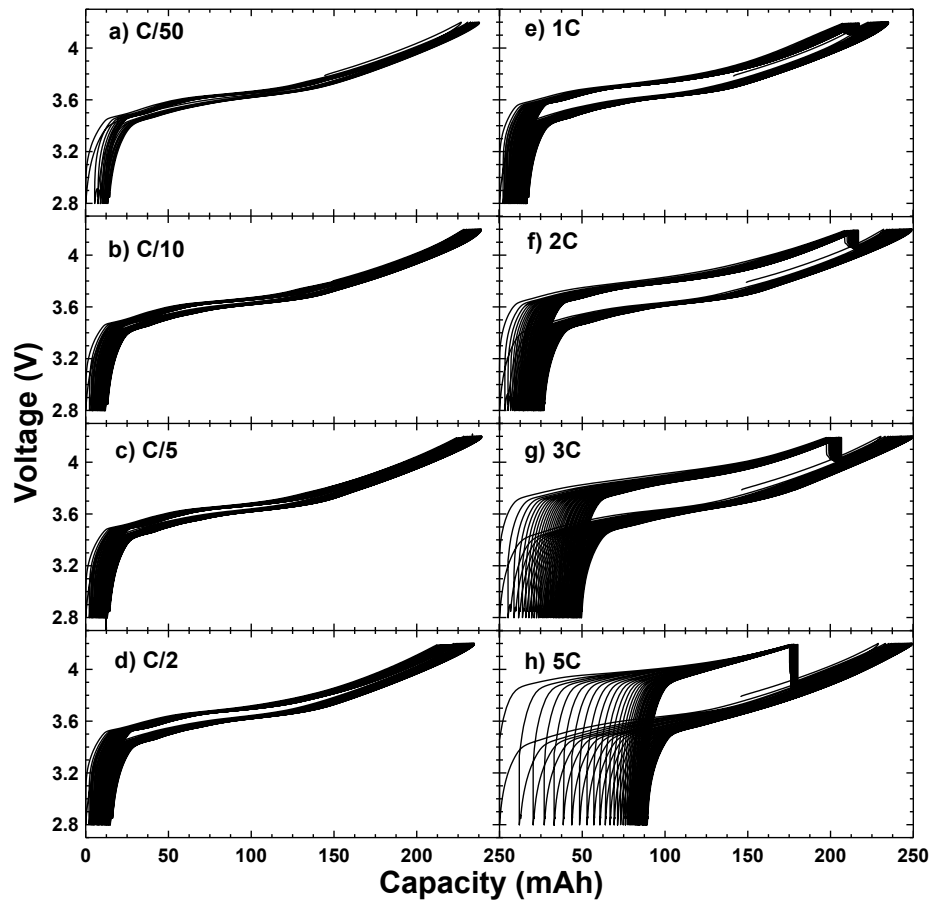


Figure 8.2 Voltage versus capacity curves for pouch cells under test at 30°C during cycling with a two-step charge process from C/50 to 5C charge rates (a-h).

Figure 8.2 shows the voltage versus capacity curves of cells cycled with the two stage procedure at 30°C. At the high rates the two stage charge becomes more apparent due to the large polarization in the voltage curve when being charged with high currents. As the charge rate becomes greater than 1C the slippage of the voltage curves to higher absolute capacities becomes quite dramatic which is due to large inefficiencies within the cells, likely from lithium plating. When more closely examining the voltage profile when charged at a 5C rate, about 60% of the capacity comes from the high rate step and 40% from the C/30 segment. This was done to approach the endpoint more slowly and not overshoot the upper voltage limit of 4.2 V, but in fact it could be adversely impacting cell

performance by changing the average charge voltage. Although it is 40% of the capacity during charge, that segment takes roughly 12 hours while the initial 60% of capacity in the high rate step only takes  $\sim 7$  minutes. Therefore, this dramatically increases the average voltage during charge which also contributes to lowering the coulombic efficiency in addition to any lithium plating that occurs. In order to eliminate this possible variable, cells were also cycled with single step charges to compare the efficiency data.

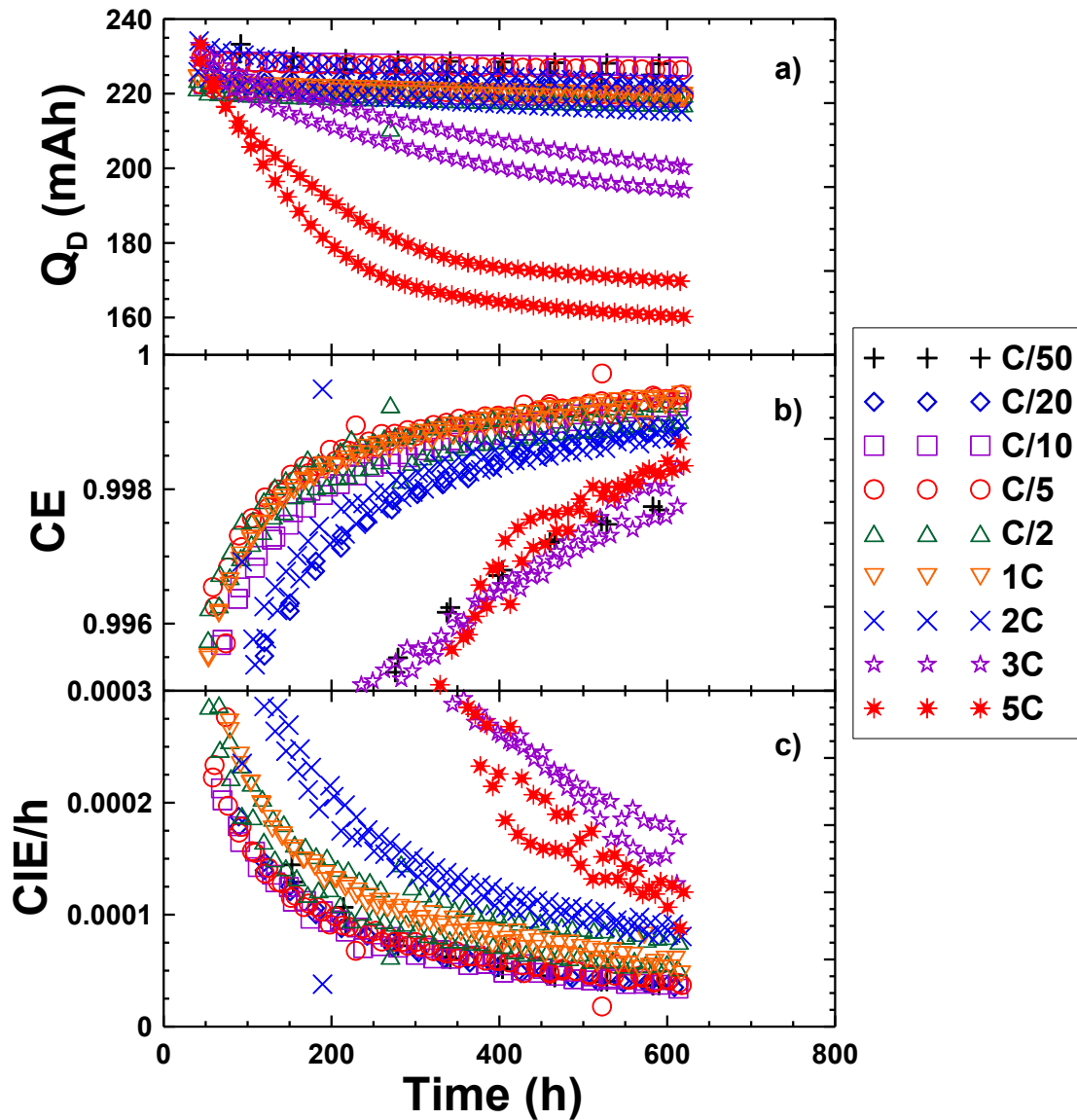


Figure 8.3 Capacity (a), coulombic efficiency (b) and coulombic inefficiency per hour (CIE/h) (c) versus time for pouch cells cycling at 30°C during cycling with a two-step charge process from C/50 to 5C charge rates.

Figure 8.3 shows the capacity, coulombic efficiency and CIE/h versus time data for the same cells presented in Figure 8.2. There is minimal difference in the capacity loss rates (panel a) until charge rates of 1C or higher which start to show progressively more capacity loss. The cell cycled with a 5C charge rate shows significant capacity loss for the first ~200 hours which then slows down dramatically. The rapid capacity loss in the early cycles is due to significant amounts of lithium plating occurring during each cycle. As the cell continues to cycle and lose capacity, the graphite electrode is charged to lesser relative states of charge with each subsequent cycle. Therefore, after ~200 hours of cycling, the graphite electrode is no longer charged to a state of charge that drives the electrode potential below 0 V vs. Li/Li<sup>+</sup> so no more lithium plating occurs which causes the capacity loss rate to decrease significantly. Apart from the cells charged with very high currents, it is difficult to distinguish between the performance of cells based on the capacity loss rates.

Figure 8.3b shows that the coulombic efficiency changes significantly for cells charged at different currents. However, the coulombic efficiency has both time and cycle dependent contributions to its deviation from unity and therefore time normalizing the data will show the cycle dependent differences between cells. Figure 8.3c shows the CIE/h for the cells which should be identical when all cells have a constant degradation rate. All cells cycled with charge rates less than 1C fall on a universal curve that shows that there is no cycle dependent contribution to cell degradation and thus no lithium plating should be occurring. As the charge rate increases beyond 1C, the CIE/h becomes increasingly worse as more lithium plating occurs at the higher rates. Therefore, the onset of lithium plating can easily be identified using the coulombic efficiency during normal cell cycling.

Cells were cycled under the same conditions at both -12 and 50°C to investigate the temperature dependence of the onset of lithium plating. Figure 8.4 shows a summary of all cells tested in this experiment showing the fade, coulombic efficiency and CIE/h versus charge rate. The error bars are taken from the difference between pair cells under a given set of experimental conditions. At 30 and 50°C, additional cells were cycled with a single stage charge, near where the onset of lithium plating was detected from the initial cells, to ensure there was no systematic error due to the two stage cycling conditions as

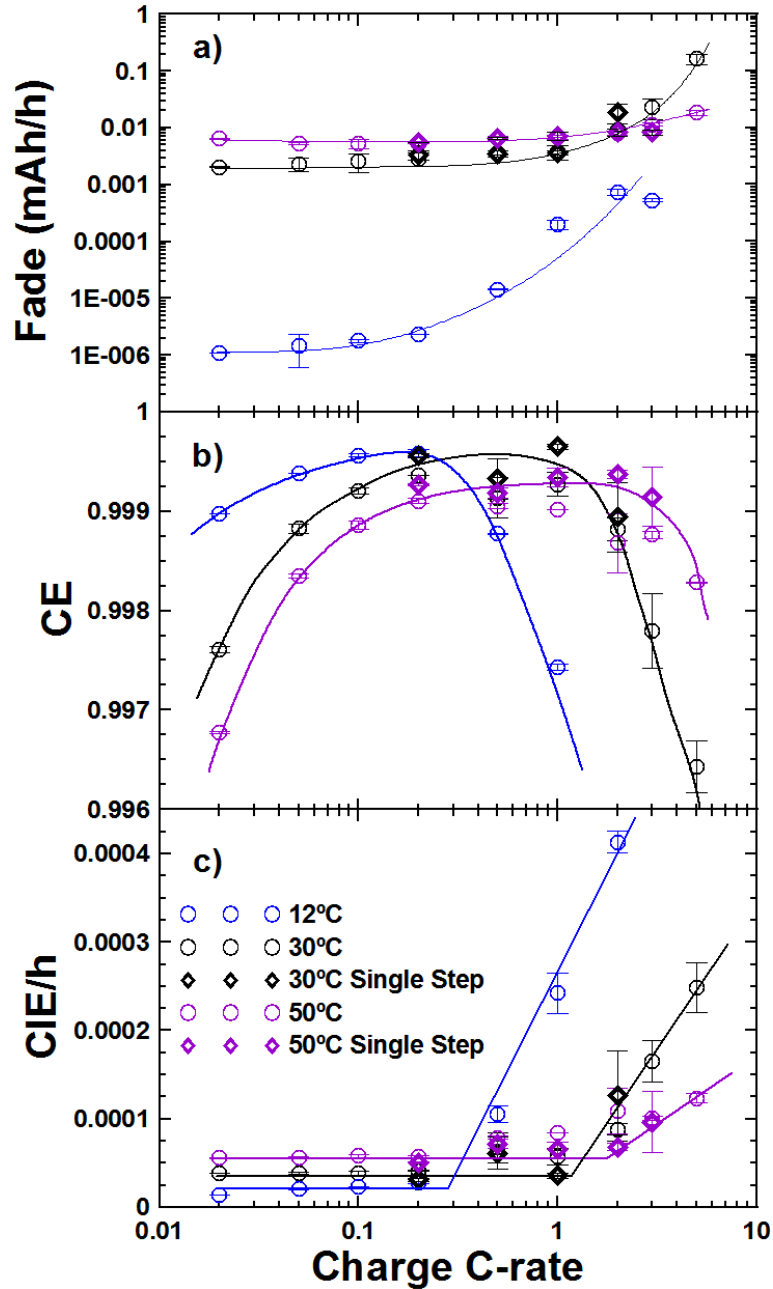


Figure 8.4 A summary of fade (a), coulombic efficiency (b) and coulombic inefficiency per hour (CIE/h) (c) versus charge rate for all pouch cells at different temperatures and rates using both the single and two-stage charge process.

discussed previously. Since the degradation rates are so small at 12°C, the difference in average charge voltage has little impact on cell degradation. Therefore, no additional cells were made as the onset of lithium plating is quite clear from the CIE/h data. The CIE/h curves show a constant value for low charge rates that then increase rapidly at a

given charge rate for each temperature. This “kink” in the CIE/h curve indicates the onset of lithium plating at that temperature. Note that the lines drawn in Figure 8.4C are drawn as two distinct lines. The first line is drawn with a zero slope during rates proposed to be in the time-dependent failure regime. More data collected closer to the proposed location of the “kinks” would be necessary to confidently identify the exact rates at which lithium plating begins at these different temperatures. For  $-12^{\circ}\text{C}$ , the onset of lithium plating is between  $C/5$  and  $C/2$ ; for  $30^{\circ}\text{C}$ , the onset of lithium plating is around  $1C$ ; and for  $50^{\circ}\text{C}$ , the onset of lithium plating is around  $2C$ . Figure 8.4b shows the CE versus rate which exhibit the expected “hump” shapes. While the curves are not symmetric as initially proposed, they agree well with the concept proposed in the discussion surrounding Figure 8.1. The curves shift to the right with increasing temperature and also shift down as the elevated temperature increases the degradation rates.

In order to verify that these measurements are truly detecting lithium plating, cells were disassembled at 50% state of charge in an argon-filled glove box for examination. Figure 8.5 shows photographs of the disassembled negative electrodes for the cells cycled at  $12$  and  $50^{\circ}\text{C}$ . Exactly as expected, the cells cycled up to  $C/5$  at  $12^{\circ}\text{C}$  show no indication of lithium plating while the cell charged at  $C/2$  shows small metallic lithium deposits. At  $12^{\circ}\text{C}$  the cells charged at  $1C$  or higher have metallic lithium covering the entire surface of the negative electrode which explains why the coulombic efficiency dropped off so severely at those high rates. At  $50^{\circ}\text{C}$  there is no evidence of lithium plating through the cells charged up to  $1C$  and the cell charged at  $2C$  shows a few very small lithium deposits primarily along the wrapping edges of the prismatically wound electrode stack. The cell charged at  $3C$  shows more significant lithium deposits and the cell charged at  $5C$  shows a thin layer of metallic lithium across the entire electrode along with larger deposits. Therefore it is clear that the measurements of coulombic efficiency do in fact detect the onset of lithium plating in these cells without the need for a reference electrode or additional testing of any sort, simply cycling under normal operating conditions in terms of rate, temperature and upper voltage limit.

This result is important to the battery management industry as almost all consumers want devices with batteries to have shorter recharge times. Electric vehicles



are an excellent example of an application where consumers want quick recharge times but the cells need to still maintain the long lifetime to meet manufacturers' warranties. Therefore this type of information can be used to monitor and adjust the maximum allowable charging current by the battery management system depending on the temperature of the pack to achieve the fastest charge time without inducing lithium plating. As the cell ages, the onset of lithium plating will change but with additional work this could also be accounted for in order to maximize cell lifetime while optimizing the cell performance for a given application.

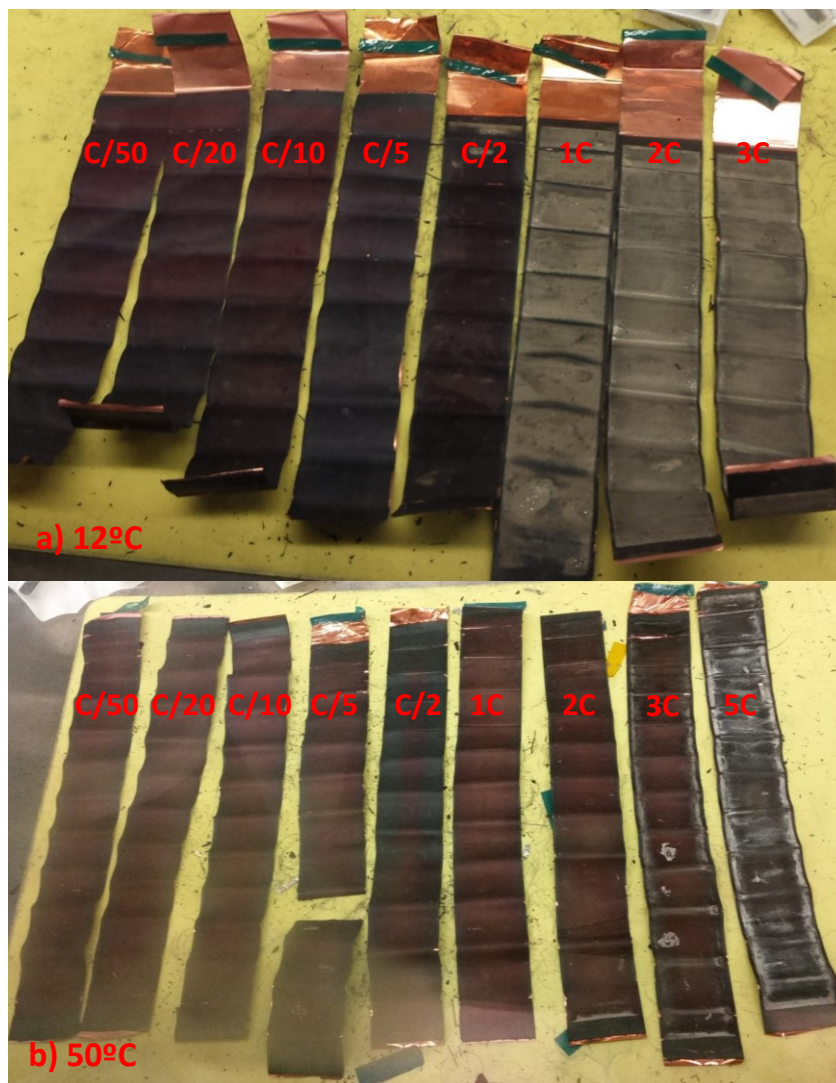


Figure 8.5 Photograph of the negative electrode after cycling for cells cycled at different rates and 12°C (a) and 50°C (b) to examine for confirmation of the occurrence of lithium plating.

## Chapter 9      Conclusions and Future Work

### 9.1 Conclusions

One of the most important criteria that would enable Li-ion batteries to be more widely used in new applications such as electric vehicles and grid energy storage is lifetime. The fundamental issue is that to state a lifetime of a cell with absolute certainty, one must test the cell under application conditions until failure. Therefore if attempting to prove that a Li-ion cell will last ten years, an experiment must be conducted that is ten years long. This process is obviously not feasible as the energy storage technology would lag applications due to the length of the research and development process. Currently, researchers attempt to accelerate failure from the actual usage conditions by, for example, increasing the cycle rate to achieve more cycles, elevating the operating temperature or keeping the cells at high states of charge. However, these testing protocols do not always extrapolate back to give realistic estimates of performance under the true operating conditions (note the staggering difference in failure mode seen in Figure 7.11 when cells are cycled at different temperatures). This work presented in this thesis shows that high precision coulometry can be used as a reliable metric in anticipating cell lifetime under realistic conditions.

Precise measurements of the coulombic efficiency and charge endpoint capacity slippage measure the rate of parasitic reactions occurring within a cell that can eventually limit the cell lifetime. In this work, in-house equipment was used to make such measurements at a higher level of precision and accuracy than available from commercial equipment. Coupling high precision cycling data collected at low rates with other short term experiments such as open circuit storage and impedance spectroscopy allows for better insight into how these parasitic reactions are manifesting within the cell. These parasitic reactions can cause gradual capacity loss, as discussed in Chapter 4, or lead to the sudden onset of rapid capacity loss after very stable cycling, as discussed in Chapter 7.

This work shows that one of the most powerful uses of high precision coulometry is as a tool to screen electrolyte additives (or the impact of water in the electrolyte) used in cells with the same base chemistry. The use of electrolyte additives can lead to large improvements in cell performance in the areas of safety, impedance, gas generation and cycle life. Electrolyte additives are by far the most easily implemented change in cell manufacturing as it does not require changes to the cell building process, only the formulation of electrolyte injected into the cell. The impact on coulombic efficiency and charge endpoint capacity slippage were almost always (impedance can be an important factor as well) directly correlated to the cycle life of the cell. This allows for cycling experiments that only take a few weeks to be used as a predictor of cell lifetime that could be many years.

The three most important results from this thesis are the results of the aged cells when cycled on the High Precision Charger, the long term cycling results of the cells containing TMOBX, presented in Chapter 5, and the “zero-fade” cells, presented in Chapter 7. The results from the cells that had been cycled for up to twelve years show the evolution of coulombic efficiency and charge slippage over time. The parasitic reaction rates slow down due to the thickening of surface films on the electrode leading to higher coulombic efficiency and lower charge slippage, but the rate of these reactions never goes to zero. After many years of cycling the SEI layer on the graphite is very stable and leads to minimal loss of active lithium, and thus capacity. However, even to only a modest upper voltage limit of 4.075 V, the oxidation of electrolyte at the positive electrode never stops and becomes the primary inefficiency within the cell. Although this does not lead directly to capacity loss, it can lead to cell failure after sufficient electrolyte has been oxidized within the cell.

Some researchers believe that coulombic efficiency is not a valid metric in predicting cell lifetime [153] as they studied the impact of VC and saw minimal difference in the capacity loss rates over 400 cycles. However, the results of the cells containing VC and/or TMOBX presented in this work show that when TMOBX was added to VC-containing electrolyte in the  $\text{LiCoO}_2$  cells, the coulombic efficiency decreased and charge slippage rate increased. This did not result in the VC + TMOBX cells showing higher capacity fade, but after 4 years of cycling has resulted in the VC +

TMOBX cells showing the onset of “roll-over” failure before the cells containing only VC due to the increased rate of electrolyte oxidation. Also, when comparing the cells cycled to 4.175 V and 4.075 V, there was minimal difference in coulombic efficiency but a decrease in charge slippage. The long term cycling showed comparable capacity loss in the first ~400 cycles until the capacity loss rate became very small but then the onset of “roll-over” failure occurred much earlier in the cells cycled to higher voltage due to the increased electrolyte oxidation rate captured by the early measurements of the charge slippage. Therefore the results from the coulombic efficiency and charge slippage do predict the cell that will have the longest cycle life. Deshpande *et al.* [153] cycle the cells measuring capacity loss until ~80% capacity is reached. However, if the cycling experiment had not been stopped, the cells would likely eventually show sudden capacity loss where the cell containing VC would achieve more cycles until the onset of this “roll-over” failure.

The results of the “zero-fade” cells in Chapter 7 are important as without measurements differentiating the coulombic efficiency, charge slippage and impedance of the cells in the early cycles, there would be no way to predict cell failure from the capacity versus cycle number plots. While the experiment was conducted on cells with at most a two year lifetime, the results would hold for cells with 10 + year lifetimes which shows the importance of measurements of coulombic efficiency and charge endpoint capacity slippage. Due to the failure mechanism being lack of ion transport into the negative electrode, impedance was an important factor in the cycle life as well. Therefore, it is clear that while information from the coulombic efficiency and charge endpoint capacity slippage can give insight into the cycle life, they must be coupled with other techniques to fully understand cell failure.

The study on the impact of high charge rate on the coulombic efficiency and therefore cell performance opens the door to a new line of work. The testing of electrolyte additives was all done at low rates, to probe the chemistry as a function of voltage and temperature, but the results from the high charge rate study show that coulombic efficiency can be measured under real application conditions and give insight into cell lifetime. Very few applications would conduct such a simple cycling protocol as a constant current charge and discharge at rates such as C/20. Therefore it is important to

understand the performance of cells under real conditions. The detection of lithium plating through the measurements of coulombic efficiency shows that high precision coulometry can be used not only to detect differences in the cell chemistry but the performance under operating conditions that vary the temperature, cycling rate, etc.

## **9.2 Future Work**

The continued validation of high precision coulometry as a reliable short term metric to predict long term cell performance opens the door to many areas where the technique could be applied and suggests directions for continued research. Using coulombic efficiency as a metric to screen electrolyte additives for different cell chemistries has been identified as an important use of high precision coulometry and is being continued in this research group [124,125]. Since the options for electrolyte additives are so vast, coulombic efficiency measurements offer a good short term metric to narrow down additives of interest for long lifetime cells. In addition to electrolyte additives, completely new electrolyte systems with changes to the salt or solvents can be studied under the same premise. For example, fluorinated solvents have been shown to have greater oxidative stability in Li-ion cells and therefore could be used in cells cycled to higher voltage limits [31]. Even more fundamental changes to the electrolyte such as changing to a solid electrolyte or room temperature ionic liquid could be studied using high precision coulometry to understand the stability in the actual cell configuration.

In order to improve the energy density of Li-ion cells, new positive electrode materials that can be cycled to higher voltage are of great interest [31]. However, cycle life is one of the largest challenges of these materials as they operate at the extent or beyond the voltage stability of the electrolyte. Therefore the formation of stable surface films to prevent electrolyte oxidation is essential in enabling such materials. Electrolyte additives can be used to form such films and the effectiveness of these surface films in reducing electrolyte oxidation can be measured through changes in the coulombic efficiency and charge slippage of either half cells or full cells. In addition to studying the impact of electrolyte formulations on new materials, studies of the coulombic efficiency

of different materials can be compared to select those which will have better performance under the conditions being tested [154].

As cell performance continues to increase and the coulombic efficiency becomes closer to 1.0000, it becomes more difficult to distinguish between the performance of cells with different electrolyte formulations. There are two approaches to solving this problem: improve equipment accuracy and precision, or test cells under conditions where the performance is worse. From the initial High Precision Charger, a great deal of work was done in attempts to optimize the performance in terms of accuracy and precision [108]. Therefore, it would likely take a fundamental change to the system design in order to improve upon the current performance of the Ultra High Precision Charger. However the two areas that would likely lead to the greatest improvement is stability (low noise) and accuracy of the current source and temperature control of cells. Currently cells are placed in thermal chambers that accommodate up to twenty cells with circulating air for temperature stability and uniformity. Individual cell temperature control could lead to more consistent and stable cell temperature lowering the noise level and improving the accuracy in measurements of pair cells.

The other approach to distinguishing cell performance is to test cells under conditions that lower the coulombic efficiency and thus the differences between cells with different chemistry will therefore be greater. Such experiments would typically involve more time at higher voltage or at elevated temperature. This could be done with constant voltage holds or open circuit storage at the top of charge or by cycling with lower charge rates at high states of charge. Exposing cells to higher states of charge for longer during each cycle will decrease the coulombic efficiency and therefore spread the performance of cells with different chemistries so that they are easily distinguishable. While this approach can help distinguish between high performing cell chemistries, it must be confirmed that cycling under non-standard conditions does not introduce any unknown changes to the high precision cycling data and that the results still correlate well with the long term performance.

While all of the work presented in this thesis concerned the impact of electrolyte additives on cell performance, it does not address the question of why certain additives result in the benefits that are measured. Developing an understanding for how different

additives react in the cell and impact the surface films will give better insight into developing better cell chemistry. In Chapter 2, it was mentioned that different groups use post mortem techniques such as XPS, FTIR, TEM, etc. to study the properties of the surface films after cycling. These types of techniques can be used to identify properties of surface films that result when certain beneficial additives (as per HPC cycling) are used within cells. The goal would be to correlate benefits seen in the cycling performance to commonalities in the surface films identified in post mortem analysis. This type of work [68] has begun in this research group and will hopefully grow to develop better understanding of what makes some additives so beneficial to performance. The use of computational studies can also help to understand possible reaction pathways that can lead to the surface films found through post mortem analysis.

If a better understanding is developed about how additives react within a cell and the result of those reactions in terms of passivation films and impact on cell performance, it can lead to designing new additives. Currently, screening of additives is based on previously reported results and finding families of additives that appear to show benefits to cycling performance and studying other similar molecules. However, if greater knowledge is developed about how certain molecular structures react within a cell and can impact the surface films, molecules can be synthesized that should give benefit to the cell in a known way. This would lead to more efficient testing of electrolyte additives in continued attempts to improve the lifetime of current and next generation cell chemistries.

Another important path forward for the uses of high precision coulometry is to provide quantitative predictions of cell performance as opposed to the mostly qualitative predictions given in this thesis. As this work was all done in an academic environment and generally as proof of concept, there was not a great deal of time spent in attempting to quantitatively model the lifetime of cells using the short term measurements of coulombic efficiency and charge slippage. The work presented in Chapter 7 about the “zero-fade” cells shows the first effort for quantitative predictions of lifetime which required the coupling of coulombic efficiency (or charge slippage in this case) and measurements of the charge transfer resistance. However, a deeper understanding of a function that would fit the data was never studied as the purpose of the study was not to develop a model for that cell chemistry but rather to show that the short term

measurements could anticipate the long term performance. Given that the coulombic efficiency and charge slippage are direct measures of the charge transferred by parasitic reactions within the cell, quantitative predictions of cycle life based on the consumption of active lithium or electrolyte within the cell should be possible. Understanding how these metrics vary over time, as presented in Chapter 4, is essential in developing these types of models as the cell performance varies as a function of age. Such work becomes difficult as effects from the negative and positive electrode must be decoupled and additionally those reactions that involve both electrodes, as seen in Chapter 7, must be identified as well. It is very unlikely that a simplistic model could be developed for a given cell type and therefore many other factors will likely need to be taken into account, for example, the rise in cell impedance over time.

Harlow *et al.* [155] attempt to make quantitative predictions of the lifetime of cells based on the short term measurements of coulombic efficiency and charge endpoint capacity slippage. The proposed model assumes electrolyte oxidation consumes solvent within the cell and below a certain fraction of solvent remaining, the cell can no longer function. Therefore, the cycle life can be calculated from the rate of solvent oxidation (from the charge endpoint capacity slippage) if the fraction of solvent needed for cell operation is known. This is an excellent step towards using high precision coulometry quantitatively but, to develop a proper understanding of how the impacts in coulombic efficiency and charge slippage affect cycle life, a greater understanding of the cell chemistry must be known.

Currently, high precision coulometry has only been used on cells with graphite or LTO negative electrodes. Many of the novel negative electrode materials still struggle to meet the lifetime requirements of Li-ion cells (especially as the lifetime requirement continues to increase for new applications) and therefore traditional electrochemical testing methods are sufficient in improving the materials. However, as the performance of novel negative electrodes such as silicon-based materials continue to improve, the materials will reach a level of performance where precision measurements of the coulombic efficiency can help to optimize performance. Materials that suffer from an electrode expansion problem will lead to interesting high precision coulometry studies as it can be used to decouple the impact of time dependent and cycle dependent degradation.



In addition to studying new materials for Li-ion cells, high precision coulometry may be useful in diagnosing problems in other types of electrochemical energy storage systems. A somewhat clear transition into other electrochemical energy storage systems is to other metal-ion cells such as sodium or magnesium based chemistries. However, it may prove useful to study completely different cell types such as supercapacitors, lithium-sulfur, molten salt, etc. These different cell types have different failure modes and fundamental issues, however working to improve the coulombic efficiency of any energy storage system should improve its cycle life.

Chapter 8 presented work moving high precision coulometry from only low rate cycling to understand the impact of cell chemistry on lifetime to application relevant testing conditions with high charging rates. There is a great deal of opportunity to study the impact of different charge/discharge profiles and how they impact coulombic efficiency and charge endpoint capacity slippage, and thus lifetime. Applications such as electric vehicles and grid storage for renewable power generation (ie photovoltaic or wind) have much more complex charge/discharge profiles to accommodate the needs of the application. While a great deal of optimizing batteries for these types of applications lies in the engineering and design of the battery, each cell within the pack still must be able to meet some power, energy and lifetime requirements. Therefore, testing cells under the conditions that meet the energy and power density required for a given application can compare the predicted lifetime of the different cells. This allows for the best cells to be selected when constructing battery packs for different applications since different cell design/configurations will be required to meet the criteria of different applications.

The work presented in this thesis is a large step in confirming the validity of using high precision coulometry as a short term metric that is indicative of long term performance. It continued to develop an understanding of the experimental design, interpretation of the data and how these metrics vary over time and between cell chemistries. Therefore, the future work outlined here is only that which comes directly from this work. However, as new cell chemistries emerge and understanding of cell chemistry and reactions continue to develop, new applications for such techniques may

become apparent and continue to advance the field of rechargeable energy storage devices.

Based on the results shown in this work, many other researchers in the industry in the Li-ion community have expressed interest in using high precision coulometry. However, few groups have the expertise and resources (both time and money) to construct systems built from Keithley Instruments as was done in this work. This led to an interesting business opportunity to provide such systems to the Li-ion research community. Novonix Battery Testing Services Inc. has spun out of Dr. Dahn's lab and commercialized 1 Amp high precision charger systems that perform with the same level of accuracy and precision as the UHPC discussed in this thesis. The company offers HPC systems and cell/material testing services to help the Li-ion research community achieve the necessary lifetime goals to enable wider spread usage of Li-ion batteries in energy storage applications as well as enter into new applications.

## Bibliography

- [1] T. Reddy, *Linden's Handbook of Batteries*, 4th ed., McGraw-Hill Professional, (2010).
- [2] *2015 Spark EV Electric Vehicle* [accessed April 5, 2015] <http://www.chevrolet.com/spark-ev-electric-vehicle.html>.
- [3] *BMW I3 Drive* [accessed April 5, 2015] <http://www.bmw.ca/ca/en/newvehicles/i3/2013/showroom/drive.html>.
- [4] *Model S* [accessed April 5, 2015] [http://www.teslamotors.com/en\\_CA/models](http://www.teslamotors.com/en_CA/models).
- [5] *Nissan USA* [accessed April 5, 2015] <http://www.nissanusa.com/electric-cars/leaf/charging-range/battery>.
- [6] *AES Energy Storage* [accessed April 5, 2015] <http://www.aesenergystorage.com/advancion/advantages/>.
- [7] *Energy Storage Renewables* [accessed April 5, 2015] <http://www.saftbatteries.com/market-solutions/energy-storage-renewables>.
- [8] *Energy Storage Systems* [accessed April 5, 2015] <http://www.a123systems.com/energy-storage-systems.htm>.
- [9] *ESSEnergy Storage Systems Overview* [accessed April 5, 2015] <http://www.samsungsdi.com/ess/overview>.
- [10] A. J. Smith, J. C. Burns, S. Trussler, and J. R. Dahn, *J. Electrochem. Soc.*, **157**, A196 (2010).
- [11] A. J. Smith, J. C. Burns, D. Xiong, and J. R. Dahn, *J. Electrochem. Soc.*, **158**, A1136 (2011).
- [12] A. J. Smith, J. C. Burns, and J. R. Dahn, *Electrochem. Solid-State Lett.*, **13**, A177 (2010).
- [13] R. Koksang, J. Barker, H. Shi, and M. Y. Saïdi, *Solid State Ion.*, **84**, 1 (1996).
- [14] Y. M. Tsutomu Ohzuku, *Chem. Lett.*, 642 (2001).
- [15] Z. Lu, D. D. MacNeil, and J. R. Dahn, *Electrochem. Solid-State Lett.*, **4**, A191 (2001).
- [16] F. Zhou, X. Zhao, A. van Bommel, X. Xia, and J. R. Dahn, *J. Electrochem. Soc.*, **158**, A187 (2011).

- [17] S. K. Martha, H. Sclar, Z. Szmuk Framowitz, D. Kovacheva, N. Saliyski, Y. Gofer, P. Sharon, E. Golik, B. Markovsky, and D. Aurbach, *J. Power Sources*, **189**, 248 (2009).
- [18] J. K. Ngala, N. A. Chernova, M. Ma, M. Mamak, P. Y. Zavalij, and M. S. Whittingham, *J. Mater. Chem.*, **14**, 214 (2004).
- [19] R. J. Gummow, A. de Kock, and M. M. Thackeray, *Solid State Ion.*, **69**, 59 (1994).
- [20] A. Yamada, S. C. Chung, and K. Hinokuma, *J. Electrochem. Soc.*, **148**, A224 (2001).
- [21] J. R. Dahn, T. Zheng, Y. Liu, and J. S. Xue, *Science*, **270**, 590 (1995).
- [22] D. Guerard and A. Herold, *Carbon*, **13**, 337 (1975).
- [23] K. M. Colbow, J. R. Dahn, and R. R. Haering, *J. Power Sources*, **26**, 397 (1989).
- [24] T. Ohzuku, A. Ueda, and N. Yamamoto, *J. Electrochem. Soc.*, **142**, 1431 (1995).
- [25] Y. Hamon, T. Brousse, F. Jousse, P. Topart, P. Buvat, and D. M. Schleich, *J. Power Sources*, **97-98**, 185 (2001).
- [26] M. N. Obrovac and L. Christensen, *Electrochem. Solid-State Lett.*, **7**, A93 (2004).
- [27] M. Winter and J. O. Besenhard, *Electrochimica Acta*, **45**, 31 (1999).
- [28] N. Tamura, R. Ohshita, M. Fujimoto, S. Fujitani, M. Kamino, and I. Yonezu, *J. Power Sources*, **107**, 48 (2002).
- [29] M. N. Obrovac and L. J. Krause, *J. Electrochem. Soc.*, **154**, A103 (2007).
- [30] A. D. W. Todd, P. P. Ferguson, M. D. Fleischauer, and J. R. Dahn, *Int. J. Energy Res.*, **34**, 535 (2010).
- [31] M. Hu, X. Pang, and Z. Zhou, *J. Power Sources*, **237**, 229 (2013).
- [32] C. R. Fell, K. J. Carroll, M. Chi, and Y. S. Meng, *J. Electrochem. Soc.*, **157**, A1202 (2010).
- [33] A. van Bommel, L. J. Krause, and J. R. Dahn, *J. Electrochem. Soc.*, **158**, A731 (2011).
- [34] S. S. Zhang and T. R. Jow, *J. Power Sources*, **109**, 458 (2002).
- [35] K. Xu, *Chem. Rev.*, **104**, 4303 (2004).
- [36] A. B. McEwen, H. L. Ngo, K. LeCompte, and J. L. Goldman, *J. Electrochem. Soc.*, **146**, 1687 (1999).

- [37] J. L. Nowinski, P. Lightfoot, and P. G. Bruce, *J. Mater. Chem.*, **4**, 1579 (1994).
- [38] A. B. McEwen, S. F. McDevitt, and V. R. Koch, *J. Electrochem. Soc.*, **144**, L84 (1997).
- [39] M. C. Smart, B. V. Ratnakumar, and S. Surampudi, *J. Electrochem. Soc.*, **149**, A361 (2002).
- [40] M. C. Smart, B. L. Lucht, and B. V. Ratnakumar, *J. Electrochem. Soc.*, **155**, A557 (2008).
- [41] J. Liu, Z. Chen, S. Busking, and K. Amine, *Electrochem. Commun.*, **9**, 475 (2007).
- [42] S. S. Zhang, *J. Power Sources*, **162**, 1379 (2006).
- [43] K. Xu and A. von Cresce, *J. Mater. Chem.*, **21**, 9849 (2011).
- [44] J. C. Burns, A. Kassam, N. N. Sinha, L. E. Downie, L. Solnickova, B. M. Way, and J. R. Dahn, *J. Electrochem. Soc.*, **160**, A1451 (2013).
- [45] M. Itagaki, N. Kobari, S. Yotsuda, K. Watanabe, S. Kinoshita, and M. Ue, *J. Power Sources*, **135**, 255 (2004).
- [46] K.-S. Lee, Y.-K. Sun, J. Noh, K. S. Song, and D.-W. Kim, *Electrochem. Commun.*, **11**, 1900 (2009).
- [47] R. Petibon, C. P. Aiken, N. N. Sinha, J. C. Burns, H. Ye, C. M. VanElzen, G. Jain, S. Trussler, and J. R. Dahn, *J. Electrochem. Soc.*, **160**, A117 (2013).
- [48] R. Petibon, N. N. Sinha, J. C. Burns, C. P. Aiken, H. Ye, C. M. VanElzen, G. Jain, S. Trussler, and J. R. Dahn, *J. Power Sources*, **251**, 187 (2014).
- [49] J. C. Burns, N. N. Sinha, G. Jain, H. Ye, C. M. VanElzen, W. M. Lamanna, A. Xiao, E. Scott, J. Choi, and J. R. Dahn, *J. Electrochem. Soc.*, **159**, A1105 (2012).
- [50] J. C. Burns, N. N. Sinha, G. Jain, H. Ye, C. M. VanElzen, W. M. Lamanna, A. Xiao, E. Scott, J. Choi, and J. R. Dahn, *J. Electrochem. Soc.*, **159**, A1095 (2012).
- [51] C. P. Aiken, J. Self, R. Petibon, X. Xia, J. M. Paulsen, and J. R. Dahn, *J. Electrochem. Soc.*, **162**, A760 (2015).
- [52] C. P. Aiken, J. Xia, D. Y. Wang, D. A. Stevens, S. Trussler, and J. R. Dahn, *J. Electrochem. Soc.*, **161**, A1548 (2014).
- [53] W. Lu, Z. Chen, H. Joachin, J. Prakash, J. Liu, and K. Amine, *J. Power Sources*, **163**, 1074 (2007).
- [54] J.-S. Shin, C.-H. Han, U.-H. Jung, S.-I. Lee, H.-J. Kim, and K. Kim, *J. Power Sources*, **109**, 47 (2002).

- [55] X. L. Yao, S. Xie, C. H. Chen, Q. S. Wang, J. H. Sun, Y. L. Li, and S. X. Lu, *J. Power Sources*, **144**, 170 (2005).
- [56] S. Chen, Z. Wang, H. Zhao, H. Qiao, H. Luan, and L. Chen, *J. Power Sources*, **187**, 229 (2009).
- [57] E.-G. Shim, T.-H. Nam, J.-G. Kim, H.-S. Kim, and S.-I. Moon, *J. Power Sources*, **172**, 919 (2007).
- [58] Y.-B. He, Q. Liu, Z.-Y. Tang, Y.-H. Chen, and Q.-S. Song, *Electrochimica Acta*, **52**, 3534 (2007).
- [59] J. Chen, C. Buhrmester, and J. R. Dahn, *Electrochem. Solid-State Lett.*, **8**, A59 (2005).
- [60] K. Shima, K. Shizuka, M. Ue, H. Ota, T. Hatozaki, and J.-I. Yamaki, *J. Power Sources*, **161**, 1264 (2006).
- [61] L. Xiao, X. Ai, Y. Cao, and H. Yang, *Electrochimica Acta*, **49**, 4189 (2004).
- [62] D. D. MacNeil, Z. Lu, Z. Chen, and J. R. Dahn, *J. Power Sources*, **108**, 8 (2002).
- [63] M. N. Richard and J. R. Dahn, *J. Electrochem. Soc.*, **146**, 2068 (1999).
- [64] Y. Wang, K. Zaghbi, A. Guerfi, F. F. C. Bazito, R. M. Torresi, and J. R. Dahn, *Electrochimica Acta*, **52**, 6346 (2007).
- [65] Z. Zhang, D. Fouchard, and J. R. Rea, *J. Power Sources*, **70**, 16 (1998).
- [66] A. M. Andersson, D. P. Abraham, R. Haasch, S. MacLaren, J. Liu, and K. Amine, *J. Electrochem. Soc.*, **149**, A1358 (2002).
- [67] D. Aurbach, *J. Power Sources*, **89**, 206 (2000).
- [68] L. Madec, J. Xia, R. Petibon, K. J. Nelson, J.-P. Sun, I. G. Hill, and J. R. Dahn, *J. Phys. Chem. C*, **118**, 29608 (2014).
- [69] Y.-H. Rho, L. F. Nazar, L. Perry, and D. Ryan, *J. Electrochem. Soc.*, **154**, A283 (2007).
- [70] J. Światowska, V. Lair, C. Pereira-Nabais, G. Cote, P. Marcus, and A. Chagnes, *Appl. Surf. Sci.*, **257**, 9110 (2011).
- [71] L. J. Hardwick, H. Buqa, M. Holzapfel, W. Scheifele, F. Krumeich, and P. Novák, *Electrochimica Acta*, **52**, 4884 (2007).
- [72] X. H. Liu and J. Y. Huang, *Energy Environ. Sci.*, **4**, 3844 (2011).

- [73] M. Nie, D. Chalasani, D. P. Abraham, Y. Chen, A. Bose, and B. L. Lucht, *J. Phys. Chem. C*, **117**, 1257 (2013).
- [74] M. Nie and B. L. Lucht, *J. Electrochem. Soc.*, **161**, A1001 (2014).
- [75] H. Wang, Y.-I. Jang, B. Huang, D. R. Sadoway, and Y.-M. Chiang, *J. Electrochem. Soc.*, **146**, 473 (1999).
- [76] D. Aurbach, B. Markovsky, A. Rodkin, M. Cojocaru, E. Levi, and H.-J. Kim, *Electrochimica Acta*, **47**, 1899 (2002).
- [77] J. Li, W. Yao, Y. S. Meng, and Y. Yang, *J. Phys. Chem. C*, **112**, 12550 (2008).
- [78] D. Ostrovskii, F. Ronci, B. Scrosati, and P. Jacobsson, *J. Power Sources*, **103**, 10 (2001).
- [79] A. Xiao, L. Yang, B. L. Lucht, S.-H. Kang, and D. P. Abraham, *J. Electrochem. Soc.*, **156**, A318 (2009).
- [80] B. Simon and J.-P. Boeue, (1997) U.S. P/N 5,626,981.
- [81] D. Aurbach, K. Gamolsky, B. Markovsky, Y. Gofer, M. Schmidt, and U. Heider, *Electrochimica Acta*, **47**, 1423 (2002).
- [82] L. El Ouatani, R. Dedryvere, C. Siret, P. Biensan, S. Reynaud, P. Iratcabal, and D. Gonbeau, *J. Electrochem. Soc.*, **156**, A103 (2009).
- [83] H. Ota, Y. Sakata, A. Inoue, and S. Yamaguchi, *J. Electrochem. Soc.*, **151**, A1659 (2004).
- [84] J. C. Burns, N. N. Sinha, D. J. Coyle, G. Jain, C. M. VanElzen, W. M. Lamanna, A. Xiao, E. Scott, J. P. Gardner, and J. R. Dahn, *J. Electrochem. Soc.*, **159**, A85 (2011).
- [85] Y. Fu, C. Chen, C. Qiu, and X. Ma, *J. Appl. Electrochem.*, **39**, 2597 (2009).
- [86] Y. Hu, W. Kong, H. Li, X. Huang, and L. Chen, *Electrochem. Commun.*, **6**, 126 (2004).
- [87] T.-H. Nam, E.-G. Shim, J.-G. Kim, H.-S. Kim, and S.-I. Moon, *J. Electrochem. Soc.*, **154**, A957 (2007).
- [88] D. Y. Wang, N. N. Sinha, J. C. Burns, R. Petibon, and J. R. Dahn, *J. Power Sources*, **270**, 68 (2014).
- [89] N.-S. Choi, K. H. Yew, K. Y. Lee, M. Sung, H. Kim, and S.-S. Kim, *J. Power Sources*, **161**, 1254 (2006).
- [90] B. Liu, B. Li, and S. Guan, *Electrochem. Solid-State Lett.*, **15**, A77 (2012).

- [91] R. McMillan, H. Slegel, Z. X. Shu, and W. Wang, *J. Power Sources*, **81–82**, 20 (1999).
- [92] I. A. Profatilova, S.-S. Kim, and N.-S. Choi, *Electrochimica Acta*, **54**, 4445 (2009).
- [93] D. Y. Wang, N. N. Sinha, J. C. Burns, C. P. Aiken, R. Petibon, and J. R. Dahn, *J. Electrochem. Soc.*, **161**, A467 (2014).
- [94] Z. Chen and K. Amine, *J. Electrochem. Soc.*, **153**, A1221 (2006).
- [95] A. von Cresce and K. Xu, *J. Electrochem. Soc.*, **158**, A337 (2011).
- [96] J. Jiang and J. R. Dahn, *Electrochimica Acta*, **49**, 4599 (2004).
- [97] Q. Wang, J. Sun, and C. Chen, *J. Power Sources*, **162**, 1363 (2006).
- [98] J. R. Dahn, J. Jiang, L. M. Moshurchak, M. D. Fleischauer, C. Buhrmester, and L. J. Krause, *J. Electrochem. Soc.*, **152**, A1283 (2005).
- [99] J. K. Feng, X. P. Ai, Y. L. Cao, and H. X. Yang, *Electrochem. Commun.*, **9**, 25 (2007).
- [100] M. Q. Xu, L. D. Xing, W. S. Li, X. X. Zuo, D. Shu, and G. L. Li, *J. Power Sources*, **184**, 427 (2008).
- [101] K. Abe, Y. Ushio, H. Yoshitake, and M. Yoshio, *J. Power Sources*, **153**, 328 (2006).
- [102] H. Mao, U. V. Sacken, and J. N. Reimers, (1999) U.S. P/N 5,891,592.
- [103] J. Shin, J. Kim, E. Hong, J. Lee, Y. Kim, and J. Kim (2003) U.S. P/N 6,645,674.
- [104] K. Abe, JP, K. Miyoshi, JP, T. Kuwata, and JP, (2009) U.S. P/N 7,629,085.
- [105] E. Peled, *J. Electrochem. Soc.*, **126**, 2047 (1979).
- [106] E. Peled, D. Golodnitsky, and G. Ardel, *J. Electrochem. Soc.*, **144**, L208 (1997).
- [107] A. Smith, (2012) [accessed April 5, 2015] <http://DalSPACE.library.dal.ca/handle/10222/14608>.
- [108] T. M. Bond, J. C. Burns, D. A. Stevens, H. M. Dahn, and J. R. Dahn, *J. Electrochem. Soc.*, **160**, A521 (2013).
- [109] J. C. Burns, L. J. Krause, D.-B. Le, L. D. Jensen, A. J. Smith, D. Xiong, and J. R. Dahn, *J. Electrochem. Soc.*, **158**, A1417 (2011).
- [110] J. Barker, R. Koksang, and M. Y. Saïdi, *Solid State Ion.*, **82**, 143 (1995).



- [111] K. Honkura, H. Honbo, Y. Koishikawa, and T. Horiba, *ECS Trans.*, **13**, 61 (2008).
- [112] I. Bloom, A. N. Jansen, D. P. Abraham, J. Knuth, S. A. Jones, V. S. Battaglia, and G. L. Henriksen, *J. Power Sources*, **139**, 295 (2005).
- [113] H. M. Dahn, A. J. Smith, J. C. Burns, D. A. Stevens, and J. R. Dahn, *J. Electrochem. Soc.*, **159**, A1405 (2012).
- [114] D. Y. Wang and J. R. Dahn, *J. Electrochem. Soc.*, **161**, A1890 (2014).
- [115] N. N. Sinha, J. C. Burns, and J. R. Dahn, *J. Electrochem. Soc.*, **160**, A709 (2013).
- [116] N. N. Sinha, T. H. Marks, H. M. Dahn, A. J. Smith, J. C. Burns, D. J. Coyle, J. J. Dahn, and J. R. Dahn, *J. Electrochem. Soc.*, **159**, A1672 (2012).
- [117] N. N. Sinha, A. J. Smith, J. C. Burns, G. Jain, K. W. Eberman, E. Scott, J. P. Gardner, and J. R. Dahn, *J. Electrochem. Soc.*, **158**, A1194 (2011).
- [118] C. H. Chen, J. Liu, and K. Amine, *J. Power Sources*, **96**, 321 (2001).
- [119] E. Barsoukov and J. R. Macdonald, *Impedance Spectroscopy: Theory, Experiment, and Applications*, John Wiley & Sons, (2005).
- [120] J. C. Burns, G. Jain, A. J. Smith, K. W. Eberman, E. Scott, J. P. Gardner, and J. R. Dahn, *J. Electrochem. Soc.*, **158**, A255 (2011).
- [121] L. Ma, D. Y. Wang, L. E. Downie, J. Xia, K. J. Nelson, N. N. Sinha, and J. R. Dahn, *J. Electrochem. Soc.*, **161**, A1261 (2014).
- [122] L. Ma, J. Xia, and J. R. Dahn, *J. Electrochem. Soc.*, **161**, A2250 (2014).
- [123] K. J. Nelson, J. Xia, and J. R. Dahn, *J. Electrochem. Soc.*, **161**, A1884 (2014).
- [124] D. Y. Wang, N. N. Sinha, R. Petibon, J. C. Burns, and J. R. Dahn, *J. Power Sources*, **251**, 311 (2014).
- [125] D. Y. Wang, J. Xia, L. Ma, K. J. Nelson, J. E. Harlow, D. Xiong, L. E. Downie, R. Petibon, J. C. Burns, A. Xiao, W. M. Lamanna, and J. R. Dahn, *J. Electrochem. Soc.*, **161**, A1818 (2014).
- [126] J. Xia, C. P. Aiken, L. Ma, G. Y. Kim, J. C. Burns, L. P. Chen, and J. R. Dahn, *J. Electrochem. Soc.*, **161**, A1149 (2014).
- [127] J. Xia, J. E. Harlow, R. Petibon, J. C. Burns, L. P. Chen, and J. R. Dahn, *J. Electrochem. Soc.*, **161**, A547 (2014).
- [128] J. Xia, N. N. Sinha, L. P. Chen, and J. R. Dahn, *J. Electrochem. Soc.*, **161**, A264 (2014).

- [129] J. Xia, N. N. Sinha, L. P. Chen, G. Y. Kim, D. J. Xiong, and J. R. Dahn, *J. Electrochem. Soc.*, **161**, A84 (2014).
- [130] R. Fathi, J. C. Burns, D. A. Stevens, H. Ye, C. Hu, G. Jain, E. Scott, C. Schmidt, and J. R. Dahn, *J. Electrochem. Soc.*, **161**, A1572 (2014).
- [131] A. J. Smith, J. C. Burns, X. Zhao, D. Xiong, and J. R. Dahn, *J. Electrochem. Soc.*, **158**, A447 (2011).
- [132] M. Armand, M. Gauthier, and D. Muller, (1991) U.S. P/N 5,021,308.
- [133] L. J. Krause, W. Lamanna, J. Summerfield, M. Engle, G. Korba, R. Loch, and R. Atanasoski, *J. Power Sources*, **68**, 320 (1997).
- [134] C.-S. Cheng, F.-M. Wang, and J. Rick, *Int. J. Electrochem. Sci.*, **7**, 8676 (2012).
- [135] J. C. Burns, N. N. Sinha, G. Jain, H. Ye, C. M. VanElzen, E. Scott, A. Xiao, W. M. Lamanna, and J. R. Dahn, *J. Electrochem. Soc.*, **160**, A2281 (2013).
- [136] J. C. Burns, N. N. Sinha, G. Jain, H. Ye, C. M. VanElzen, E. Scott, A. Xiao, W. M. Lamanna, and J. R. Dahn, *J. Electrochem. Soc.*, **161**, A247 (2014).
- [137] M. Lu, Y. Tian, X. Zheng, J. Gao, and B. Huang, *J. Power Sources*, **219**, 188 (2012).
- [138] I. Belharouak, G. M. Koenig, T. Tan, H. Yumoto, N. Ota, and K. Amine, *J. Electrochem. Soc.*, **159**, A1165 (2012).
- [139] R. Spotnitz, *J. Power Sources*, **113**, 72 (2003).
- [140] S. E. Sloop, J. B. Kerr, and K. Kinoshita, *J. Power Sources*, **119–121**, 330 (2003).
- [141] R. Dedryvère, D. Foix, S. Franger, S. Patoux, L. Daniel, and D. Gonbeau, *J. Phys. Chem. C*, **114**, 10999 (2010).
- [142] A. J. Smith, H. M. Dahn, J. C. Burns, and J. R. Dahn, *J. Electrochem. Soc.*, **159**, A705 (2012).
- [143] Y.-T. Cheng and M. W. Verbrugge, *J. Power Sources*, **190**, 453 (2009).
- [144] P. Liu, J. Wang, J. Hicks-Garner, E. Sherman, S. Soukiazian, M. Verbrugge, H. Tataria, J. Musser, and P. Finamore, *J. Electrochem. Soc.*, **157**, A499 (2010).
- [145] X. H. Liu, L. Zhong, S. Huang, S. X. Mao, T. Zhu, and J. Y. Huang, *ACS Nano*, **6**, 1522 (2012).
- [146] J. H. Ryu, J. W. Kim, Y.-E. Sung, and S. M. Oh, *Electrochem. Solid-State Lett.*, **7**, A306 (2004).

- [147] S. S. Zhang, *J. Power Sources*, **161**, 1385 (2006).
- [148] S. S. Zhang, K. Xu, and T. R. Jow, *J. Power Sources*, **160**, 1349 (2006).
- [149] L. E. Downie, L. J. Krause, J. C. Burns, L. D. Jensen, V. L. Chevrier, and J. R. Dahn, *J. Electrochem. Soc.*, **160**, A588 (2013).
- [150] M. Petzl and M. A. Danzer, *J. Power Sources*, **254**, 80 (2014).
- [151] M. C. Smart and B. V. Ratnakumar, *J. Electrochem. Soc.*, **158**, A379 (2011).
- [152] J. C. Burns, D. A. Stevens, and J. R. Dahn, *J. Electrochem. Soc.*, **162**, A959 (2015).
- [153] R. D. Deshpande, P. Ridgway, Y. Fu, W. Zhang, J. Cai, and V. Battaglia, *J. Electrochem. Soc.*, **162**, A330 (2015).
- [154] A. W. Rowe, J. Camardese, E. McCalla, and J. R. Dahn, *J. Electrochem. Soc.*, **161**, A1189 (2014).
- [155] J. E. Harlow, D. A. Stevens, J. C. Burns, J. N. Reimers, and J. R. Dahn, *J. Electrochem. Soc.*, **160**, A2306 (2013).

# Appendix A

## Request for Permission to Reproduce or Re-Publish ECS Material

Please fax this form to: The Electrochemical Society (ECS), Attn: Permissions Requests, 1.609.730.0629.  
You may also e-mail your request to: [copyright@electrochem.org](mailto:copyright@electrochem.org). Include all the information as required on this form. Please allow 3-7 days for your request to be processed.

I am preparing a (choose one):  paper  chapter  book  thesis

entitled: Studies on the Lifetime and Degradation of Li-Ion Cells

to be published by: John C Burns

in an upcoming publication entitled: Studies on the Lifetime and Degradation of Li-Ion Cells

I request permission to use the following material in the publication noted above, and request nonexclusive rights for all subsequent editions and in all foreign language translations for distribution throughout the world.

**Description of material to be used**—Indicate what material you wish to use (figures, tables, text, etc.) and give the full bibliographic reference for the source publication. You may attach a separate list, organized by ECS title.

See attached list

Signature: 

Date: January 6, 2015

Name: John C Burns

Address: 2723 George Dauphinee Ave

Halifax, NS B3L 3S5

Canada

Telephone: 902-449-9121

Fax: \_\_\_\_\_

E-mail: chris.burns@dal.ca

Permission is granted to reproduce the above-referenced material. Please acknowledge the author(s) and publication data of the original material, and include the words: "Reproduced by permission of The Electrochemical Society."

Jan. 6, 2015

Date

  
Ann F. Goedkoop, Publications Production Director

I request the rights to use any of the figures and tables from my work in the following references in my PhD thesis:

1. "Introducing Symmetric Li-Ion Cells as a Tool to Study Cell Degradation Mechanisms" *Journal of The Electrochemical Society*, **158** (12) A1417-A1422 (2011). ✓
2. "The Impact of Varying the Concentration of Vinylene Carbonate Electrolyte Additive in Wound Li-Ion Cells" *Journal of The Electrochemical Society*, **159** (2) A85-A90 (2012). ✓
3. "Impedance Reducing Additives and Their Effect on Cell Performance I.  $\text{LiN}(\text{CF}_3\text{SO}_2)_2$ " *Journal of The Electrochemical Society*, **159** (7) A1095-A1104 (2012). ✓
4. "Impedance Reducing Additives and Their Effect on Cell Performance II.  $\text{C}_3\text{H}_9\text{B}_3\text{O}_6$ " *Journal of The Electrochemical Society*, **159** (7) A1105-A1113 (2012). ✓
5. "The Effect of Trimethoxyboroxine on Carbonaceous Negative Electrodes for Li-Ion Batteries" *Journal of The Electrochemical Society*, **160** (2) A383-A386 (2013). ✓
6. "Improving Precision and Accuracy in Coulombic Efficiency Measurements of Li-Ion Batteries" *Journal of The Electrochemical Society*, **160** (3) A521-A527 (2013). ✓
7. "Predicting and Extending the Lifetime of Li-Ion Batteries" *Journal of The Electrochemical Society*, **160** (9) A1451-A1456 (2013). ✓
8. "Studies of the Effect of Varying Vinylene Carbonate (VC) Content in Lithium Ion Cells on Cycling Performance and Cell Impedance" *Journal of The Electrochemical Society*, **160** (10) A1668-A1674 (2013). ✓
9. "The Impact of Intentionally Added Water to the Electrolyte of Li-Ion Cells I. Cells with Graphite Negative Electrodes" *Journal of The Electrochemical Society*, **160** (11) A2281-A2287 (2013). ✓
10. "The Impact of Intentionally Added Water to the Electrolyte of Li-Ion Cells II. Cells with Lithium Titanate Negative Electrodes" *Journal of The Electrochemical Society*, **161** (3) A247-A255 (2014). ✓
11. "Comparative Study of Tris(trimethylsilyl) Phosphate and Tris(trimethylsilyl) Phosphite as Electrolyte Additives for Li-Ion Cells" *Journal of The Electrochemical Society*, **161** (6) A1084-A1089 (2014). ✓
12. "Ultra High-Precision Studies of Degradation Mechanisms in Aged  $\text{LiCoO}_2$ /Graphite Li-Ion Cells" *Journal of The Electrochemical Society*, **161** (10) A1572-A1579 (2014). ✓

